LAWRENCE
LIVERMORE
NATIONAL
LABORATORY

LLNL-TR-677751

Fusion Blanket Coolant Section Criteria, Methodology, and Results

J. A. DeMuth, W. R. Meier, A. Jolodosky, M. Frantoni, S. Reyes

October 2, 2015

Disclaimer

This work performed under the auspices of the U.S. Department of Energy by Lawrence Livermore National Laboratory under Contract DE-AC52-07NA27344.

Table of Contents

Figures

Tables

1 Introduction

The “blanket” that surrounds the chamber in a fusion power plant serves two primary purposes: removal of thermal energy and breeding of tritium for continuing plant operations. In considering deuterium-tritium (DT) fusion, tritium must be created or “bred” since it has a half-life of 12 years and thus is not naturally available in the quantities needed. Fortunately tritium can be readily created in the blanket surrounding the fusion plasma since it undergoes two T producing reaction with neutrons produced in the DT fusion reaction:

$$^{7}Li + n \rightarrow n' + T + \alpha$$

$$^{6}Li + n \rightarrow T + \alpha$$

The tritium breeding ratio (TBR) equals the number tritium atoms created per DT fusion reaction. Due to tritium losses by decay and in fuel cycle processing, a TBR greater than one is required to maintain operations. The fact that reactions with ^{7}Li produce a lower energy neutron in addition to a T and the ability to incorporate a neutron multiplier in the fusion blanket makes it possible to breed more than one T per DT reaction even though the DT fusion reaction only releases one neutron:

$$D + T \rightarrow n(14.1\ MeV) + \alpha(3.5\ MeV)$$

In order for the lithium to be in a position to undergo these neutron interactions, it needs to be close to the reaction source, either as a Li-bearing solid ceramic material typically cooled by high pressure helium or as a liquid metal (pure Li or an alloy) that can also serve as the blanket coolant.

Tritium breeding and energy extraction requirements place many constraints on the materials to be used in the process. Lithium in some form must then be at a sufficient concentration in either the solid or liquid breeding material to achieve a TBR greater than one. From an electrical generation perspective, conversion from heat to electricity becomes more efficient as the working fluid becomes hotter, and typical operating points are between 400C and 600C. Due to this elevated temperature, molten lithium is often considered as a blanket coolant, however it can be very problematic due to its high reactivity with oxygen, water, and nitrogen.

The focus of this LDRD was to explore potential Li alloys that would meet the tritium breeding and blanket cooling requirements but with reduced chemical reactivity, while maintaining the other attractive features of pure Li breeder/coolant. In other fusion approaches (magnetic fusion energy or MFE), 17Li-83Pb alloy is used leveraging Pb’s ability to maintain high TBR while lowering the levels of lithium in the system. Unfortunately this alloy has a number of potential draw-backs. Due to the high Pb content, this alloy suffers from very high average density, low tritium solubility, low system energy, and produces undesirable activation products in particular polonium. The criteria considered in the selection of a tritium breeding alloy are described in the following section.

1.1 Selection Criteria

The goal of this study is to determine if an alternative alloy(s) for lithium can be found that produce a coolant with the following attributes:

1.1.1 Reactivity (RX)

Low chemical reactivity is very desirable. The subsequent chemical reactivity of the potential alloy has tremendous cascading effects on plant economics as well as the safety basis of operation. If a blanket can be chemically reacted simply by exposing it to air or water (as is true in the case of Lithium) it could have the potential to mobilize tritium and other activated structural material, not to mention subsequent destructive explosions and fire scenarios.

1.1.2 Melting Point (MP)

The candidate alloy must have a sufficiently low melting point to allow for operation at as low as 400C, giving an operating margin of ~50C before the solidification temperature. The alloy should consist of a single material phase so separation (think oil and water) does not occur during operation giving rise to continuously changing performance and material properties depending on how well mixed it is.

1.1.3 Tritium Inventory (TI)

The amount of tritium stored in the coolant system is critical in the event of an accident. If the coolant is reactive (such as in the case of pure Li, or even 17Li-83Pb), there is a potential for all the tritium dissolved in the coolant to be released, generating an acute dose at the site boundary. As a general guideline, <100g is considered good, 100-1000g is considered acceptable, and >1kg is considered poor for a site boundary of 1 mile. All tritium dissolved in potentially volatilized material must be considered in this calculation. This includes all coolant volumes and the structures containing them such as all the piping, the blanket, tritium extractor, pumps, and heat exchangers. These concentrations ultimately depend on the environment of all these components as well as their respective tritium solubilities and diffusivities.

1.1.4 Power Handling (PH)

The fraction of energy spent on moving the primary coolant around the plant should not constitute a signification fraction of the total energy generated. This factor is dependent on material properties, primarily operating temperature window (difference between melt temperature and maximum operating temperature of 600C), material density, specific heat, viscosity, and thermal conductivity.

1.1.5 Blanket Multiplication Factor (GAIN)

System GAIN plays a very large part in the system economics. Higher gain means that for the same electrical energy output, less fusion power is needed, reducing the capital costs of the laser and all driver systems accordingly. This is especially economical if higher GAIN can be achieved through careful selection of the blanket coolant material. Blanket GAIN is defined as:

$$GAIN = \frac{Total\ Thermal\ Energy}{Fusion\ Energy}$$

1.1.6 Tritium Breeding Ratio (TBR)

There is a minimum TBR required for operation, anything more than that is excess, however there are scenarios such as starting up a new plant that require a stockpile of tritium to achieve. There are other alternative uses for excess tritium that have been explored in the past, however for the purposes of this study, TBR is used as a minimum requirement (of 1.02), and no merit is given to higher values.

1.1.7 Activation (ACT)

Material activation is a large concern when dealing with fusion energy. Worker dose, and waste handling all become considerations if the material gets to hot both in terms of Contact Dose, and Accident Dose.

1.1.8 Waste Disposal Rating (WDR)

Material must have a WDR<1 to qualify for shallow land burial.

1.1.9 Material Abundance (MA)

Material Abundance factor is a long term consideration. Lithium is sufficiently abundant but we must make sure alloying constituents are also available in quantities that are needed to support a fusion power economy.

1.1.10 Material Cost (MC)

Material Cost factor is an immediate factor which clearly impacts the economics of the proposed power plant. This must be low enough so as to not be commercially prohibitive.

1.2 Potential Alloys

Initial pre-screening and down selection was carried out by examining binary phase diagrams for elements alloying with lithium. The resulting elements were Ag, Ba, Bi, Cd, Cu, Ga, Hg, In, Li, Na, Pb, Sb, Sn, Sr, Ti, and Zn. The corresponding phase diagrams can be found in Appendix 6.

2 Simulations

2.1 Selection Mechanism

To down-select potential candidate alloys, a selection mechanism is required that can appropriately weight the merit of these nine criteria. Human beings are excellent at comparing two properties and distinguishing between them, but are terrible at simultaneous comparison of many. To that end, the Analytic Hierarchy Process (AHP)(*1*) was implemented to determine the criteria weights. AHP uses pair wise comparison technique to determine the criteria weights. First a matrix is created where each criteria is compared one at a time to the other criteria and importance is evaluated on a scale of 0-5 as follows. Here the results of the selection are tabulated in Table 1.

1 = Equally Important
2 = Moderately More Important
3 = Strongly More Important
4 = Very Strongly More Important
5 = Extremely More Important

Criteria	GAIN	TI	RX	PH	MC	MA
GAIN	1	3	0.5	2	4	4
TI	0.333	1	0.25	0.25	4	4
RX	2	4	1	4	5	5
PH	0.5	4	0.25	1	3	3
MC	0.25	0.25	0.2	0.2	1	1.5
MA	0.25	0.25	0.2	0.333	0.667	1

Table 1: Criteria Importance Matrix

The diagonals in this matrix are always (1) (white), and the yellow values are calculated as the inverse of the values generated by the pairwise comparison (green). Values less than (1) take the reciprocal comparison. For instance in this comparison, row 1, column 2, GAIN is valued as “Strongly more Important” than the tritium inventory (TI), however for row 1, column 3, Reactivity (RX) is valued as “Moderately more Important” than GAIN so the value is ½, or 0.5.

$$PairWiseComparison = PWC_{i,j} = \begin{pmatrix} 1 & 3 & 0.5 & 2 & 4 & 4 \\ 0.333 & 1 & 0.25 & 0.25 & 4 & 4 \\ 2 & 4 & 1 & 4 & 5 & 5 \\ 0.5 & 4 & 0.25 & 1 & 3 & 3 \\ 0.25 & 0.25 & 0.2 & 0.2 & 1 & 1.5 \\ 0.25 & 0.25 & 0.2 & 0.333 & 0.667 & 1 \end{pmatrix}$$

This matrix is then squared, and each row summed:

$$PWC_{sumsq} = \sum_{j=1}^{6} PWC_{i,j}^2 = \begin{pmatrix} 101.9 \\ 66.9 \\ 161.4 \\ 43.8 \\ 19.9 \\ 18.5 \end{pmatrix}$$

Then normalized to determine the correct weighting:

$$Weights = \frac{PWC_{sumsq}}{\sum_{i=1}^{6} PWC_{sumsq}} = \begin{pmatrix} 0.247 \\ 0.162 \\ 0.391 \\ 0.106 \\ 0.048 \\ 0.045 \end{pmatrix}$$

The process is then repeated to check if the results are consistent, giving:

$$FinalWeights = \begin{pmatrix} 0.243 \\ 0.16 \\ 0.389 \\ 0.11 \\ 0.051 \\ 0.047 \end{pmatrix}$$

2.2 Material Properties

2.2.1 Melting Point (MP)

Ternary melting point data is used in the calculation of power handling and tritium inventory, as well as baseline usability of the ternary alloy for a coolant, but is not directly used as a criteria value.

While a Li-Sn binary yields ideal results in terms of TBR and GAIN, unfortunately, the mixture optimized for Gain and TBR has a melting point over 700C, and is a solid at blanket operating temperatures. The creation of a Li/Sn/X ternary mixture has potential to lower the melt temperature as long as the ternary constituent doesn't interfere with the current blanket properties. In examining phase diagrams for nearly every elemental binary combination of lithium and tin with a ternary partner that was liquid in some form below 400C.

Using an interpolation algorithm, Equation 1, the three binary diagrams for all combinations of Li and the 15 other elements is used to create an estimation of the ternary liquidus line. These binary diagrams are listed in Appendix 6.1. Here a, b, and c represent species Li, X and Y, and F(a,b) is the temperature of the binary combination of a and b as a function of the relative mole fraction of a to b.

Equation 1:
$$\boldsymbol{T_{Li-X-Y} = \frac{ab*F\left(\frac{a}{a+b}\right) + bc*F\left(\frac{b}{b+c}\right) + ca*F\left(\frac{c}{a+c}\right)}{ab+bc+ca}}$$

2.2.2 Heat Transfer Properties

While heat transfer properties are not used directly in the criteria, they are subsets, and can give a good feel for which materials are enhancing the alloy, and which are not. The ability to quickly transfer thermal energy, or store large amounts is highly desirable in power plant or heat exchanger systems. The physical

properties of the ternary candidates, vary a good deal from species to species. For evaluating the heat transfer coefficient based on material properties for liquid metals, the important scale factor goes as $(\rho C_p)^{0.8} k^{0.2}$, this is reduced from the heat transfer coefficient (h) and Nusselt number (Nu) correlations given by Equation 4, and Equation 5, where Prandtl Number (Pr) and Reynolds number (Re) are given by Equation 2 and Equation 3. Based on this scaling factor, the heat transfer coefficient increases with increasing volumetric heat capacity and thermal conductivity.

Equation 2: $$Pr = \frac{C_p \mu}{k}$$

Equation 3: $$Re = \frac{\rho V D}{\mu}$$

Equation 4: $$Nu = 5.0 + 0.025(Pr * Re)^{.8}$$

Equation 5: $$h = \frac{Nu * k}{D}$$

By examining the thermal properties of the materials in question in

Material	Thermal Conductivity [W/m-K]	Density [g/cc]	Molar Mass [g/mol]	Dynamic Viscosity [Pa-s]	Specific Heat [J/kg-K]	Volumetric Heat [J/cm^3-K]	Heat Transfer Coefficient [kW/m^2-K]
Ag	430	10.50	107.87	0.00180	235	2.47	26.15
Ba	18	3.51	137.33	0.00074	205	0.72	4.50
Bi	8	9.78	208.98	0.00169	122	1.19	5.59
Cd	97	8.65	112.41	0.00152	230	1.99	14.63
Cu	400	8.92	63.55	0.00156	384	3.43	32.00
Ga	29	5.90	69.72	0.00160	371	2.19	11.87
Hg	8.3	13.40	200.59	0.00210	140	1.88	8.05
In	82	7.31	114.82	0.00104	233	1.70	12.48
Li	85	0.53	6.94	0.00376	3570	1.89	13.63
Na	140	0.97	22.99	0.00025	1230	1.19	11.15
Pb	35	11.30	207.20	0.00215	127	1.44	8.93
Sb	24	6.70	121.76	0.00122	207	1.39	7.98
Sn	67	7.30	118.71	0.00109	217	1.58	11.24
Sr	35	2.63	87.62	0.00060	300	0.79	5.66
Ti	22	4.51	47.87	0.00089	520	2.35	11.80
Zn	120	7.14	65.38	0.00385	388	2.77	19.77

, it is clear that the materials with the highest volumetric heat are Cu, Zn, Ag, and Ti at 3.43, 2.77, 2.47, and 2.34 $\frac{J}{cm^3-K}$ respectively. Using an example scenario of 2m/s flow down a 50cm diameter tube gives heat transfer coefficients, the largest of which are for Cu, Ag, Zn, and Cd at 32, 26.15, 19.77, and 14.63 $\frac{kW}{m^2-K}$. If designing the blanket for heat transfer purposes alone, Cu would be the optimal heat transfer fluid, with a high volumetric heat capacity, it could accommodate a given temperature drop with the lowest flow rate. Additionally, the high heat transfer coefficient for liquid Cu would allow it to maintain the wall temperatures closer to that of the bulk fluid. The transition metals in period 4 of the periodic table have the best heat transfer properties, essentially they have the largest volumetric heat capacity, with Ni being one of the highest. Unfortunately, most of these transition metals have very high melting points which make them unusable as a heat transfer fluid. Zinc is the exception to this rule with its low melting point, and has good potential for providing excellent heat transfer.

Table 2: Thermophysical Properties of Potential Coolant Constituents at STP

Material	Thermal Conductivity [W/m-K]	Density [g/cc]	Molar Mass [g/mol]	Dynamic Viscosity [Pa-s]	Specific Heat [J/kg-K]	Volumetric Heat [J/cm^3-K]	Heat Transfer Coefficient [kW/m^2-K]
Ag	430	10.50	107.87	0.00180	235	2.47	26.15
Ba	18	3.51	137.33	0.00074	205	0.72	4.50
Bi	8	9.78	208.98	0.00169	122	1.19	5.59
Cd	97	8.65	112.41	0.00152	230	1.99	14.63
Cu	400	8.92	63.55	0.00156	384	3.43	32.00
Ga	29	5.90	69.72	0.00160	371	2.19	11.87
Hg	8.3	13.40	200.59	0.00210	140	1.88	8.05
In	82	7.31	114.82	0.00104	233	1.70	12.48
Li	85	0.53	6.94	0.00376	3570	1.89	13.63
Na	140	0.97	22.99	0.00025	1230	1.19	11.15
Pb	35	11.30	207.20	0.00215	127	1.44	8.93
Sb	24	6.70	121.76	0.00122	207	1.39	7.98
Sn	67	7.30	118.71	0.00109	217	1.58	11.24
Sr	35	2.63	87.62	0.00060	300	0.79	5.66
Ti	22	4.51	47.87	0.00089	520	2.35	11.80
Zn	120	7.14	65.38	0.00385	388	2.77	19.77

2.3 Criteria Values

In the subsequent sections, all material data in an alloy is linearly weighted by constituent except for solubility which is scaled according to the lithium concentration curve fit for Lithium Lead. For flow and geometry: pipe roughness $\left(\frac{\varepsilon}{d} = 0.004\right)$, R=13m, t=1.5m, v=2m/s, Dh=2t, and $\Delta T_{io} = 650 - T_{melt}$.

2.3.1 Reactivity (RX)

Reactivity weightings for the merit function are based on MSDS until more extensive data can be added. These sheets rate the different elements based on chemical reactivity on a scale between 0 and 3, where 3 is most reactive. This scale is normalized to [0, 1]. Scaling is linear. Merit function value is given by Equation 6. Merit function aims to minimize this criterion.

Equation 6: $$Merit_{RX} = 1 - \frac{RX}{\max(RX)}$$

2.3.2 GAIN

Gain data is calculated using MCNP and a geometrical model of the fusion chamber by Jolodosky et al(*2*). Ternary mixtures were swept in 5% increments for each ternary combination. Lithium was combined with 88 different binary mixtures, of which there were 210 data points per ternary for a total of 18,480 MCNP runs to evaluate the ternary data space. Gain data is in the range [0, 1.5] and is normalized to [0, 1]. Scaling is linear. Merit function value is given by Equation 7. Merit function aims to maximize this criterion.

Equation 7: $$Merit_{GAIN} = \frac{GAIN - 1}{\max(GAIN) - 1}$$

2.3.3 Tritium Inventory (TI)

Tritium inventory is the most complicated criteria to calculate (other than the MCNP physics involved in generating TBR and GAIN). In this simulation, an eight state flow loop is modeled. All pipes are assumed to be made of steel. Volumes of coolant and steel, wall thicknesses, temperatures, diffusion rates, solubilities for each of the eight states are calculated based upon known parameters. The states are defined in Figure 1, showing the direction of flow, and calling out all pipe number lengths.

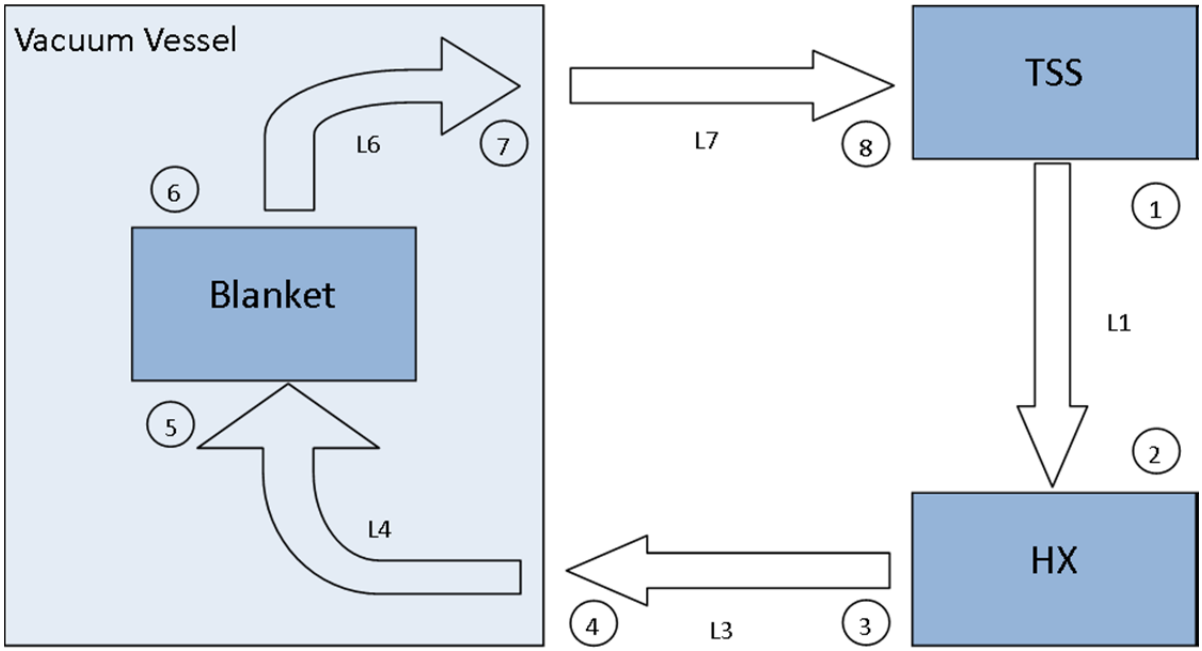

Figure 1: Tritium Inventory System Layout

In this system there are four major components, the Vacuum Vessel (which defines the barriers to clear Ar and heavily tritium laden Xe), the blanket (where tritium is created, and the coolant heated), the Tritium Separation System (TSS – where tritium is removed), and the Heat Exchanger (HX) where the heat is removed. Outside the vacuum vessel, all pipes are assumed to be double walled with zero tritium in the gas phase outside the pipe wall. Inside the vacuum vessel, the pipes are single walled, and gaseous tritium concentration is calculated based on gas clearing rates. States 1, 2, 6, 7, and 8 are taken to be "hot" (600C), and States 3, 4, and 5 are taken to be "cold" (Tmelt+50C). Cross sectional flow areas of the pipes are calculated by Equation 8 where all the flow is assumed to go through one single pipe for the entire blanket. Assuming a circular cross-section, the radius and surface area to volume ratio of the pipes can be calculated.

Equation 8: $$Ac_{pipe} = \frac{q_{plant}}{v_{max}\rho C_p \Delta T_{io}}$$

Pipe length in state (1) is taken to be 30m, state (3) to be 60m, state (4) and state (6) to be the difference between the vacuum vessel and blanket radii (5m), and state (7) 30m.

2.3.3.1 State 1 – Just after Tritium Separation System (TSS) to HX

Tritium concentration is set at this point to the designed level of 0.1appm. In this model, the TSS is the first stop for flow exiting the blanket to take advantage of the high temperature diffusion rates of tritium to extract it from the system. Temperature is "hot" (600C). State one starts just after the TSS and encompasses the pipe between state 1 and state 2. The pipe is assumed to be thermally well insulated, but permeable to tritium (which is swept away by helium in a double walled tube).

2.3.3.2 State 2 – Inside the Heat Exchanger

Heat exchanger hydraulic diameter is taken as a general assumption to be 0.1m. Based on general liquid to liquid heat exchanger design, surface area to volume ratio for the heat exchanger is taken to be 250 $\frac{m^2}{m^3}$(*3*). Since the temperature of this state varies from hot to cold, temperature dependent parameters are calculated at both the inlet and outlet, and then averaged (especially important for highly non-linear parameters such as diffusivity and solubility). Peclet number is calculated by Equation 9, and Nusselt number by Equation 10. Nusselt is then used to calculate the heat transfer coefficient on the coolant side of the HX wall. HX walls are assumed to be made of 1mm thick steel with a thermal conductivity of 20 $\frac{w}{m-K}$, and the heat transfer coefficient on the other side of the HX is assumed to be to a molten salt secondary loop with htc=2,000 $\frac{W}{m^2-K}$. Overall heat transfer coefficient can then be calculated by Equation 11.

Equation 9: $$Pe_{HX} = \frac{\rho C_p}{k} * v_{max} D_h$$

Equation 10: $$Nu_{HX} = 5.0 + 0.025 Pe_{HX}^{0.8}$$

Equation 11: $$U_{HX} = \frac{1}{\frac{1}{htc_1} + \frac{t_{HX}}{k_{HX}} + \frac{1}{htc_2}}$$

Based on the power output of the fusion plant, temperature drop, heat transfer coefficient and surface area to volume ratio of the HX, the total volume of coolant in the heat exchanger can be calculated by Equation 12.

Equation 12: $$V_{c_{HX}} = \frac{q_{plant}}{U_{HX} \Delta T_{io} \left(\frac{A_{s_{HX}}}{V_{HX}}\right)}$$

Length of the HX is taken as the cubed root of the volume, and volume of steel in the HX is taken as the product of the HX wall thickness, surface area to volume ratio, and coolant volume in the HX, Equation 13.

Equation 13: $$Vs_{HX} = \left(\frac{A_{s_{HX}}}{V_{HX}}\right) t_{HX} V_{c_{HX}}$$

2.3.3.3 State 3 – Heat Exchanger to the Vacuum Vessel

State 3 is “cold” with very low tritium concentration. Not much leaks out in this leg. This state continues up to the vacuum vessel wall.

2.3.3.4 State 4 – Vacuum Vessel to the Blanket

Inside the vacuum vessel, there is a relatively high concentration of tritium due to target and hohlraum debris. Radius of the vacuum vessel is taken to be 18m. Mass of the target is taken to be 1.7 mg of D+T. Chamber gas is 6000K, clearing ratio is 0.5% per shot. Steady state gas concentration can be found as a function of clearing ratio(*4,5*) by Equation 14. Knowing the mass of tritium in the vacuum vessel, volume, and temperature, the partial pressure of tritium can be found.

Equation 14: $$m_T = \frac{m_{target}}{x_{clear}}$$

2.3.3.5 State 5 – The Blanket

The blanket is where the tritium is created, and the coolant heated. Tritium creation rates are based on alloy TBR and plant power (taken to be 2 GW) and are calculated in Tritium generated per second. Surface area to volume for the blanket is calculated based upon chamber radius and thickness assuming spherical geometry. Gas surrounding the blanket is at the same partial pressure as in state 4.

2.3.3.6 State 6 – Blanket to the Vacuum Vessel

State 6 is nearly identical to state 4 except this time at high temperature, meaning higher tritium permeation rates. Depending on the coolant and wall concentrations, that rate could be either in or out of the coolant.

2.3.3.7 State 7 – Vacuum Vessel to the Tritium Separation System

State 7 is the last stretch of tubing, no tritium is assumed to be outside of the tube walls, so tritium can only be leaving the system.

2.3.3.8 Tritium Inventory Calculations

Once all the hydraulic diameters have been calculated, the pressure drop in the system can then be found with some very basic assumptions and is given by Equation 15. Here K_{eff} is the piping flow losses and is taken to be 20, h_{cham} is the vertical height of the chamber and is taken to be $2R_{cham}$.

Equation 15: $$\Delta P = \rho g \left(\frac{K_{eff} v_{max}^2}{2} + h_{cham} + \sum_i \frac{f L_i}{D_{h_i}} \frac{v_{max}^2}{2g} \right)$$

With a known system pressure drop, minimum wall thicknesses can be found based on the stress limits of the pipes and a 3x safety margin as compared to a 1mm thick pipe (Equation 16). With the pipe thickness known, pipe volumes can be calculated and the volume of steel and volume of coolant for each state determined.

Equation 16: $$t_{pipe} = \max\left(\left[\frac{3 \Delta P r}{\sigma_{pipe}}, 1mm \right] \right)$$

Concentration of tritium in the coolant can be modeled by the differential equation of the form of Equation 17, resulting in a solution of the form of Equation 19, which after re-substitution gives Equation 20. In this equation, D is the diffusivity of tritium in steel, K_{ss} is the Sieverts constant in steel, P_{T_2} is the partial pressure of tritium in the gas outside the pipe, t is the pipe thickness, SA/V is the surface Area to Volume Ratio, L is the pipe length, and v is the coolant velocity(*6–12*). This gives the final concentration at the end of the pipe depending on surrounding conditions in a continuum, allowing tritium to either be absorbed into the pipes, or dissipate to the surroundings. Equation 21 adds on the one additional source term that is needed to increase the concentration in the blanket due to the tritium generation due to neutron irradiance. Finally, Equation 22 and Equation 23 give the average tritium concentration in the coolant and the steel for each segment of the loop. This can be converted to moles by multiplying by the respective zone volume. Sum to total with Equation 24.

Equation 17: $$C(t) = C(0) + \frac{dC}{dt}$$

Equation 18: $$\frac{dC}{dt} = \left[K_{ss} P_{T_2}^{\frac{1}{2}} - C(t) \right] \frac{D}{t} \frac{SA}{V} = a[b - x]$$

Equation 19: $$C(t) = [ab + C_0] e^{-at}$$

Equation 20: $$C_{x+1} = \left[\frac{D}{t} \frac{SA}{V} K_{ss} P_{T_2}^{\frac{1}{2}} + C_x \right] e^{\left(-\frac{D}{t} * \frac{SA}{V} * \frac{L}{v} \right)}$$

Equation 21: $$C_{x+1} = \left[\frac{D}{t} \frac{SA}{V} K_{ss} P_{T_2}^{\frac{1}{2}} + C_x \right] e^{\left(-\frac{D}{t} * \frac{SA}{V} * \frac{L}{v} \right)} + \frac{T_{2_{gen}}}{V_{c_{state}}}$$

Equation 22: $$C_{x_{coolant}} = \frac{C_x + C_{x+1}}{2}$$

Equation 23: $$C_{x_{steel}} = \frac{\left(C_{x_{coolant}} \frac{K_{ss}}{K_{Li}} + K_{ss} P_T^{\frac{1}{2}}\right)}{2}$$

Equation 24: $$TI = \left[\sum_x C_{x_{steel}} * V_{x_{steel}} + \sum_x C_{x_{coolant}} * V_{x_{coolant}}\right] * M_T$$

Equation 25: $$Merit_{TI} = 1 - \frac{TI}{\max(TI)}$$

2.3.4 Power Handling (PH)

Power handling is explicitly calculated as the ratio of circulating power to output power. Values from this calculation are in the range of [0.000192 to 3.62]. Maximum allowed value for this criterion is 0.1 or 10%. Data is normalized to [0, 1] after the cap with a linear scaling. The value for power handling for each alloy is given by Equation 26, and the merit function by Equation 27. In these equations, f is the friction factor, v is the flow velocity (estimated to be 2m/s), Cp is the specific heat of the coolant, ΔT_{io} is the temperature window between the minimum coolant temperature and 650C, R is the radius of the blanket (13m), and t is the blanket thickness (1.5m). Equation 26 derives from basic heat transfer equations, and using assumptions with regards to spherical chamber geometry of a given thickness.

Equation 26: $$\frac{W}{Q} = \frac{\Delta P A_c v}{\dot{m} C_p \Delta T_{io}} = \frac{f v^2}{2 C_p \Delta T_{io}} \frac{L}{D_h} = \frac{f v^2}{C_p \Delta T_{io}} \left[\frac{(R+t)^3 - R^3}{3\pi^2 t^2 R}\right]$$

Equation 27: $$Merit_{PH} = 1 - \frac{\frac{W}{Q}}{\max\left(\frac{W}{Q}\right)}$$

2.3.5 Material Cost (MC)

Material Cost data is in $\frac{\$}{m^3}$ in the range [116,000-119,000,000]. Data is gathered from Alfa Aesar in terms of bar stock when possible. It is expected that actual bulk prices will be considerably less. This metric is used to get an estimate on the value. The data is capped at 10,000,000 and is then normalized to [0, 1]. Scaling is linear. Merit function value is given by Equation 28. Merit function aims to minimize this criterion.

Equation 28: $$Merit_{MC} = 1 - \frac{MC}{max(MC)}$$

2.3.6 Material Abundance (MA)

Gain data is in the range [0.0000067% to 2.3%] and is normalized to [0, 1]. Data is gathered from ptable.com(*13*) in terms of crust abundance. Scaling is logarithmic. Merit function value is given by Equation 29. Merit function aims to maximize this criterion.

Equation 29: $$Merit_{MA} = \frac{\log_{10} MA - min\left(MA(MA>0)\right)}{\log_{10} max(MA) - min\left(MA(MA>0)\right)}$$

2.3.7 Tritium Breeding Ratio (TBR)

TBR is not directly used as a merit function weighting, but it is used as a cutoff. If the TBR is <1.02 it is typically excluded. The exception is when examining alloys for use with enriched lithium in which case this cutoff is not imposed.

2.3.8 Melt Temperature

While the melt temperature is not directly used in the merit function as a weighting, it is used as a cutoff. Any alloys with a melt temp over 650C are not considered.

Table 3: Summary of Criterion and Li-Pb Alloy Examples

Criteria	Weight	Min Value	Max Value	Maximize/Minimize?	Scale	Max Limit
Gain	0.243	0	1.5	Maximize	Linear	None
Tritium Inventory	0.16	0	1.00E+21	Minimize	Linear	3000
Reactivity	0.389	0	3	Minimize	Linear	None
Power Handling	0.11	1.92E-04	3.62E+00	Minimize	Linear	0.1
Cost	0.051	1.16E+05	1.19E+08	Minimize	Linear	3.00E+07
Availability	0.043	6.70E-06	2.30E+00	Maximize	Logaritmic	None
TBR	0/1	0.00E+00	1.6062	Binary	Linear	1.02 (Min Value)
Melt Temp	0/1		6.50E+02	Binary	Linear	650C

Criteria	Lithium	Lead	5Li-PB	10Li-Pb	15Li-Pb	20Li-Pb
Gain	1.0395	1.0195	1.0079	1.0142	1.0194	1.024
Tritium Inventory	27.315	114.71	53.372	39.101	33.588	31.941
Reactivity	3	0	0.15	0.3	0.45	0.6
Power Handling	0.0001941	0.0084052	0.0032509	0.001902	0.0012828	0.0010354
Cost	1.16E+05	4.45E+05	4.29E+05	4.12E+05	3.96E+05	3.79E+05
Availability	0.0017	0.00099	0.0010255	0.001061	0.0010965	0.001132
TBR	1.6062	0	1.0011	1.1434	1.2302	1.2941
Melt Temp	180.85	327.85	301.28	275.92	248.04	255.98

3 Results

Running results of the various criterion calculations through the merit function with the appropriate weights shows that a few key alloys do very well. Table 3 lays out the various criterion, weights, minimum and maximum values, maximization vs minimization and scale. For key lithium lead alloys it also lays out the different merit function results for comparison and evaluation. When sorting by merit function, bismuth and lead alloys show up as winners because of their ability to allow for very low lithium content, but still maintain sufficient TBR to operate a plant. While lead is an acceptable coolant, bismuth produces polonium when irradiated, and is a non-starter with respect to plant operation.

Lithium-Lead-Zinc is a very predominant alloy in the merit function results and shows up as having compositions in many of the top contending ranks (Table 4). Some of the interesting results are those with the highest gain such as rank 1, 2, and 13.

Table 4: Merit Function Results

Rank	Mixture Name	MeritF	Gain	TBR	Tritium Invento	Reactivit y	Power Handling	Cost Per Volume	Availabil ity	MeltC	Acomp	Bcomp	Ccomp	MixInd
1	'li-pb-zn'	0.73567	1.1385	1.08E+00	35.213	0.45	0.001419	3.95E+05	0.001437	288.15	15	80	5	52
2	'li-pb-zn'	0.73198	1.1692	1.07E+00	39.115	0.6	0.0015107	3.77E+05	0.001813	371.54	20	70	10	52
3	'li-ag-pb'	0.72884	1.0566	1.02E+00	53.379	0.15	0.0032509	4.29E+05	0.001026	301.28	5	0	95	6
4	'li-pb-ba'	0.72881	1.0565	1.03E+00	53.382	0.15	0.0032509	4.29E+05	0.001026	301.28	5	95	0	49
5	'li-pb-bi'	0.72881	1.0565	1.03E+00	53.382	0.15	0.0032509	4.29E+05	0.001026	301.28	5	95	0	50
6	'li-pb-zn'	0.72881	1.0565	1.03E+00	53.382	0.15	0.0032509	4.29E+05	0.001026	301.28	5	95	0	52
7	'li-ti-bi'	0.72848	1.1188	1.06E+00	106.16	0.3	0.0074512	4.89E+07	0.099175	525.95	10	15	75	64
8	'li-ti-bi'	0.72746	1.1069	1.10E+00	58.599	0.3	0.0034207	5.17E+07	0.066176	432.36	10	10	80	64
9	'li-pb-zn'	0.72071	1.1864	1.064	46.659	0.75	0.0018175	3.59E+05	0.002189	444.35	25	60	15	52
10	'li-ti-bi'	0.71892	1.0925	1.1417	43.163	0.3	0.0022888	5.45E+07	0.033176	339.21	10	5	85	64
11	'li-pb-ba'	0.71496	1.0627	1.18E+00	39.104	0.3	0.001902	4.12E+05	0.001061	275.92	10	90	0	49
12	'li-pb-bi'	0.71496	1.0627	1.1754	39.104	0.3	0.001902	4.12E+05	0.001061	275.92	10	90	0	50
13	'li-pb-zn'	0.71496	1.0627	1.18E+00	39.104	0.3	0.001902	4.12E+05	0.001061	275.92	10	90	0	52
14	'li-ag-pb'	0.71493	1.0626	1.1682	39.104	0.3	0.001902	4.12E+05	0.001061	275.92	10	0	90	6
15	'li-zn-bi'	0.71488	1.1456	1.094	33.579	0.45	0.0013123	5.10E+07	0.000651	260.73	15	5	80	67
16	'li-zn-bi'	0.71428	1.1737	1.077	34.429	0.6	0.0012283	4.46E+07	0.001125	317.84	20	10	70	67
17	'li-na-bi'	0.71393	1.0761	1.0724	43.713	0.3	0.0024279	5.73E+07	0.11509	257.94	5	5	90	42
18	'li-in-pb'	0.71389	1.0606	1.12E+00	39.098	0.3	0.001902	4.12E+05	0.001061	275.92	10	0	90	35
19	'li-pb-bi'	0.71353	1.065	1.0207	43.428	0.15	0.0023996	4.15E+07	0.000386	190.85	5	30	65	50
20	'li-pb-bi'	0.71326	1.0632	1.166	41.693	0.3	0.0021292	3.57E+06	0.001012	310.35	10	85	5	50
21	'li-ga-pb'	0.71323	1.0593	1.09E+00	39.095	0.3	0.001902	4.12E+05	0.001061	275.92	10	0	90	25
22	'li-pb-zn'	0.71295	1.1313	1.1704	33.524	0.6	0.0011554	3.78E+05	0.001473	296.56	20	75	5	52
23	'li-pb-bi'	0.71207	1.0636	1.1622	40.822	0.3	0.0020624	6.73E+06	0.000963	300.81	10	80	10	50
24	'li-pb-bi'	0.71196	1.0658	1.02E+00	44.074	0.15	0.0024937	4.47E+07	0.000337	205.96	5	25	70	50
25	'li-pb-bi'	0.71086	1.0639	1.16E+00	39.593	0.3	0.0019613	9.90E+06	0.000914	285.21	10	75	15	50
26	'li-pb-bi'	0.71017	1.0664	1.0264	44.91	0.15	0.0026064	4.78E+07	0.000288	222.68	5	20	75	50
27	'li-pb-bi'	0.70991	1.0647	1.16E+00	38.484	0.3	0.0018637	1.31E+07	0.000864	268.56	10	70	20	50
28	'li-pb-bi'	0.70857	1.0649	1.1583	37.615	0.3	0.0017819	1.62E+07	0.000815	253.15	10	65	25	50
29	'li-ti-bi'	0.70856	1.1038	1.2022	54.194	0.45	0.0028205	4.85E+07	0.06626	448.31	15	10	75	64
30	'li-pb-bi'	0.70846	1.0674	1.03E+00	45.882	0.15	0.0027285	5.10E+07	0.000239	239.26	5	15	80	50
31	'li-pb-zn'	0.7078	1.1598	1.14E+00	39.316	0.75	0.001365	3.60E+05	0.001849	390.08	25	65	10	52
32	'li-pb-bi'	0.70757	1.0658	1.1582	36.73	0.3	0.0016897	1.94E+07	0.000766	234.05	10	60	30	50
33	'li-ti-bi'	0.70703	1.1133	1.17E+00	109.67	0.45	0.0080505	4.57E+07	0.09926	548.37	15	15	70	64
34	'li-pb-bi'	0.70657	1.0683	1.0336	46.891	0.15	0.0028483	5.42E+07	0.00019	254.14	5	10	85	50
35	'li-zn-bi'	0.70647	1.1895	1.0712	36.768	0.75	0.0012196	3.83E+07	0.001599	367.37	25	15	60	67
36	'li-pb-bi'	0.70639	1.0664	1.16E+00	36.032	0.3	0.0016093	2.25E+07	0.000717	215.56	10	55	35	50
37	'li-pb-zn'	0.70505	1.1959	1.0604	56.818	0.9	0.0024433	3.42E+05	0.002565	501.9	30	50	20	52
38	'li-pb-bi'	0.70498	1.0666	1.16E+00	35.502	0.3	0.0015425	2.57E+07	0.000668	198.68	10	50	40	50
39	'li-pb-ba'	0.70472	1.1226	1.05E+00	33.67	0.6	0.0012975	6.34E+06	0.001061	254.13	15	80	5	49
40	'li-pb-bi'	0.70447	1.0693	1.04E+00	47.755	0.15	0.0029483	5.73E+07	0.000141	265.58	5	5	90	50
41	'li-pb-bi'	0.70379	1.0674	1.1609	35.107	0.3	0.0014895	2.89E+07	6.19E-04	184.18	10	45	45	50
42	'li-pb-bi'	0.7025	1.068	1.1628	34.774	0.3	0.0014424	3.20E+07	5.69E-04	170.39	10	40	50	50
43	'li-sr-bi'	0.70225	1.1247	1.0474	43.253	0.5	0.0023232	5.22E+07	3.78E-03	341.96	10	10	80	58
44	'li-ag-bi'	0.70207	1.0702	1.0422	47.26	0.15	0.0029097	6.05E+07	9.16E-05	260.86	5	0	95	2
45	'li-ba-bi'	0.70207	1.0702	1.04E+00	47.26	0.15	0.0029097	6.05E+07	9.16E-05	260.86	5	0	95	12
46	'li-cu-bi'	0.70207	1.0702	1.0422	47.26	0.15	0.0029097	6.05E+07	9.16E-05	260.86	5	0	95	15
47	'li-ga-bi'	0.70207	1.0702	1.0422	47.26	0.15	0.0029097	6.05E+07	9.16E-05	260.86	5	0	95	21
48	'li-in-bi'	0.70207	1.0702	1.0422	47.26	0.15	0.0029097	6.05E+07	9.16E-05	260.86	5	0	95	32
49	'li-na-bi'	0.70207	1.0702	1.0422	47.26	0.15	0.0029097	6.05E+07	9.16E-05	260.86	5	0	95	42
50	'li-pb-bi'	0.70207	1.0702	1.0422	47.26	0.15	0.0029097	6.05E+07	9.16E-05	260.86	5	0	95	50

Table 5 shows results in the absence of bismuth. Here other alloys begin to surface such as 10Li-10Na-20Pb, but for the most part, Li-Pb-Zn still dominates the scene of alloys. 25Li-60Pb-15Zn is most likely one of the top candidates, with high gain (1.186), moderate TBR (1.064), and a hypothesized acceptable melting point of 444C, this alloy has low lithium content and lower lead content that the traditional 17Li-83Pb. It is interesting that the top performing alloy is not Li-Pb, but a ternary Li-Pb-Zn with composition very close to that of the chosen MFE community.

Table 5: Merit Function Results, No Bismuth

Rank	Mixture Name	MeritFxn	Gain	TBR	Tritium Inventory	Reactivity	Power Handling	Cost Per Volume	Availability	Melt C	Acomp	Bcomp	Ccomp	MixInd
1	'li-pb-zn'	0.7364	1.14	1.08	28.628	0.45	0.001419	3.95E+05	0.00144	288	15	80	5	52
2	'li-pb-zn'	0.7328	1.17	1.07	32.25	0.6	0.0015107	3.77E+05	0.00181	372	20	70	10	52
3	'li-ag-pb'	0.7323	1.06	1.02	29.889	0.15	0.0032509	4.29E+05	0.00103	301	5	0	95	6
4	'li-pb-ba'	0.7323	1.06	1.03	29.889	0.15	0.0032509	4.29E+05	0.00103	301	5	95	0	49
5	'li-pb-zn'	0.7323	1.06	1.03	29.889	0.15	0.0032509	4.29E+05	0.00103	301	5	95	0	52
6	'li-pb-zn'	0.7219	1.19	1.06	37.796	0.75	0.0018175	3.59E+05	0.00219	444	25	60	15	52
7	'li-pb-ba'	0.7163	1.06	1.18	28.55	0.3	0.001902	4.12E+05	0.00106	276	10	90	0	49
8	'li-pb-zn'	0.7163	1.06	1.18	28.55	0.3	0.001902	4.12E+05	0.00106	276	10	90	0	52
9	'li-ag-pb'	0.7163	1.06	1.17	28.55	0.3	0.001902	4.12E+05	0.00106	276	10	0	90	6
10	'li-in-pb'	0.7153	1.06	1.12	28.55	0.3	0.001902	4.12E+05	0.00106	276	10	0	90	35
11	'li-ga-pb'	0.7146	1.06	1.09	28.55	0.3	0.001902	4.12E+05	0.00106	276	10	0	90	25
12	'li-pb-zn'	0.7134	1.13	1.17	28.741	0.6	0.0011554	3.78E+05	0.00147	297	20	75	5	52
13	'li-pb-zn'	0.7085	1.16	1.14	33.342	0.75	0.001365	3.60E+05	0.00185	390	25	65	10	52
14	'li-pb-zn'	0.7069	1.20	1.06	43.801	0.9	0.0024433	3.42E+05	0.00257	502	30	50	20	52
15	'li-pb-ba'	0.7054	1.12	1.05	27.847	0.6	0.0012975	6.34E+06	0.00106	254	15	80	5	49
16	'li-pb-ba'	0.6998	1.07	1.26	27.752	0.45	0.0012828	3.96E+05	0.0011	248	15	85	0	49
17	'li-pb-zn'	0.6998	1.07	1.26	27.752	0.45	0.0012828	3.96E+05	0.0011	248	15	85	0	52
18	'li-ag-pb'	0.6998	1.07	1.26	27.752	0.45	0.0012828	3.96E+05	0.0011	248	15	0	85	6
19	'li-in-pb'	0.6982	1.06	1.21	27.752	0.45	0.0012828	3.96E+05	0.0011	248	15	0	85	35
20	'li-pb-zn'	0.6973	1.18	1.13	39.041	0.9	0.0017174	3.43E+05	0.00222	459	30	55	15	52
21	'li-ga-pb'	0.6972	1.06	1.19	27.752	0.45	0.0012828	3.96E+05	0.0011	248	15	0	85	25
22	'li-na-pb'	0.6971	1.06	1.04	28.663	0.6	0.0015933	3.80E+05	0.23096	287	10	10	80	44
23	'li-na-pb'	0.6922	1.06	1.08	27.89	0.6	0.0012188	3.79E+05	0.11605	259	15	5	80	44
24	'li-pb-sn'	0.6918	1.01	1.14	28.55	0.3	0.001902	4.12E+05	0.00106	276	10	90	0	51
25	'li-pb-zn'	0.6913	1.13	1.24	29.839	0.75	0.0010689	3.62E+05	0.00151	328	25	70	5	52
26	'li-na-pb'	0.6908	1.05	1.03	27.752	0.45	0.0012828	3.96E+05	0.0011	248	15	0	85	44
27	'li-sr-pb'	0.6908	1.05	1.03	27.752	0.45	0.0012828	3.96E+05	0.0011	248	15	0	85	60
28	'li-pb-zn'	0.6892	1.20	1.05	49.741	1.05	0.0038095	3.24E+05	0.00294	545	35	40	25	52
29	'li-sr-pb'	0.6891	1.07	1.04	28.082	0.55	0.0013354	9.84E+05	0.00285	266	15	5	80	60
30	'li-pb-sn'	0.6875	1.08	1.05	28.846	0.6	0.0011796	4.03E+05	0.00109	300	20	75	5	51
31	'li-sr-pb'	0.6857	1.08	1.04	28.615	0.65	0.0014093	1.57E+06	0.0046	288	15	10	75	60
32	'li-pb-zn'	0.6853	1.15	1.20	34.881	0.9	0.0013047	3.44E+05	0.00188	412	30	60	10	52
33	'li-ga-pb'	0.6834	1.11	1.07	29.725	0.75	0.0010596	1.07E+06	0.00121	326	25	5	70	25
34	'li-pb-ba'	0.683	1.12	1.16	27.959	0.75	0.0010631	6.32E+06	0.0011	267	20	75	5	49
35	'li-pb-ba'	0.6828	1.07	1.33	27.759	0.6	0.0010354	3.79E+05	0.00113	256	20	80	0	49
36	'li-pb-zn'	0.6828	1.07	1.33	27.759	0.6	0.0010354	3.79E+05	0.00113	256	20	80	0	52
37	'li-ag-pb'	0.6827	1.07	1.33	27.759	0.6	0.0010354	3.79E+05	0.00113	256	20	0	80	6
38	'li-na-pb'	0.6825	1.07	1.08	28.548	0.75	0.0014474	3.63E+05	0.34591	285	10	15	75	44
39	'li-pb-zn'	0.6824	1.19	1.11	45.04	1.05	0.0024264	3.25E+05	0.0026	514	35	45	20	52
40	'li-sr-pb'	0.6817	1.10	1.03	29.523	0.75	0.0015224	2.16E+06	0.00635	315	15	15	70	60
41	'li-in-pb'	0.6808	1.07	1.28	27.759	0.6	0.0010354	3.79E+05	1.13E-03	256	20	0	80	35
42	'li-ga-pb'	0.6799	1.07	1.25	27.759	0.6	0.0010354	3.79E+05	1.13E-03	256	20	0	80	25
43	'li-na-pb'	0.6787	1.06	1.12	27.909	0.75	0.0011403	3.63E+05	2.31E-01	262	15	10	75	44
44	'li-pb-ba'	0.6758	1.15	1.05	29.345	0.9	0.0012331	1.23E+07	1.06E-03	314	20	70	10	49
45	'li-pb-sn'	0.6753	1.02	1.23	27.752	0.45	0.0012828	3.96E+05	1.10E-03	248	15	85	0	51
46	'li-na-pb'	0.6737	1.06	1.13	28.03	0.75	0.0010145	3.63E+05	1.16E-01	271	20	5	75	44
47	'li-pb-zn'	0.6737	1.17	1.18	40.641	1.05	0.0017068	3.26E+05	2.26E-03	476	35	50	15	52
48	'li-na-pb'	0.672	1.05	1.08	27.759	0.6	0.0010354	3.79E+05	1.13E-03	256	20	0	80	44
49	'li-sr-pb'	0.672	1.05	1.08	27.759	0.6	0.0010354	3.79E+05	1.13E-03	256	20	0	80	60
50	'li-pb-zn'	0.6705	1.20	1.04	50.152	1.2	0.0036598	3.06E+05	3.32E-03	550	40	30	30	52

Another interesting way of examining the results is to consider enrichment such as in **Error! Not a valid bookmark self-reference.**. Here, Sn-Zn binaries are the key players with very high gain up to 1.475. The idea here would be to add small amounts of enriched Li so as to not dilute the high gain Sn-Zn mixture and maintain high gain. These curves can be seen in more detail in Figure 2.

Table 6: Merit Function Results, No TBR Limit (for enrichment)

Rank	Mixture Name	MeritF	Gain	TBR	Tritium Invento	Reactivity	Power Handli	Cost Per Volum	Availability	MeltC	Acomp	Bcomp	Ccomp	MixInd
1	'li-sn-zn'	0.9618	1.4754	1.00E-05	60.093	0	0.003219	7.90E+05	0.002115	252.56	0	75	25	56
2	'li-sn-zn'	0.96164	1.476	1.00E-05	58.123	0	0.003113	8.14E+05	0.001736	228.43	0	80	20	56
3	'li-sn-zn'	0.96146	1.4742	1.00E-05	61.992	0	0.003304	7.65E+05	0.002494	272.24	0	70	30	56
4	'li-sn-zn'	0.96101	1.4759	1.00E-05	56.147	0	0.002984	8.39E+05	0.001357	198.84	0	85	15	56
5	'li-sn-zn'	0.96053	1.4718	2.00E-05	63.692	0	0.003362	7.41E+05	0.002873	287.84	0	65	35	56
6	'li-sn-zn'	0.95918	1.4688	2.00E-05	65.543	0	0.003421	7.16E+05	0.003252	302.45	0	60	40	56
7	'li-sn-zn'	0.95916	1.4751	0.00E+00	57.421	0	0.003152	8.63E+05	0.000978	206.33	0	90	10	56
8	'li-sn-zn'	0.95751	1.4653	2.00E-05	67.472	0	0.003478	6.91E+05	0.003631	315.8	0	55	45	56
9	'li-sn-zn'	0.95609	1.4732	0	59.132	0	0.003364	8.88E+05	0.000599	217.06	0	95	5	56
10	'li-sn-ti'	0.95601	1.4646	0	123.35	0	0.007944	1.23E+06	0.033209	442.46	0	95	5	55
11	'li-sn-zn'	0.95526	1.4607	3.00E-05	69.389	0	0.003526	6.67E+05	0.00401	327.66	0	50	50	56
12	'li-na-sn'	0.95341	1.4664	0	54.474	0.15	0.002931	8.73E+05	0.11521	229.69	0	5	95	45
13	'li-sn-zn'	0.95266	1.4555	3.00E-05	71.21	0	0.003564	6.42E+05	0.004389	337.91	0	45	55	56
14	'li-sn-zn'	0.95063	1.4705	0	61.598	0	0.003646	9.13E+05	0.00022	232.85	0	100	0	56
15	'li-ag-sn'	0.95001	1.4693	0	61.598	0	0.003646	9.13E+05	0.00022	232.85	0	0	100	8
16	'li-cu-sn'	0.95001	1.4693	0	61.598	0	0.003646	9.13E+05	0.00022	232.85	0	0	100	17
17	'li-ga-sn'	0.95001	1.4693	0	61.598	0	0.003646	9.13E+05	0.00022	232.85	0	0	100	27
18	'li-in-sn'	0.95001	1.4693	0.00E+00	61.598	0	0.003646	9.13E+05	0.00022	232.85	0	0	100	37
19	'li-na-sn'	0.95001	1.4693	0	61.598	0	0.003646	9.13E+05	0.00022	232.85	0	0	100	45
20	'li-sn-ba'	0.95001	1.4693	0	61.598	0	0.003646	9.13E+05	0.00022	232.85	0	100	0	53
21	'li-sn-bi'	0.95001	1.4693	0.00E+00	61.598	0	0.003646	9.13E+05	0.00022	232.85	0	100	0	54
22	'li-sn-ti'	0.95001	1.4693	0	61.598	0	0.003646	9.13E+05	0.00022	232.85	0	100	0	55
23	'li-sr-sn'	0.95001	1.4693	0	61.598	0	0.003646	9.13E+05	0.00022	232.85	0	0	100	61
24	'li-sn-zn'	0.94974	1.4496	3.00E-05	72.732	0	0.003578	6.18E+05	0.004768	345.97	0	40	60	56
25	'li-cu-sn'	0.94763	1.4611	0.00E+00	71.585	0	0.004353	8.93E+05	0.000549	303.86	0	5	95	17
26	'li-ga-sn'	0.94637	1.4596	0	59.349	0	0.003409	1.59E+06	0.000304	220.77	0	5	95	27
27	'li-sn-zn'	0.94626	1.4425	4.00E-05	74.065	0	0.003578	5.93E+05	0.005147	352.6	0	35	65	56
28	'li-sn-bi'	0.94439	1.461	0	60.886	0	0.003619	4.05E+06	0.000209	221.83	0	95	5	54
29	'li-ga-sn'	0.94251	1.4501	0	57.419	0	0.003201	2.27E+06	0.000388	209.52	0	10	90	27
30	'li-cu-sn'	0.94244	1.4536	0.00E+00	91.102	0	0.00558	8.74E+05	0.000878	377.22	0	10	90	17
31	'li-sn-zn'	0.94238	1.4347	4.00E-05	75.34	0	0.003572	5.69E+05	0.005526	358.46	0	30	70	56
32	'li-sn-bi'	0.93885	1.4529	0	60.363	0	0.003605	7.19E+06	0.000199	211.59	0	90	10	54
33	'li-sr-sn'	0.93863	1.4637	0.00E+00	83.271	0.1	0.005367	1.48E+06	0.002009	355.25	0	5	95	61
34	'li-sn-ti'	0.93823	1.446	0.1168	55.291	0.15	0.00313	1.19E+06	0.033283	367.86	5	90	5	55
35	'li-ga-sn'	0.93814	1.4401	0	55.671	0	0.00301	2.95E+06	0.000472	198.06	0	15	85	27
36	'li-sn-zn'	0.93804	1.4261	4.00E-05	76.641	0	0.003564	5.44E+05	0.005905	363.93	0	25	75	56
37	'li-cu-sn'	0.93528	1.4449	0	115.38	0	0.006999	8.55E+05	0.001207	428.51	0	15	85	17
38	'li-na-sn'	0.9349	1.4627	0.00E+00	53.227	0.3	0.002748	8.33E+05	0.2302	267.88	0	10	90	45
39	'li-ag-sn'	0.93474	1.4413	0.00E+00	61.949	0	0.003612	2.96E+06	0.000209	230.91	0	5	95	8
40	'li-sn-ti'	0.93428	1.459	0.00E+00	255.1	0	0.01604	1.55E+06	0.066198	526.76	0	90	10	55
41	'li-sn-zn'	0.93408	1.4543	0.11218	41.635	0.15	0.001953	7.74E+05	1.81E-03	244.94	5	75	20	56
42	'li-ga-sn'	0.93395	1.4307	0	54.15	0	0.002841	3.63E+06	5.56E-04	187.32	0	20	80	27
43	'li-sn-zn'	0.93386	1.4552	0.11337	40.458	0.15	0.001861	7.99E+05	1.43E-03	219.43	5	80	15	56
44	'li-sn-zn'	0.93375	1.4526	0.11116	42.803	0.15	0.00203	7.50E+05	2.19E-03	265.17	5	70	25	56
45	'li-sn-zn'	0.93334	1.4168	5.00E-05	78.097	0	0.003562	5.20E+05	6.28E-03	369.47	0	20	80	56
46	'li-sn-bi'	0.93318	1.4446	0	59.912	0	0.003592	1.03E+07	1.88E-04	201.12	0	85	15	54
47	'li-sn-zn'	0.933	1.4504	0.11042	44.02	0.15	0.0021	7.25E+05	2.57E-03	282.63	5	65	30	56
48	'li-sn-zn'	0.93261	1.4551	0.11512	40.655	0.15	0.001907	8.24E+05	1.05E-03	220.89	5	85	10	56
49	'li-sn-ti'	0.93211	1.4404	0.1182	90.452	0.15	0.005648	1.51E+06	6.63E-02	476.04	5	85	10	55
50	'li-sn-zn'	0.93179	1.4473	0.10988	45.284	0.15	0.002164	7.01E+05	2.95E-03	298.04	5	60	35	56

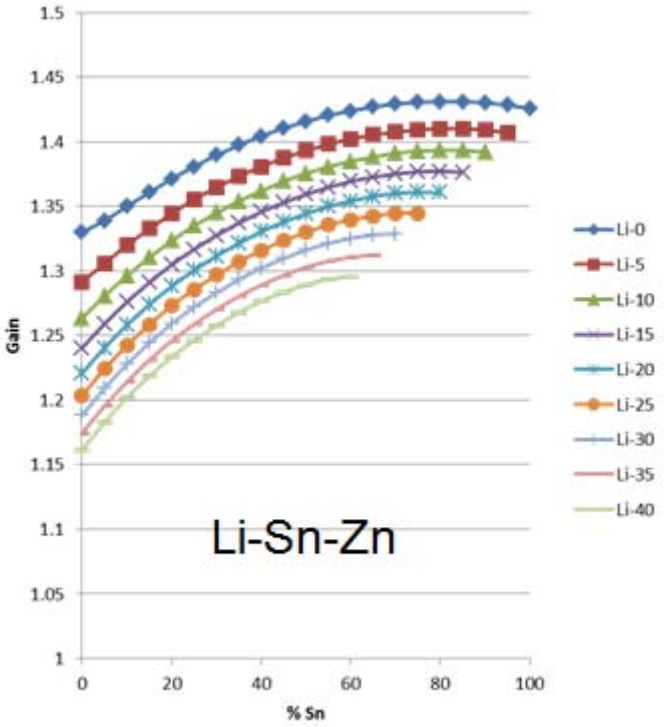

Figure 2: Lithium-Tin-Zinc Gain with minimal Lithium.

4 Conclusions

Lithium-Lead-Zinc alloys are some of the frontrunners in the ternary alloy selection. There is, however, little difference between the merit functions, and quite a wide spread of possible alloys that are competitive. Further analysis on waste stream, WDR, and activation would help to augment this list and down select options that are un-feasible due to negative effect. Lithium-Tin-Zinc alloys show great promise for use with enriched lithium to enable very high gain blankets with low chemical reactivity and low activation. In the absence of enrichment, and excluding Bismuth, Lithium-Lead-Zinc alloys show perhaps the most promise. It is worth noting that the reactivity scaling used in this exercise is merely a place holder to help ground the alloys in reality, however it is only a excerpt from MSDS sheets and contains very minimal data. Similarly the ternary interpolation on melt temperature is a “refined” estimate, and not a hard calculation. Therefore eliminating various alloys because of their performance in these metrics could be premature.

5 References

1. T. L. Saaty, "Decision Making with the Analytic Hierarchy Process," *Int. J. Services Sciences*, **1,** 83-98 (2008).

2. A. Jolodosky, M. Fratoni, W. Meier, J. DeMuth, S. Reyes, "Neutronic and Activation Analysis of Lithium-based Ternary Alloys in IFE Blankets," Submitted to *Fusion Engineering and Design* (2015).

3. F. P. Incropera, D. P. DeWitt, T. L. Bergman, A. S. Lavine, *Fundamentals of Heat and Mass Transfer*, John Wiley & Sons, ed. 6th (2007).

4. J. A. DeMuth *et al.*, "Equilibrium Chemistry Simulations for the LIFE Chamber," LLNL internal memo, 2012.

5. J. A. DeMuth, A. J. Simon, "LIFE Chamber Chemical Equilibrium Simulations with Additive Hydrogen, Oxygen, and Nitrogen BRIEF" (2009).

6. H. Katsuta, H. Iwamoto, H. Ohno, "Hydrogen Solubility In Liquid Li17Pb," *J. Nucl. Mater.* **133**, 167–170 (1985).

7. H. Katsuta, T. Ishigai, K. Furukawa, "Equilibrium Pressure and Solubility of Hydrogen in Liquid Lithium," *Nucl. Technol.* **32**, 297–303 (1977).

8. H. R. Ihle, C. H. Wu, in *Hydrogen In Metals* (Pergamon Press, Paris, France, 1977).

9. S. Kumar, A. Tirpude, N. Krishnamurthy, "Studies on the Solubility of Hydrogen in Molten Pb83Li17 Eutectic Alloy," *Int. J. Hydrogen Energy*, 1–6 (2013).

10. F. J. Smith, A. M. Batistoni, G. M. Begun, J. F. Land, "The Solubility of Hydrogen Isotopes in Lithium," EUR-5602, Commission of the European Communities (CEC) (1976).

11. G. G. Eichholz, W.J. Park, C.A Hazin, "Tritium Penetration Through Concrete," *Nuclear and Chemical and Waste Management*, **9** (1), 27-36 (1989).

12. E. Veleckis, "Thermodynamics of the Lithium-Lithium Deuteride System," *J. Phys. Chem.*, **81** (6), 526–531 (1977).

13. M. Dayah, Dynamic Periodic Table (2013), (available at http://www.ptable.com).

6 Appendix

6.1 Binary Phase Diagrams

6.1.1 Ag-Ba

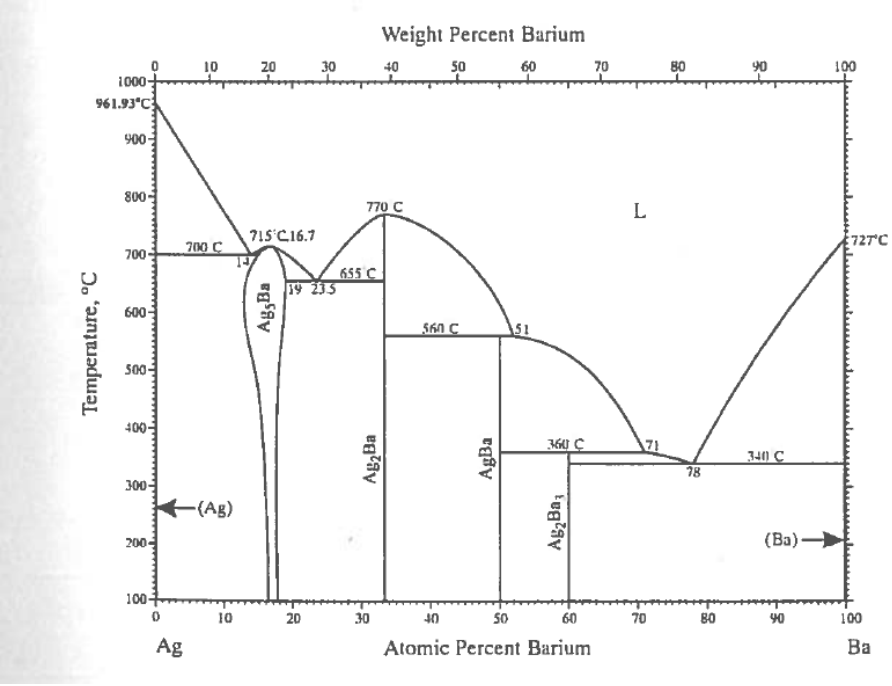

Ag-Ba

Ag-Ba

Phase	Composition, at.% Ba	Pearson symbol	Space group	Strukturbericht designation	Prototype
(Ag)	0	*cF*4	$Fm\bar{3}m$	*A*1	Cu
Ag_5Ba	13 to 19	*hP*6	*P*6/*mmm*	$D2_d$	$CaCu_5$
Ag_2Ba	33.3	*oI*12	*Imma*	…	$CeCu_2$
AgBa	50	*oP*8	*Pnma*	*B*27	FeB
Ag_2Ba_3	60	*hR*45	$R\bar{3}$	…	Er_3Ni_2
(Ba)	100	*cI*2	$Im\bar{3}m$	*A*2	W

H. Okamoto, *J. Phase Equilibria*, *13*(4), 434-435 (1992)

6.1.2 Ag-Bi

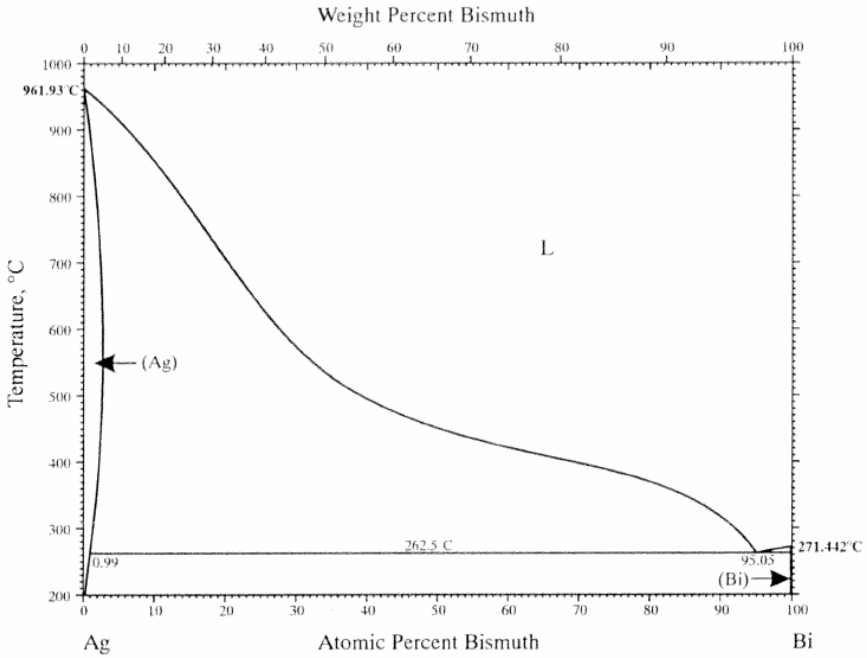

Ag-Bi

Phase	Composition, at.% Bi	Pearson symbol	Space group	Struktur-bericht designation	Prototype
(Ag)	0 to 2.76	*cF*4	$Fm\bar{3}m$	*A*1	Cu
(Bi)	100	*hR*2	$R\bar{3}m$	*A*7	αAs

I. Karakaya and W.T. Thompson, *J. Phase Equilibria*, *14*(4), 525-530 (1993)

6.1.3 Ag-Cd

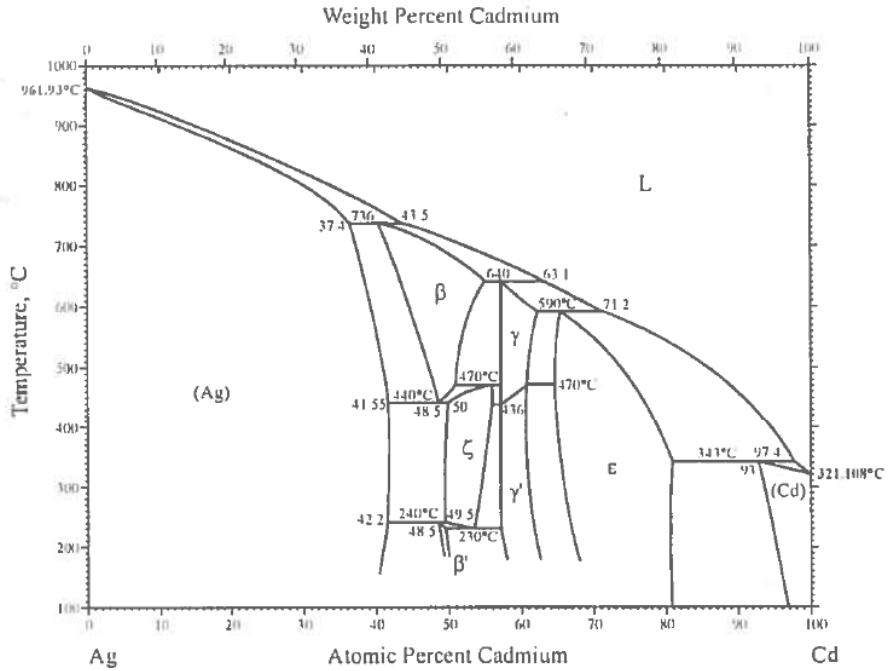

Ag-Cd

Ag-Cd

Phase	Composition, at.% Cd	Pearson symbol	Space group	Strukturbericht designation	Prototype
(Ag)	0 to 42.2	*cF*4	$Fm\bar{3}m$	*A*1	Cu
β	40 to 55	*cI*2	$Im\bar{3}m$	*A*2	W
β'	48.5 to 50	*cI**	...	...	...
ζ	49.5 to 56	*hP**	...	...	...
γ'	57 to 62.5	...	...	...	...
γ	57 to 62.5	*cI*52	$I\bar{4}3m$	$D8_2$	Cu_5Zn_8
ε	64.5 to 81	*hP*2	$P6_3/mmc$	*A*3	Mg
(Cd)	93 to 100	*hP*2	$P6_3/mmc$	*A*3	Mg

Binary Alloy Phase Diagrams, 2nd ed., T.B. Massalski, H. Okamoto, P.R. Subramanian, and L. Kacprzak, ed., ASM International, Materials Park, OH, 22-23 (1990)

6.1.4 Ag-Cu

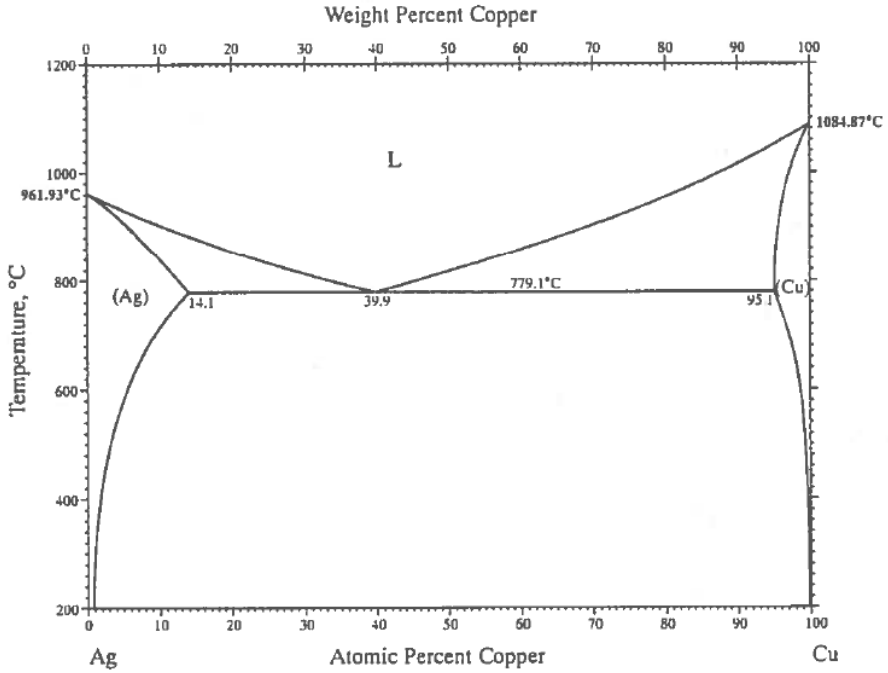

Ag-Cu

Phase	Composition, at.% Cu	Pearson symbol	Space group	Struktur-bericht designation	Prototype
(Ag)	0 to 14.1	*cF*4	$Fm\bar{3}m$	*A*1	Cu
(Cu)	95.1 to 100	*cF*4	$Fm\bar{3}m$	*A*1	Cu

P.R. Subramanian and J.H. Perepezko, *Phase Diagrams of Binary Copper Alloys*, ASM International, Materials Park, Ohio, 5-17 (1994)

6.1.5 Ag-Ga

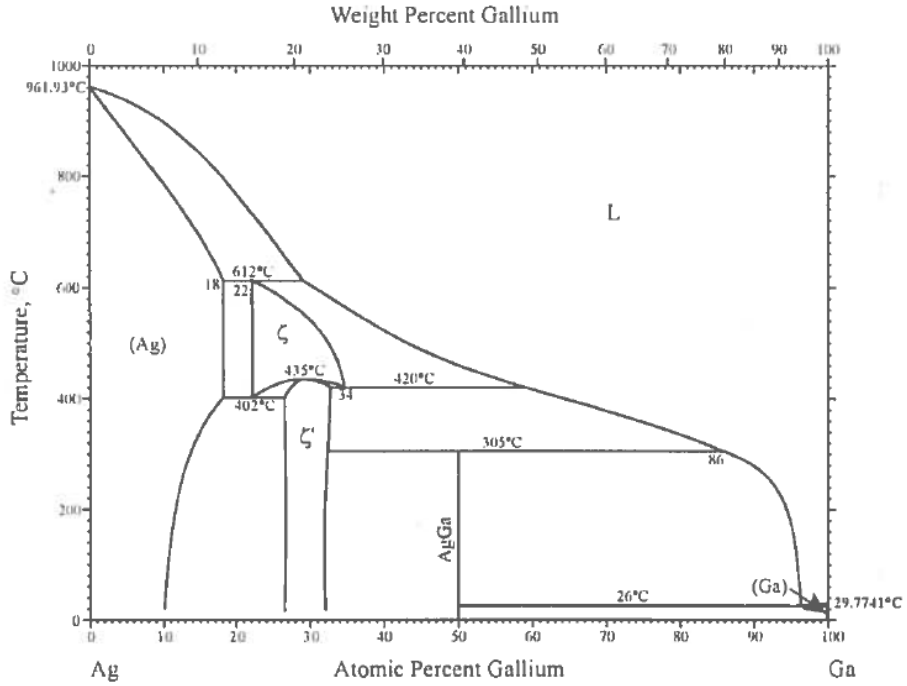

Ag-Ga

Ag-Ga

Phase	Composition, at.% Ga	Pearson symbol	Space group	Strukturbericht designation	Prototype
(Ag)	0 to 18	*cF*4	$Fm\bar{3}m$	*A*1	Cu
ζ	22 to 34	*hP*2	$P6_3/mmc$	*A*3	Mg
ζ'	26 to 33	*hP*9	$P\bar{3}$	B_b	ζAgZn
AgGa	50	*cI*2	$Im\bar{3}m$	*A*2	W
(Ga)	100	*oC*8	*Cmca*	*A*11	αGa

H. Okamoto, *J. Phase Equilibria*, *13*(3), 324-325 (1992)

6.1.6 Ag-Hg

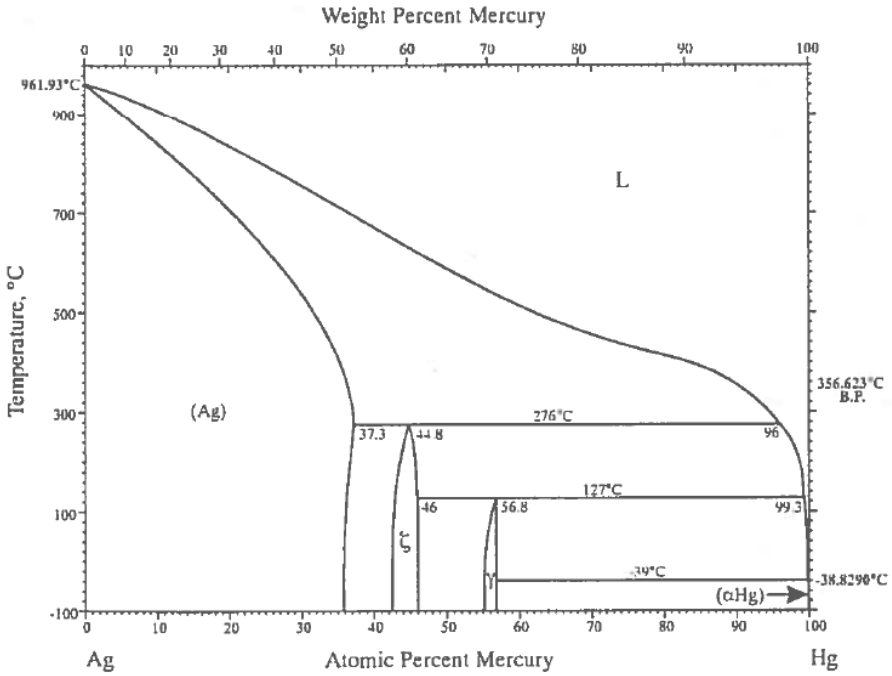

Ag-Hg

Ag-Hg

Phase	Composition, at.% Hg	Pearson symbol	Space group	Strukturbericht designation	Prototype
(Ag)	0 to 37.3	*cF*4	$Fm\bar{3}m$	*A*1	Cu
ζ	42.5 to 46.0	*hP*2	$P6_3/mmc$	*A*3	Mg
γ	55.1 to 56.8	*cI**	*I*23	…	…
(αHg)	100	*hR*1	$R\bar{3}m$	*A*10	αHg
(βHg)	100	*tI*2	*I*4/*mmm*	…	βHg

M.R. Baren, *J. Phase Equilibria*, *17*(2), 122-128 (1996)

6.1.7 Ag-In

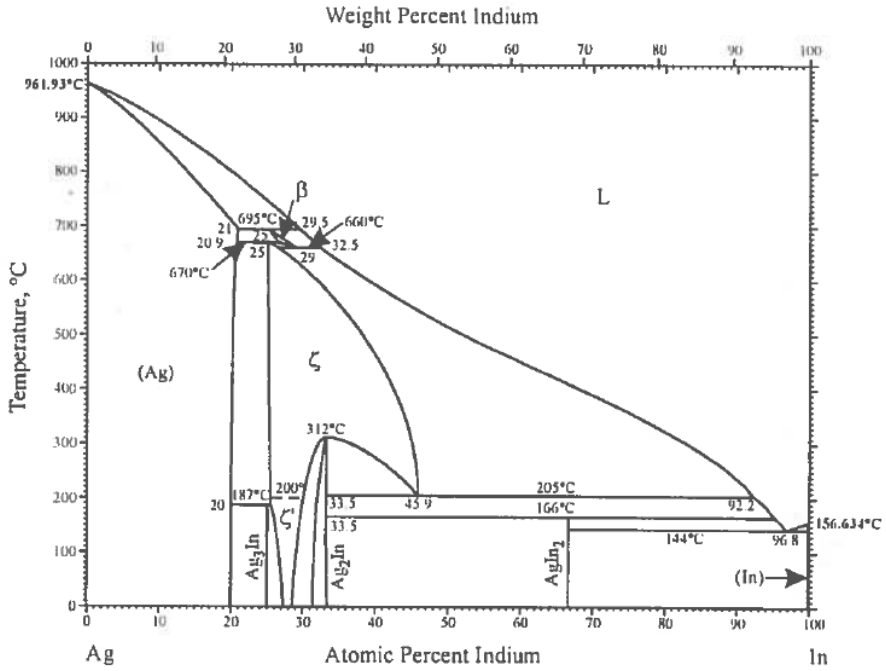

Ag-In

Ag-In

Phase	Composition, at.% In	Pearson symbol	Space group	Strukturbericht designation	Prototype
(Ag)	0 to 21	*cF*4	$Fm\bar{3}m$	*A*1	Cu
β	25 to 29	*cI*2	$Im\bar{3}m$	*A*2	W
Ag_3In	25	*cP*4	$Pm\bar{3}m$	$L1_2$	$AuCu_3$
ζ	25 to 45.9	*hP**	...	...	...
ζ'	?	*hP*8	$P6_3/mmc$	$D0_{19}$	Ni_3Sn
Ag_2In	31.1 to 33.6	*cP*52	$P\bar{4}3m$	$D8_3$	Cu_9Al_4
$AgIn_2$	66.7	*tI*12	*I*4/*mcm*	*C*15	$CuAl_2$
(In)	100	*tI*2	*I*4/*mmm*	*A*6	In

M.R. Baren, *Phase Diagrams of Indium Alloys and Their Engineering Applications*, C.E T. White and H. Okamoto, ed., ASM International, Materials Park, OH, 15-19 (1992)

6.1.8 Ag-Li

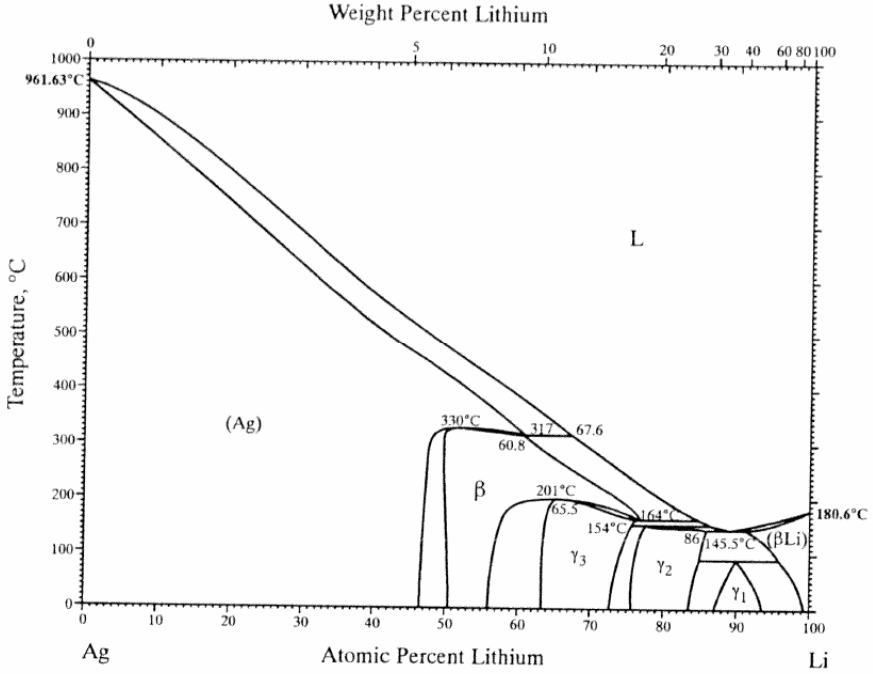

Ag-Li

Ag-Li

Phase	Composition, at.% Li	Pearson symbol	Space group	Struktur-bericht designation	Prototype
(Ag)	0 to 61	*cF*4	$Fm\bar{3}m$	*A*1	Cu
β	50 to 77	*cP*2	$Pm\bar{3}m$	*B*2	CsCl
γ_3	63.5 to 76	*cP*52?	$P\bar{4}3m$?	$D8_3$?	…
γ_2	76 to 86	*cI*52?	$I\bar{4}3m$?	$D8_2$?	…
γ_1	87 to 94	*c***	…	…	…
(βLi)	91 to 100	*cI*2	$Im\bar{3}m$	*A*2	W
(αLi)	100	*hP*2	$P6_3/mmc$	*A*3	Mg

A.D. Pelton, *Bull. Alloy Phase Diagrams*, 7(3), 223-228 (1986)

6.1.9 Ag-Na

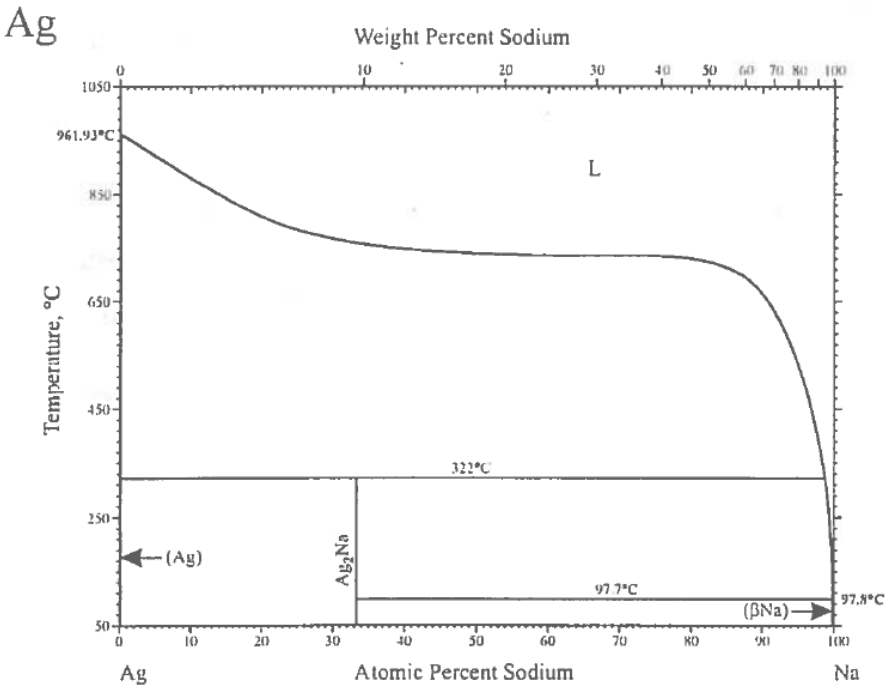

Ag-Na

Ag-Na

Phase	Composition, at.% Na	Pearson symbol	Space group	Struktur-bericht designation	Prototype
(Ag)	0	*cF*4	$Fm\bar{3}m$	*A*1	Cu
Ag_2Na	33.3	*cF*24	$Fd\bar{3}m$	*C*15	Cu_2Mg
(βNa)	100	*cI*2	$Im\bar{3}m$	*A*2	W

A. D. Pelton, *Bull. Alloy Phase Diagrams*, 7(2), 133-136 (1986)

6.1.10 Ag-Pb

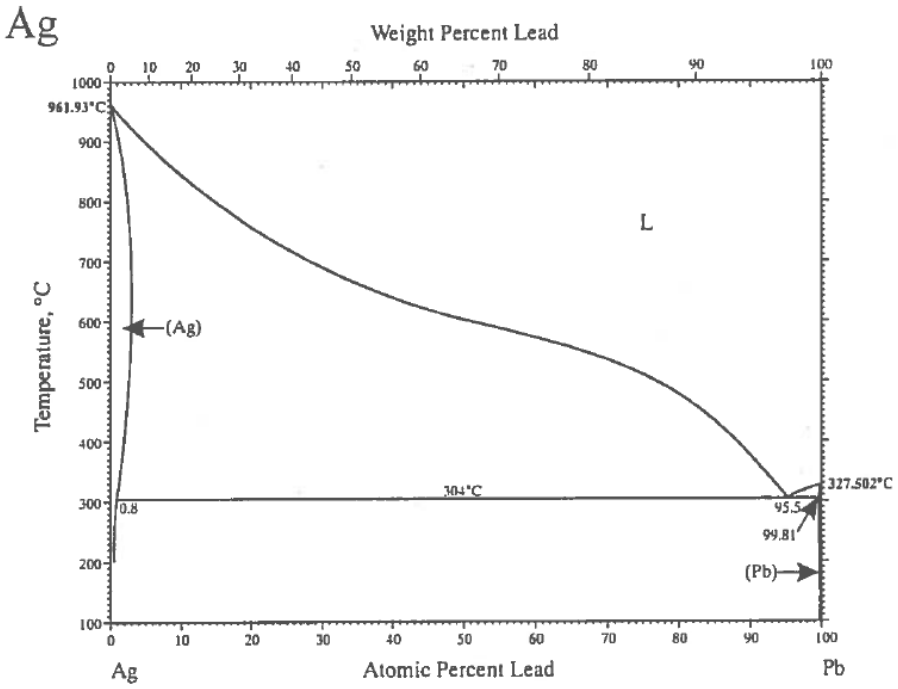

Ag-Pb

Phase	Composition, at.% Pb	Pearson symbol	Space group	Strukturbericht designation	Prototype
(Ag)	0 to 2.8	*cF*4	$Fm\bar{3}m$	*A*1	Cu
(Pb)	99.81 to 100	*cF*4	$Fm\bar{3}m$	*A*1	Cu

I. Karakaya and W.T. Thompson, *Bull. Alloy Phase Diagrams*, *8*(4), 326-334 (1987)

6.1.11 Ag-Sb

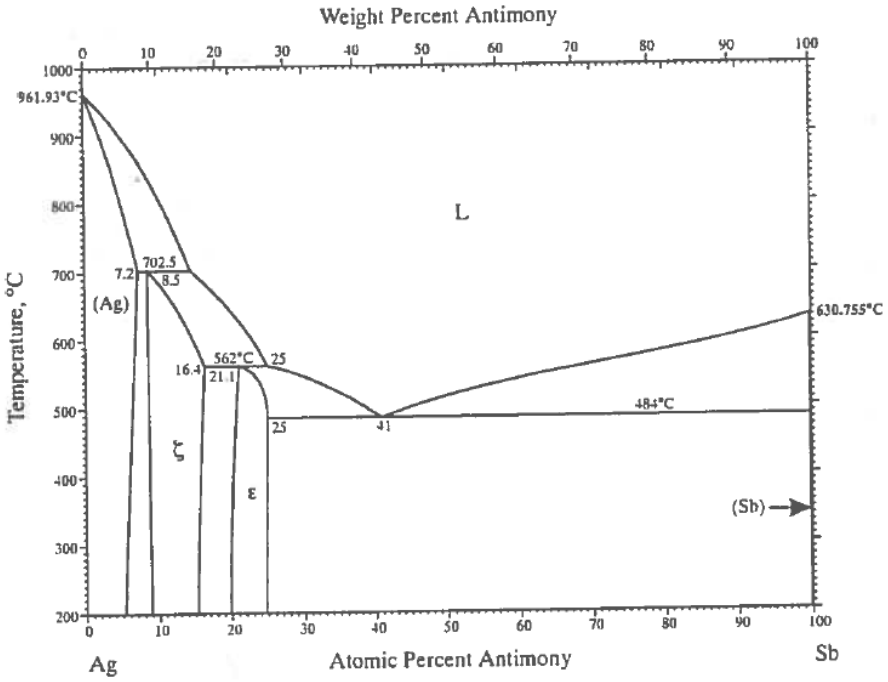

Ag-Sb

Ag-Sb

Phase	Composition, at.% Sb	Pearson symbol	Space group	Struktur-bericht designation	Prototype
(Ag)	0 to 7.2	*cF*4	$Fm\bar{3}m$	*A*1	Cu
ζ	8.5 to 16.4	*hP*2	$P6_3/mmc$	*A*3	Mg
ε	20 to 25	*tP*4	*P*4/*mmm*	$L6_0$	Cu_3Ti
(Sb)	100	*hR*2	$R\bar{3}m$	*A*7	αAs

H. Okamoto, *J. Phase Equilibria*, *14*(4), 531-532 (1993)

6.1.12 Ag-Sn

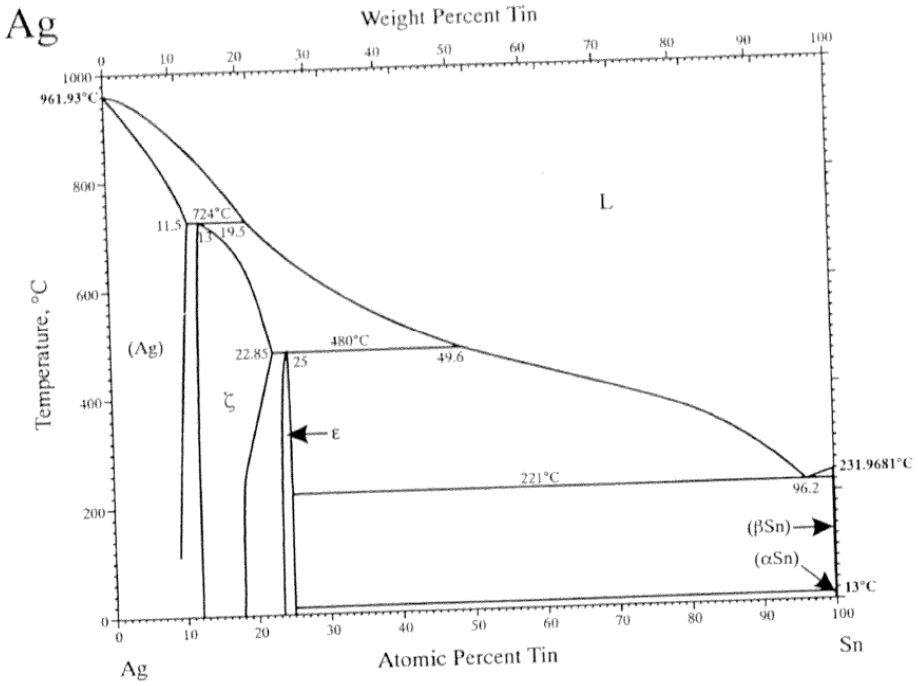

Ag-Sn

Ag-Sn

Phase	Composition, at.% Sn	Pearson symbol	Space group	Strukturbericht designation	Prototype
(Ag)	0 to 11.5	*cF*4	$Fm\bar{3}m$	*A*1	Cu
ζ	11.8 to 22.85	*hP*2	$P6_3/mmc$	*A*3	Mg
ε	23.2 to 25	*oP*8	*Pmmn*	$D0_a$	βCu_3Ti
(βSn)	99.91 to 100	*tI*4	$I4_1/amd$	*A*5	βSn
(αSn)	100	*cF*8	$Fd\bar{3}m$	*A*4	C (diamond)

I. Karakaya and W.T. Thompson, *Bull. Alloy Phase Diagrams*, *8*(4), 340-347 (1987)

6.1.13 Ag-Sr

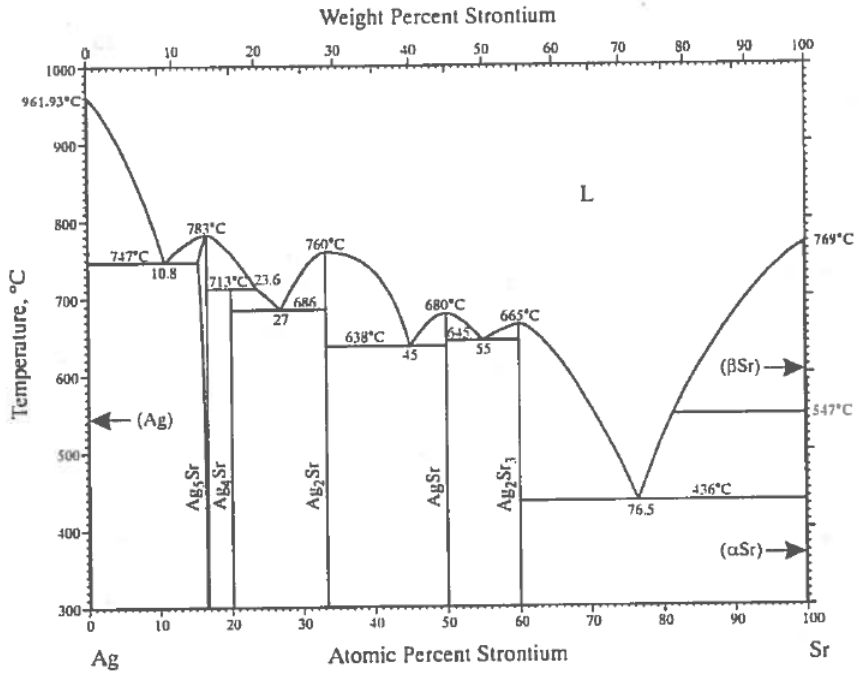

Ag-Sr

Ag-Sr

Phase	Composition, at.% Sr	Pearson symbol	Space group	Struktur-bericht designation	Prototype
(Ag)	0	*cF*4	$Fm\bar{3}m$	*A*1	Cu
Ag_5Sr	15.4 to 16.8	*hP*6	*P*6/*mmm*	$D2_d$	$CaCu_5$
Ag_4Sr	20	...	...	...	...
Ag_2Sr	33.3	*oI*12	*Imma*	...	$CeCu_2$
AgSr	50	*oP*8	*Pnma*	*B*27	FeB
Ag_2Sr_3	60	*hR*45	$R\bar{3}$	...	Er_3Ni_2
Ag_3Sr_7*	70	*hP*20	$P6_3mc$	$D10_2$	Fe_3Th_7
(βSr)	100	*cI*2	$Im\bar{3}m$	*A*2	W
(αSr)	100	*cF*4	$Fm\bar{3}m$	*A*1	Cu

* Not shown.

M.R. Baren, *Bull. Alloy Phase Diagrams*, *11*(2), 117-120 (1990)

6.1.14 Ag-Ti

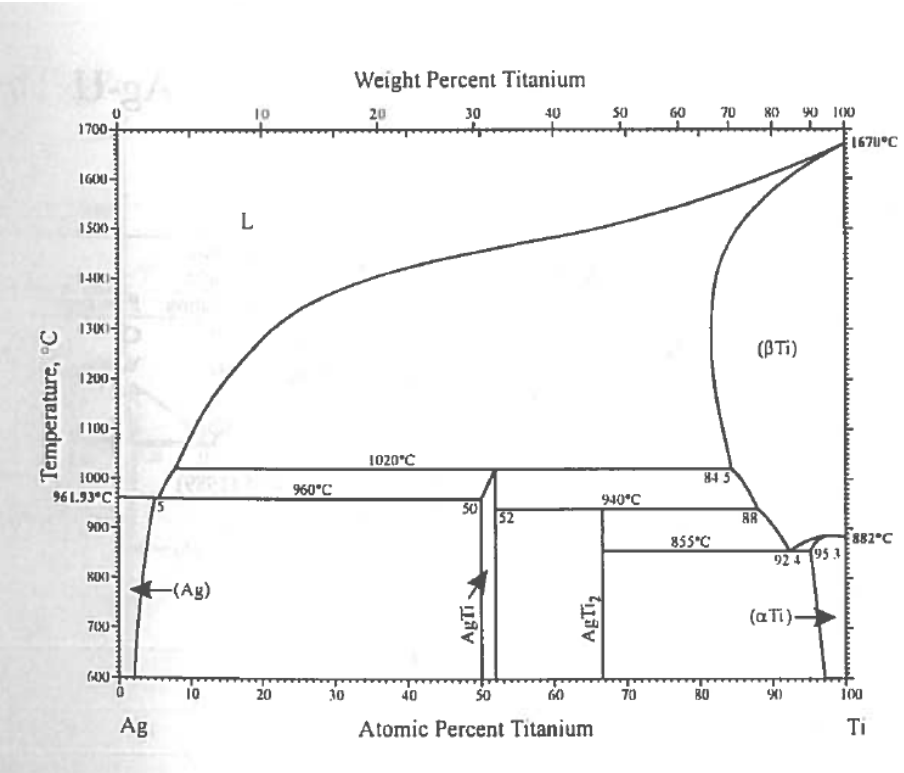

Ag-Ti

Ag-Ti

Phase	Composition, at.% Ti	Pearson symbol	Space group	Strukturbericht designation	Prototype
(Ag)	0 to 5	*cF*4	$Fm\bar{3}m$	*A*1	Cu
AgTi	50 to 52	*tP*4	*P*4/*nmm*	*B*11	CuTi
$AgTi_2$	66.7	*tI*6	*I*4/*mmm*	$C11_b$	$MoSi_2$
(βTi)	82 to 100	*cI*2	$Im\bar{3}m$	*A*2	W
(αTi)	95.3 to 100	*hP*2	$P6_3/mmc$	*A*3	Mg

J.L. Murray and K.J. Bansali, *Phase Diagrams of Binary Titanium Alloys*, J.L. Murray, ed., ASM International, Metals Park, OH, 178-183 (1987)

6.1.15 Ag-Zn

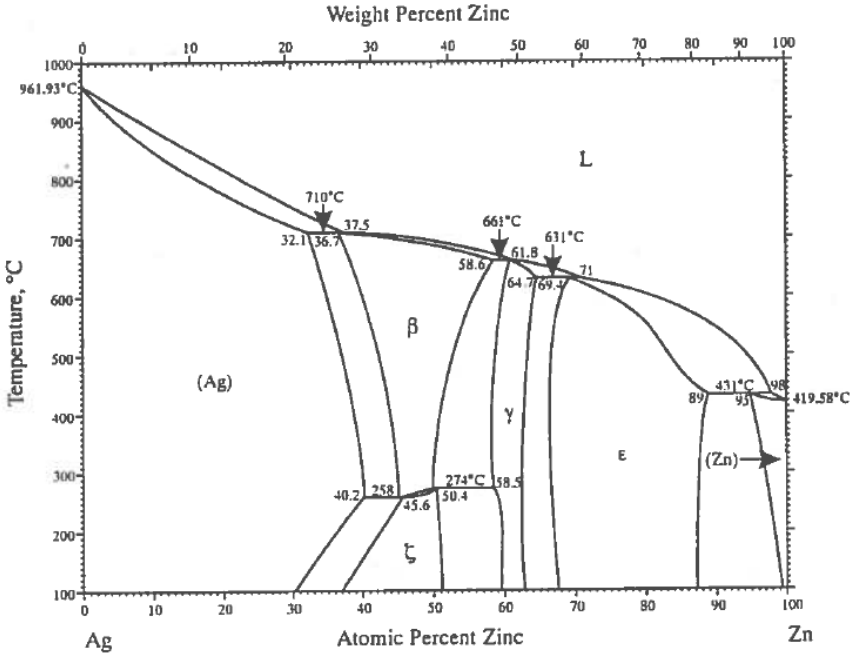

Ag-Zn

Ag-Zn

Phase	Composition, at.% Zn	Pearson symbol	Space group	Struktur-bericht designation	Prototype
(Ag)	0 to 40.2	*cF*4	$Fm\bar{3}m$	*A*1	Cu
ζ	37 to 51.2	*hP**	...	...	...
β	36.7 to 58.6	*cI*2	$Im\bar{3}m$	*A*2	W
γ	58 to 64.7	*cI*52	$I\bar{4}3m$	$D8_2$	Cu_5Zn_8
ε	66.2 to 89	*hP*2	$P6_3/mmc$	*A*3	Mg
(Zn)	95 to 100	*hP*2	$P6_3/mmc$	*A*3	Mg

Binary Alloy Phase Diagrams, 2nd ed., T.B. Massalski, H. Okamoto, P.R. Subramanian, and L. Kacprzak, ed., ASM International, Materials Park, OH, 117 (1990)

6.1.16 Ba-Bi

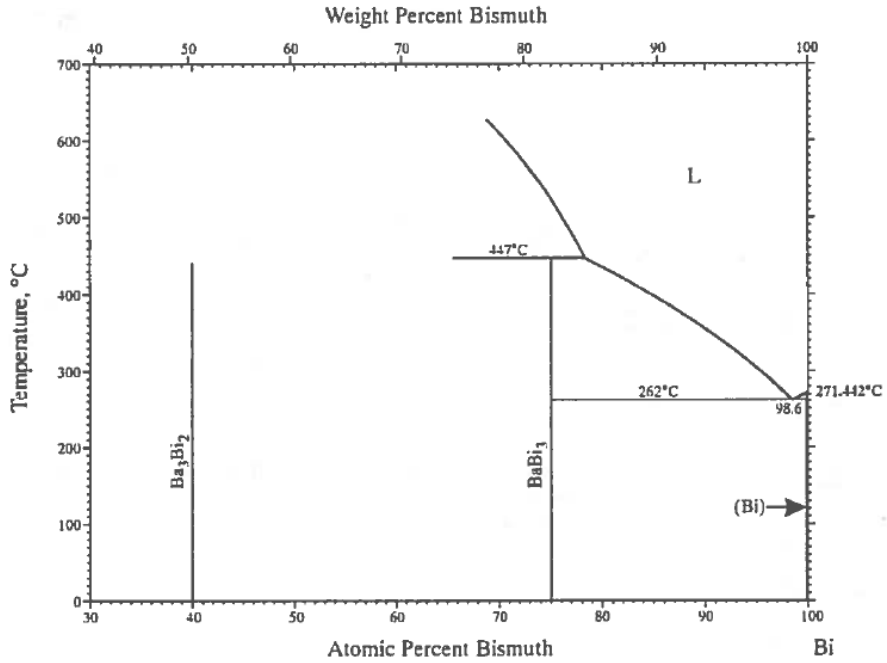

Ba-Bi

Ba-Bi

Phase	Composition, at.% Bi	Pearson symbol	Space group	Struktur-bericht designation	Prototype
Ba_3Bi_2	40	...	...	...	...
$BaBi_3$	75	*tP*4	*P*4/*mmm*	$L1_0$	AuCu
(Bi)	100	*hR*2	$R\bar{3}m$	*A*7	αAs

G. Grube and A. Dietrich, *Z. Elektrochem.*, *44*, 755-758 (1938)

6.1.17 Ba-Cd

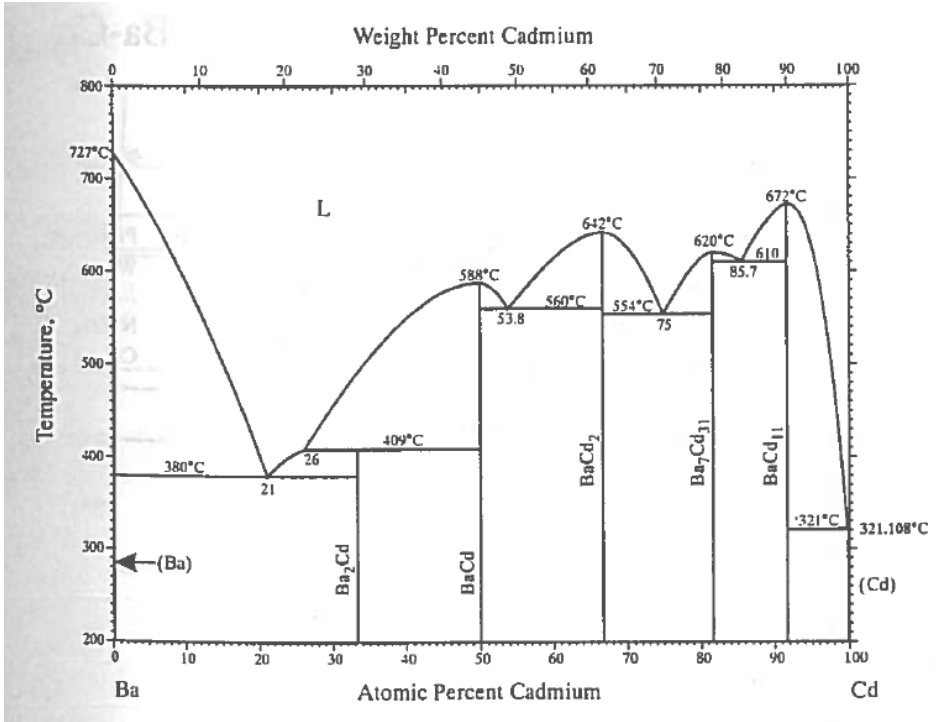

Ba-Cd

Ba-Cd

Phase	Composition, at.% Cd	Pearson symbol	Space group	Struktur-bericht designation	Prototype
(Ba)	0	*cI*2	$Im\bar{3}m$	*A*2	W
Ba_2Cd	33.3	*tI*6	*I*4/*mmm*	$C11_b$	$MoSi_2$
BaCd	50	*cP*2	$Pm\bar{3}m$	*B*2	CsCl
$BaCd_2$	66.7	*oI*12	*Imma*	...	...
Ba_7Cd_{31}	81.6	*hP*41	*P*6/*mmm*	...	...
$BaCd_{11}$	91.7	*tI*48	$I4_1/amd$	...	...
(Cd)	100	*hP*2	$P6_3/mmc$	*A*3	Mg

Binary Alloy Phase Diagrams, 2nd ed., T.B. Massalski, H. Okamoto, P.R. Subramanian, and L. Kacprzak, ed., ASM International, Materials Park, OH, 566, 568-569 (1990)

6.1.18 Ba-Cu

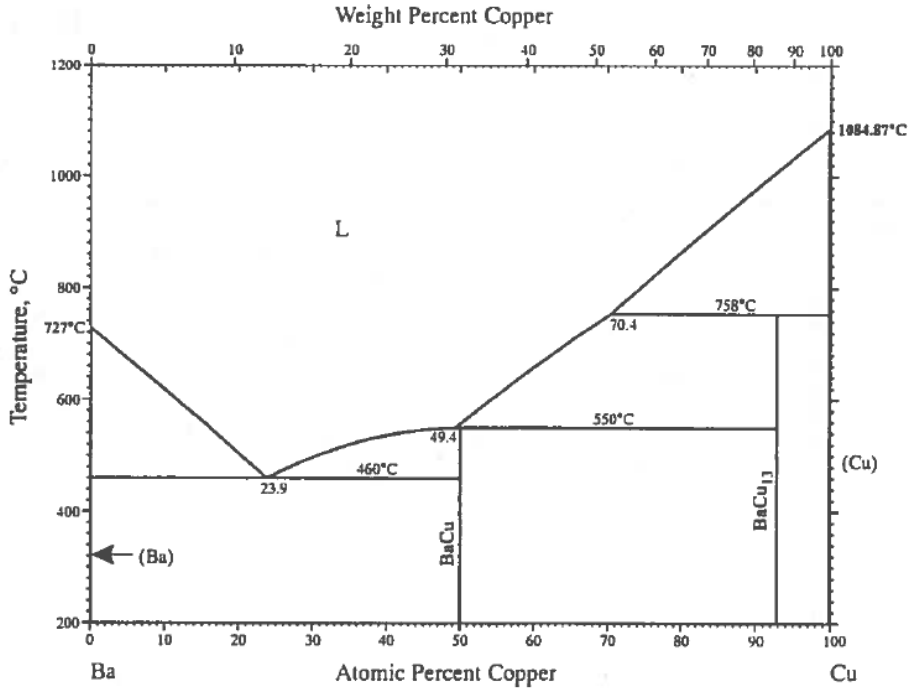

Ba-Cu

Ba-Cu

Phase	Composition, at.% Cu	Pearson symbol	Space group	Struktur-bericht designation	Prototype
(Ba)	0	*cI*2	$Im\bar{3}m$	*A*2	W
BaCu	50	*hP*8	$P6_3/mmc$	…	…
$BaCu_{13}$	92.9	*cF*112	$Fm\bar{3}c$	$D2_3$	$NaZn_{13}$
(Cu)	100	*cF*4	$Fm\bar{3}m$	*A*1	Cu

H. Okamoto, *J. Phase Equilibria*, *15*(5), 564-565 (1994)

6.1.19 Ba-Ga

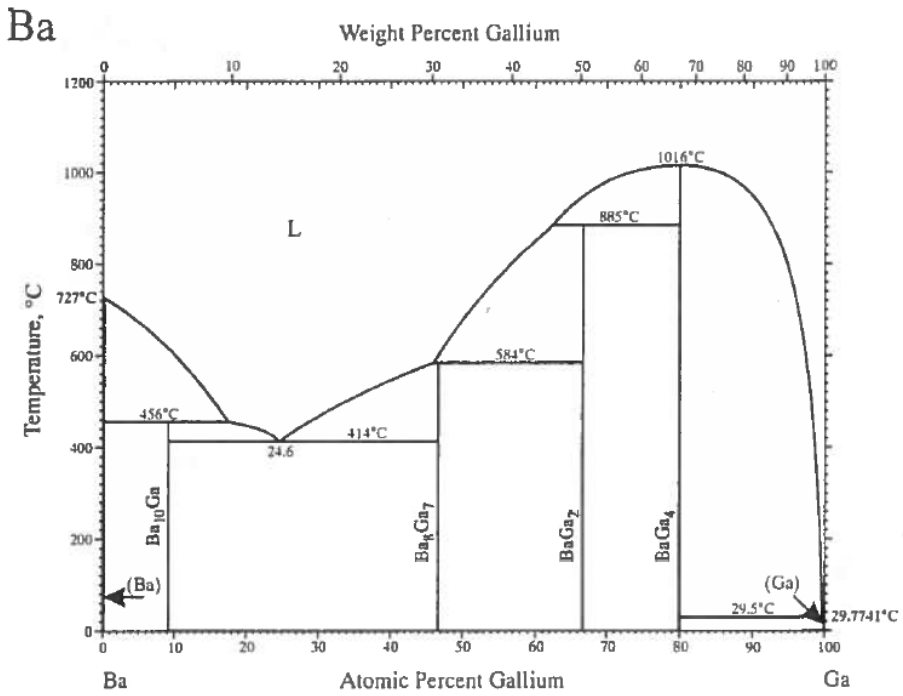

Ba-Ga

Ba-Ga

Phase	Composition, at.% Ga	Pearson symbol	Space group	Struktur-bericht designation	Prototype
(Ba)	0	*cI*2	$Im\bar{3}m$	*A*2	W
$Ba_{10}Ga$	9.1	*cF*176	$Fd\bar{3}m$	...	$Al_{10}V$
Ba_8Ga_7	46.7	*cP*60	$P2_13$	...	Al_7Sr_8
$BaGa_2$	66.7	*hP*3	*P6/mmm*	*C*32	AlB_2
$BaGa_4$	80	*tI*10	*I4/mmm*	$D1_3$	Al_2Ba
(Ga)	100	*oC*8	*Cmca*	*A*11	Ga

V.P. Itkin and C.B. Alcock, J. *Phase Equilibria*, *12*(5), 575-577 (1991)

6.1.20 Ba-Hg

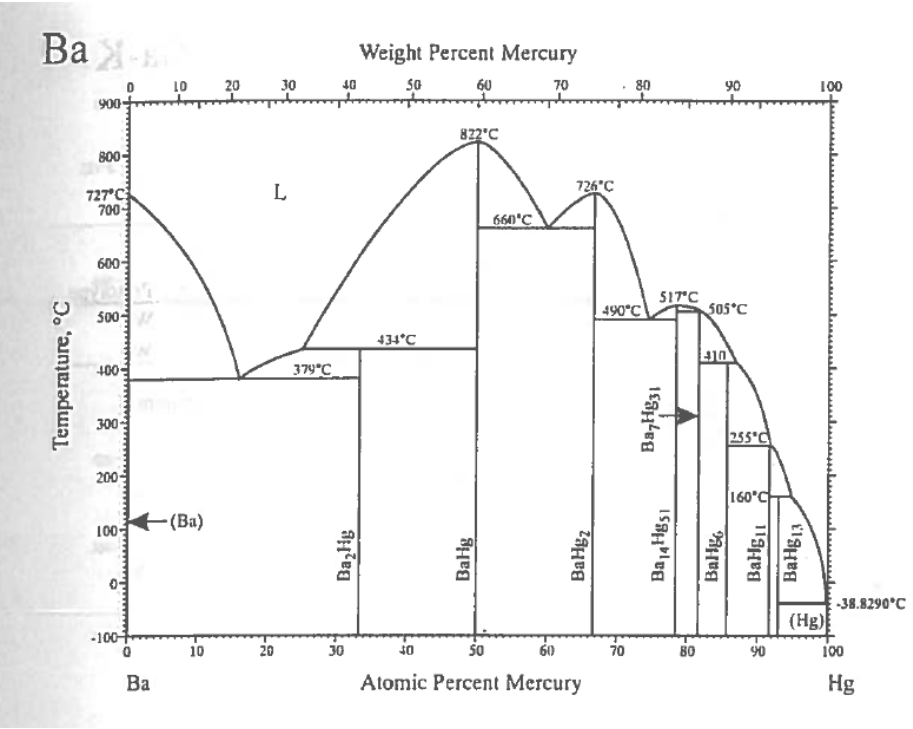

Ba-Hg

Ba-Hg

Phase	Composition, at.% Hg	Pearson symbol	Space group	Struktur-bericht designation	Prototype
(Ba)	0	*cI*2	*Im* $\bar{3}$*m*	*A*2	W
Ba_2Hg	33.3	*tI*6	*I*4/*mmm*	$C11_b$	$MoSi_2$
BaHg	50	*cP*2	*Pm* $\bar{3}$*m*	*B*2	CsCl
$BaHg_2$	66.7	*oI*12	*Imma*	…	$CeCu_2$
$Ba_{14}Hg_{51}$	78.5	*hP*65	…	…	…
Ba_7Hg_{31}	81.6	*hP*38	*P*6/*mmm*	…	Ba_7Cd_{31}
$BaHg_6$	85.7	…	…	…	…
$BaHg_{11}$	91.7	*cP*36	*Pm* $\bar{3}$*m*	$D2_c$	$BaHg_{11}$
$BaHg_{13}$	93	…	…	…	…
(Hg)	100	*hR*1	*R* $\bar{3}$*m*	*A*10	αHg

C. Guminski, *J. Phase Equilibria*, *21*(2), 173-178 (2000)

6.1.21 Ba-In

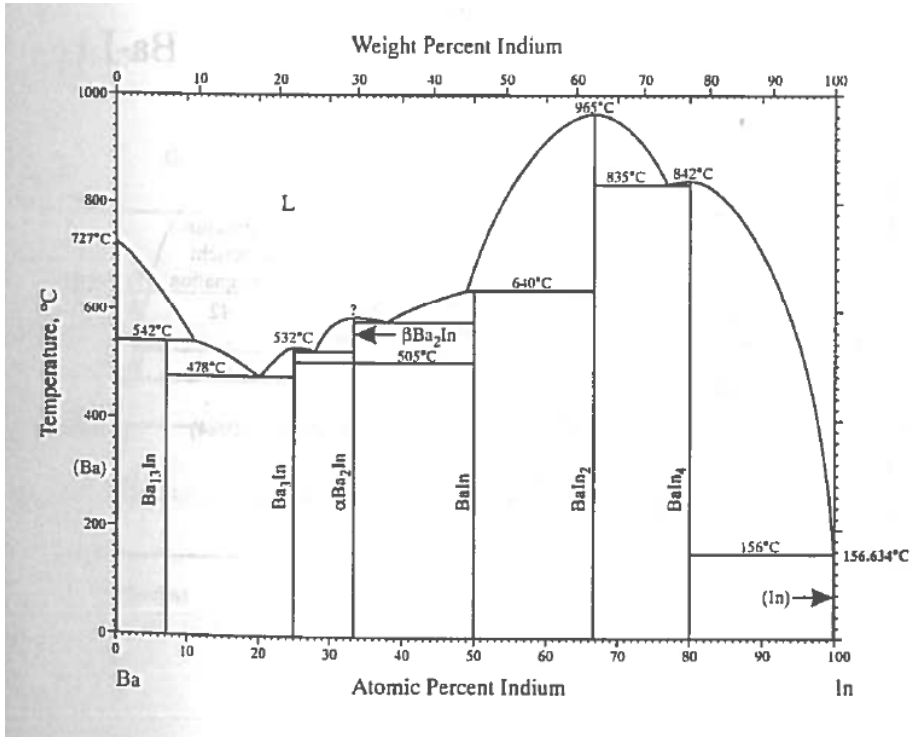

Ba-In

Ba-In

Phase	Composition, at.% In	Pearson symbol	Space group	Struktur-bericht designation	Prototype
(Ba)	0	*cI*2	*Im* $\bar{3}$*m*	*A*2	W
$Ba_{13}In$	7.1	...	...	...	...
Ba_3In	25	...	...	...	...
βBa_2In	33.3	...	...	...	...
αBa_2In	33.3	...	...	...	...
BaIn	50	...	...	...	...
$BaIn_2$	66.7	*oI*12	*Imma*	...	$CeCu_2$
$BaIn_4$	80	*tI*10	*I*4/*mmm*	$D1_3$	Al_4Ba
(In)	100	*tI*2	*I*4/*mmm*	*A*6	In

H. Okamoto, *Phase Diagrams of Indium Alloys and Their Engineering Applications*, C.E.T. White and H. Okamoto, ed., ASM International, Materials Park, OH, 42-43 (1992)

6.1.22 Ba-Li

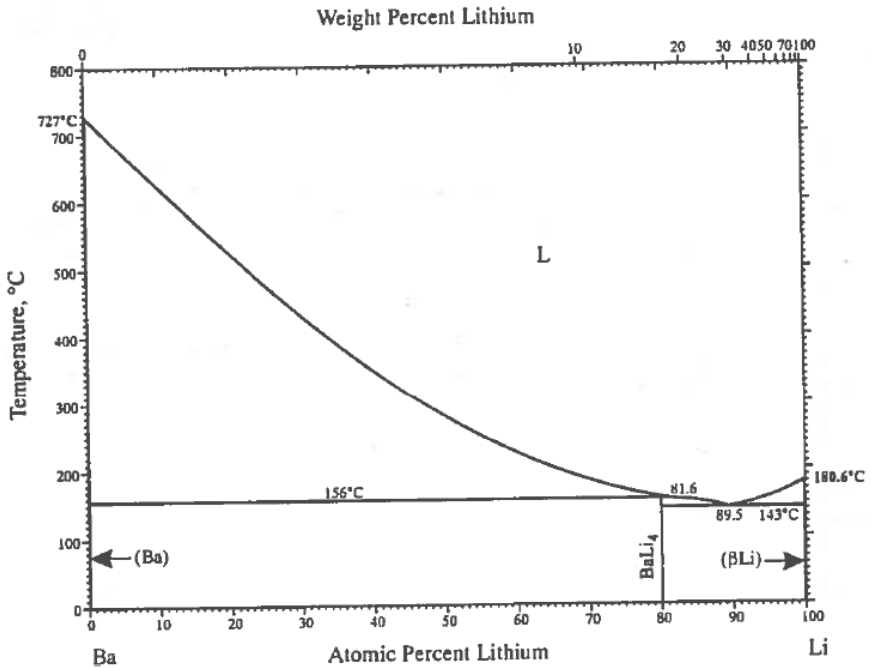

Ba-Li

Ba-Li

Phase	Composition, at.% Li	Pearson symbol	Space group	Struktur-bericht designation	Prototype
(Ba)	0	*cI*2	$Im\bar{3}m$	*A*2	W
$BaLi_4$	80	*hP*30	$P6_3/mmc$	...	...
(βLi)	100	*cI*2	$Im\bar{3}m$	*A*2	W

A.D. Pelton, *Bull. Alloy Phase Diagrams*, *5*(*5*), 452-454 (1984)

6.1.23 Ba-Na

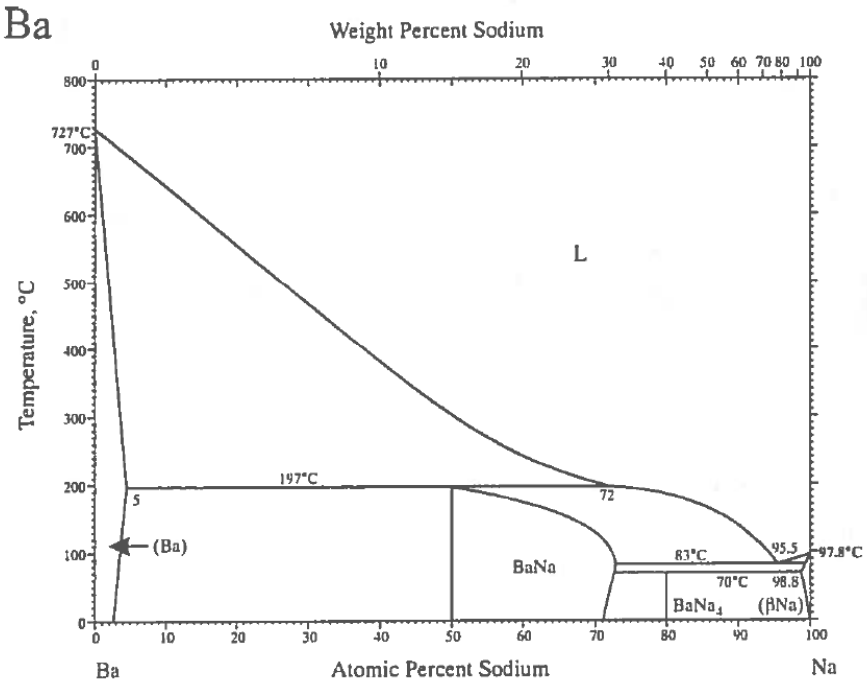

Ba-Na

Ba-Na

Phase	Composition, at.% Na	Pearson symbol	Space group	Struktur-bericht designation	Prototype
(Ba)	0 to 5	*cI*2	$Im\bar{3}m$	*A*2	W
BaNa	50 to 73	*t***	...	...	...
$BaNa_4$	80	*o***	...	...	...
(βNa)	98.8 to 100	*cI*2	$Im\bar{3}m$	*A*2	W

A.D. Pelton, *Bull. Alloy Phase Diagrams*, *6*(1), 26-29 (1985)

6.1.24 Ba-Pb

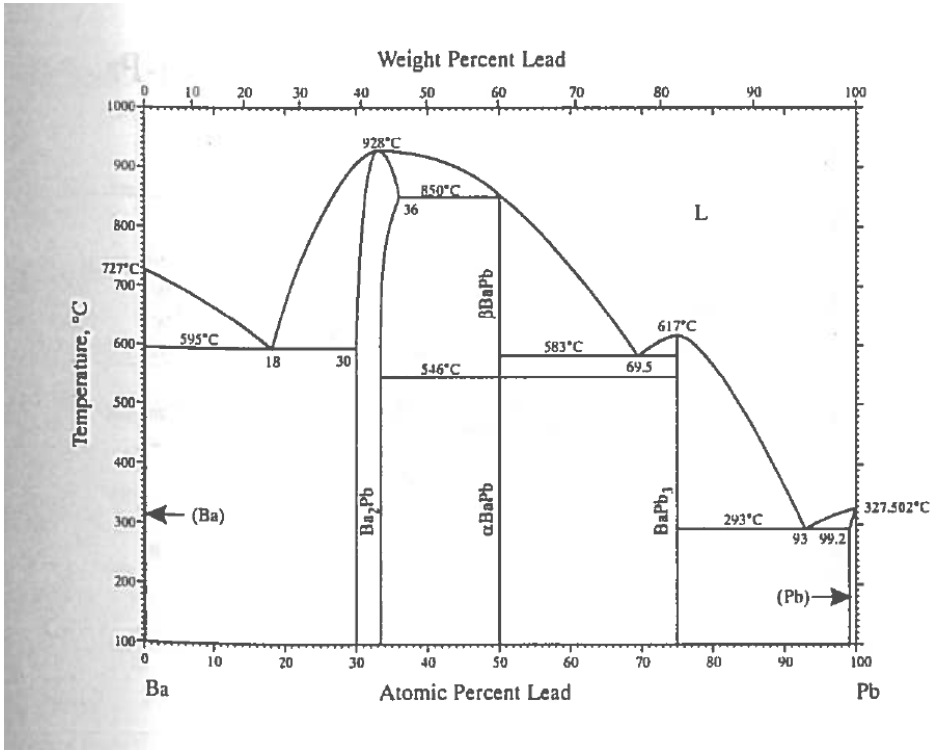

Ba-Pb

Ba-Pb

Phase	Composition, at.% Pb	Pearson symbol	Space group	Strukturbericht designation	Prototype
(Ba)	0	*cI*2	$Im\bar{3}m$	*A*2	W
Ba_2Pb	30 to 36	*oP*12	*Pnma*	*C*23	Co_2Si
βBaPb	50	...	...	...	...
αBaPb	50	*oC*8	*Cmcm*	B_f	CrB
$BaPb_3$	75	*hR*12	$R\bar{3}m$	...	...
(Pb)	99.2 to 100	*cF*4	$Fm\bar{3}m$	*A*1	Cu

G. Grube and A. Dietrich, *Z. Elektrochem.*, *44*, 755-767 (1938)

6.1.25 Ba-Sn

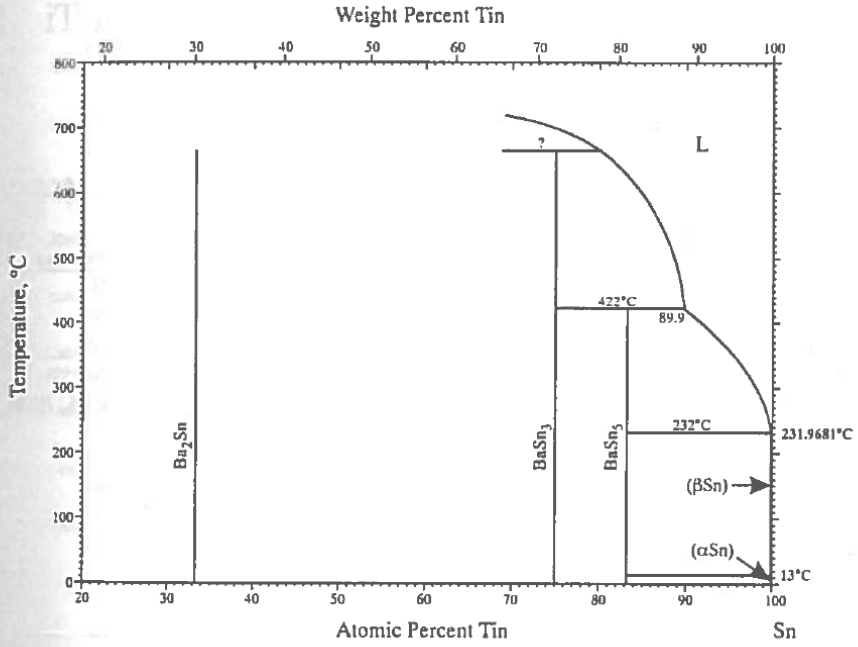

Ba-Sn

Ba-Sn

Phase	Composition, at.% Sn	Pearson symbol	Space group	Strukturbericht designation	Prototype
Ba_2Sn	33.3	*oP*12	*Pnma*	*C*23	Co_2Si
Ba_5Sn_3*	37.5	*tI*32	*I4/mcm*	$D8_l$	Cr_5B_3
BaSn*	50	*oC*8	*Cmcm*	B_f	CrB
$BaSn_3$	75	...	...	...	...
$BaSn_5$	83.3	...	...	...	...
(βSn)	100	*tI*4	$I4_1/amd$	*A*5	βSn
(αSn)	100	*cF*8	$Fd\bar{3}m$	*A*4	C (diamond)

*Not shown

Binary Alloy Phase Diagrams, 2nd ed., T.B. Massalski, H. Okamoto, P.R. Subramanian, and L. Kacprzak, ed., ASM International, Materials Park, OH, 616, 618 (1990)

6.1.26 Ba-Sr

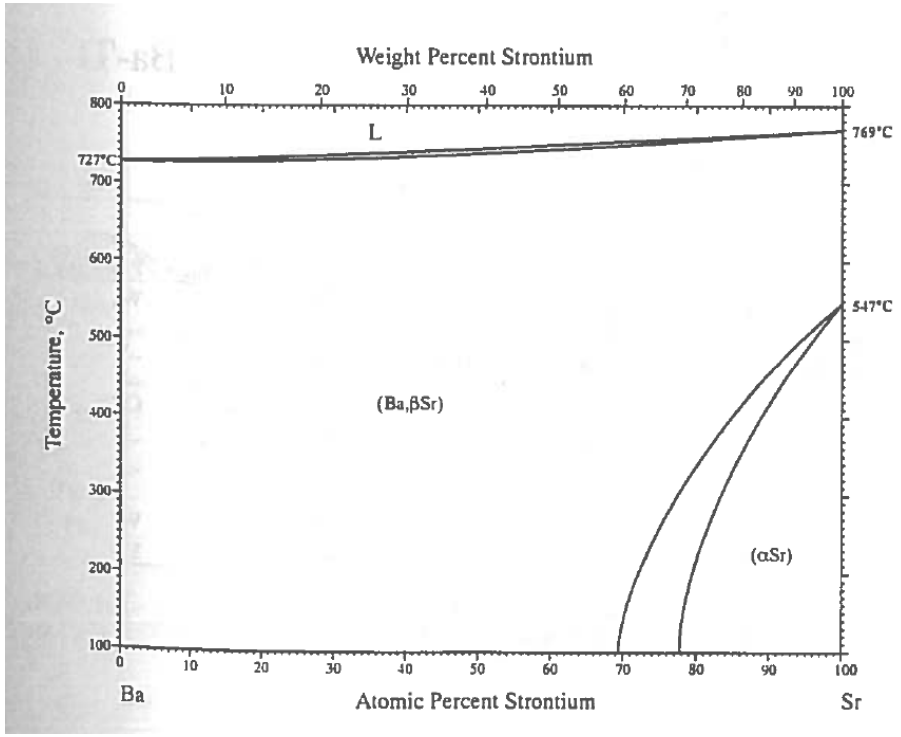

Ba-Sr

Ba-Sr

Phase	Composition, at.% Sr	Pearson symbol	Space group	Strukturbericht designation	Prototype
(Ba,βSr)	0 to 100	*cI*2	$Im\bar{3}m$	*A*2	W
(αSr)	78 to 100	*cF*4	$Fm\bar{3}m$	*A*1	Cu

C.B. Alcock and V.P. Itkin, *Bull. Alloy Phase Diagrams*, *8*(6), 534-536 (1987)

6.1.27 Ba-Ti

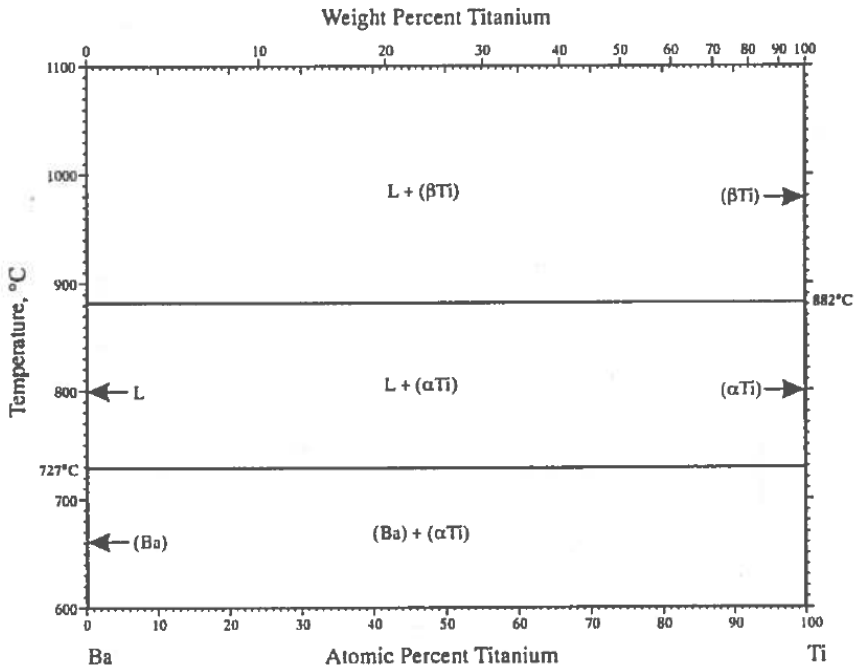

Ba-Ti

Ba-Ti

Phase	Composition, at.% Ti	Pearson symbol	Space group	Struktur-bericht designation	Prototype
(Ba)	0	*cI*2	$Im\bar{3}m$	*A*2	W
(βTi)	100	*cI*2	$Im\bar{3}m$	*A*2	W
(αTi)	100	*hP*2	$P6_3/mmc$	*A*3	Mg

J.L. Murray, *Phase Diagrams of Binary Titanium Alloys*, J.L. Murray, ed., ASM International, Metals Park, OH, 38-39 (1987)

6.1.28 Ba-Zn

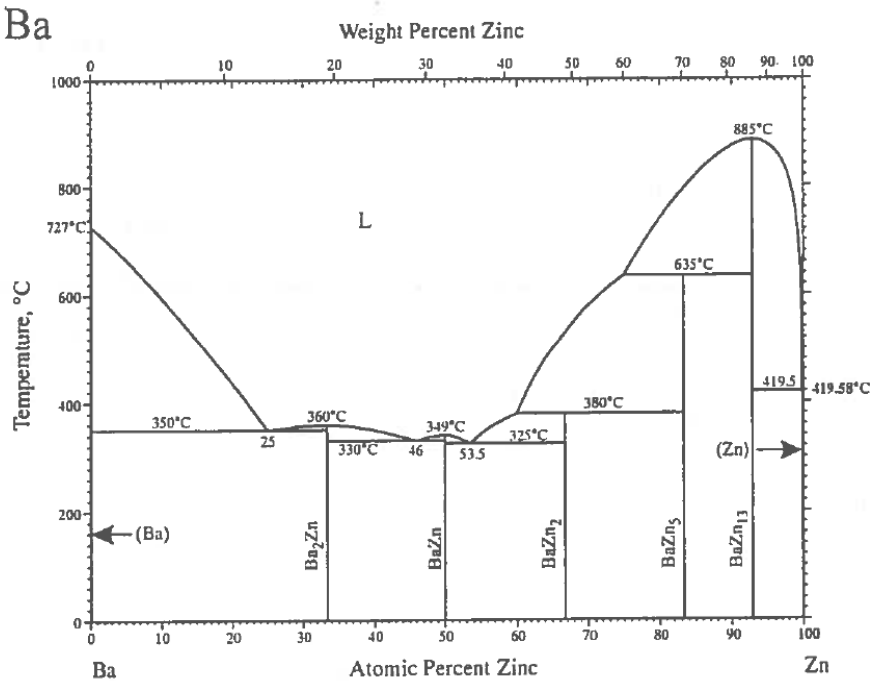

Ba-Zn

Ba-Zn

Phase	Composition, at.% Zn	Pearson symbol	Space group	Strukturbericht designation	Prototype
(Ba)	0	*cI*2	$Im\bar{3}m$	*A*2	W
Ba_2Zn	33.3	*tI*6	*I*4/*mmm*	$C11_b$	$MoSi_2$
BaZn	50	*cP*2	$Pm\bar{3}m$	*B*2	CsCl
$BaZn_2$	66.7	*oI*12	*Imma*	...	$CeCu_2$
$BaZn_5$	83.3	*oC*24	*Cmcm*	...	...
$BaZn_{13}$	92.9	*cF*112	$Fm\bar{3}c$	$D2_3$	$NaZn_{13}$
(Zn)	100	*hP*2	$P6_3/mmc$	*A*3	Mg

H. Okamoto, *J. Phase Equilibria*, *12*(4), 469-471 (1991)

6.1.29 Bi-Cd

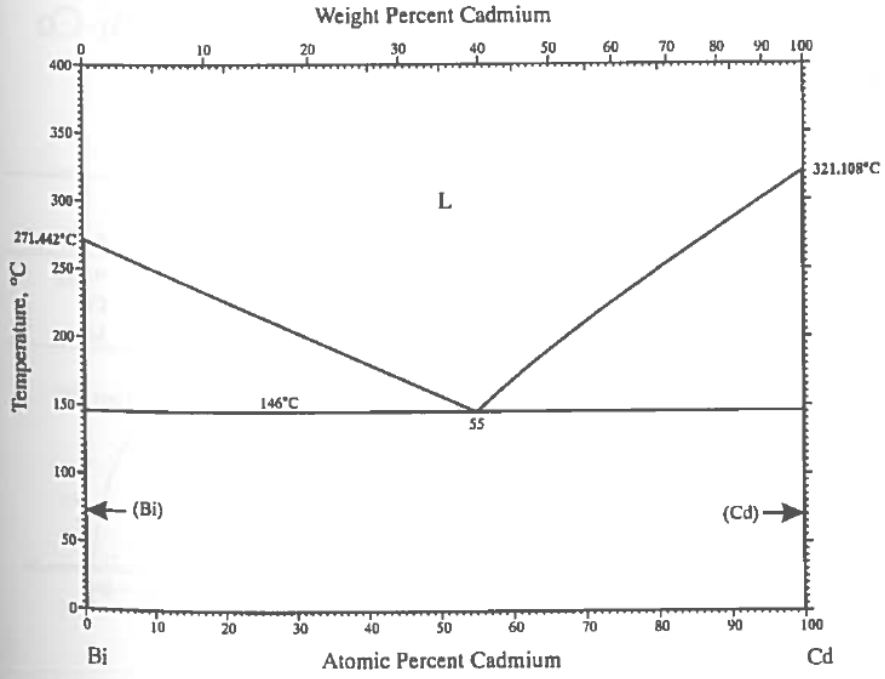

Bi-Cd

Bi-Cd

Phase	Composition, at.% Cd	Pearson symbol	Space group	Strukturbericht designation	Prototype
(Bi)	0	*hR*2	$R\bar{3}m$	*A*7	αAs
(Cd)	100	*hP*2	$P6_3/mmc$	*A*3	Mg

Z. Moser, J. Dutkiewicz, L. Zabdyr, and J. Salawa, *Bull. Alloy Phase Diagrams*, *9*(4), 445-448 (1988)

6.1.30 Bi-Cu

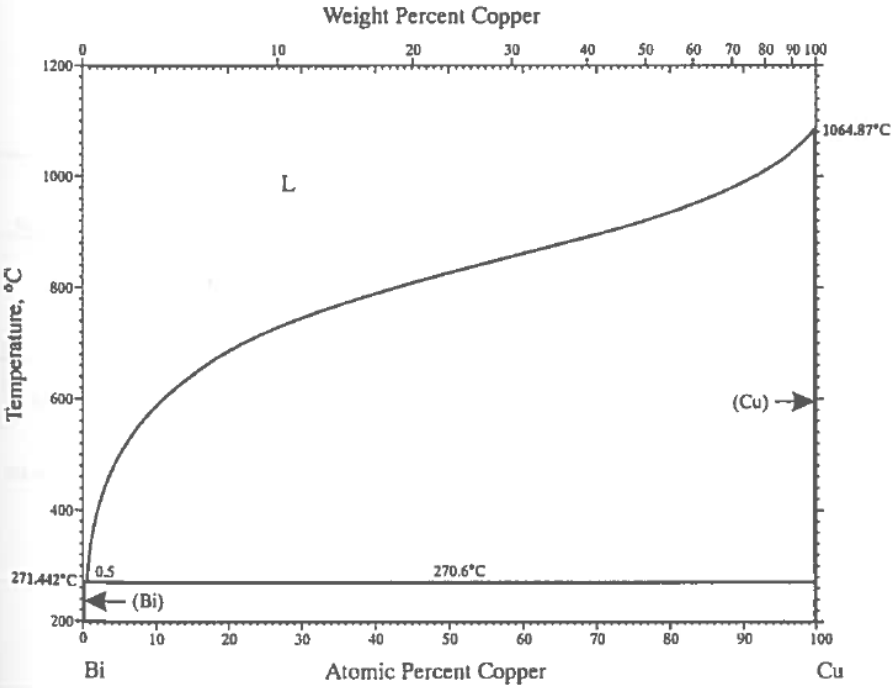

Bi-Cu

Bi-Cu

Phase	Composition, at.% Cu	Pearson symbol	Space group	Struktur-bericht designation	Prototype
(Bi)	0	*hR*2	$R\bar{3}m$	*A*7	αAs
(Cu)	100	*cF*4	$Fm\bar{3}m$	*A*1	Cu

D.J. Chakrabarti and D.E. Laughlin, *Bull. Alloy Phase Diagrams*, *5*(2), 148-155 (1984)

6.1.31 Bi-Ga

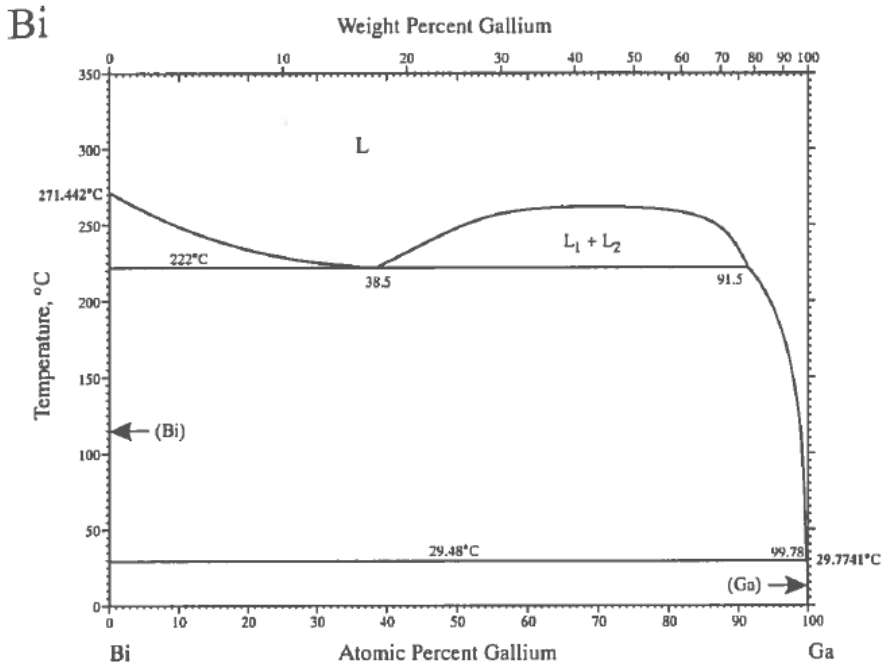

Bi-Ga

Phase	Composition, at.% Ga	Pearson symbol	Space group	Strukturbericht designation	Prototype
(Bi)	0	*hR*2	$R\bar{3}m$	*A*7	αAs
(Ga)	100	*oC*8	*Cmca*	*A*11	Ga

Binary Alloy Phase Diagrams, 2nd ed., T.B. Massalski, H. Okamoto, P.R. Subramanian, and L. Kacprzak, ed., ASM International, Materials Park, OH, 738-739 (1990)

6.1.32 Bi-Hg

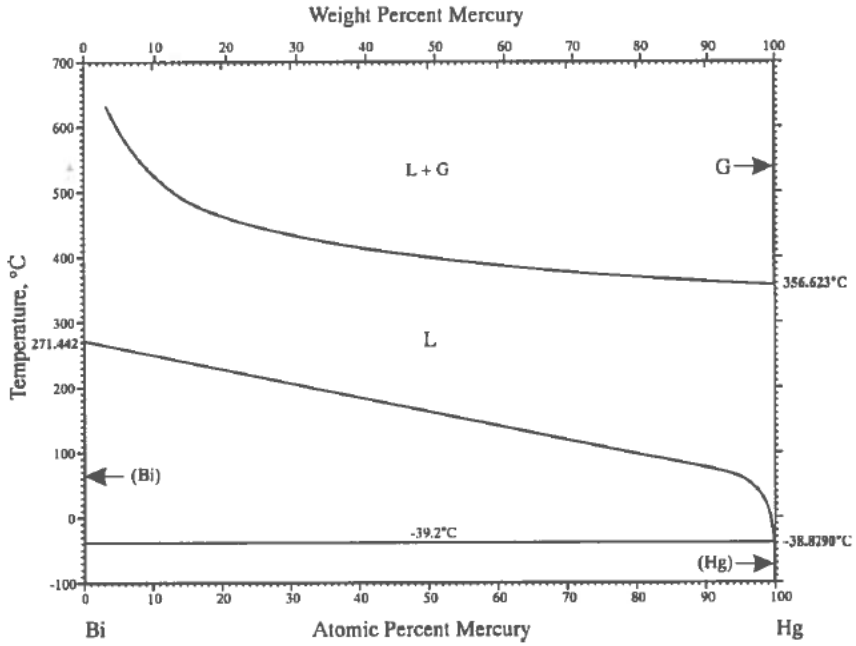

Bi-Hg

Bi-Hg

Phase	Composition, at.% Hg	Pearson symbol	Space group	Struktur-bericht designation	Prototype
(Bi)	0	*hR*2	$R\bar{3}m$	*A*7	αAs
(Hg)	100	*hR*1	$R\bar{3}m$	*A*10	αHg

L. Zabdyr and C. Guminski, *J. Phase Equilibria*, *17*(3), 230-236 (1996)

6.1.33 Bi-In

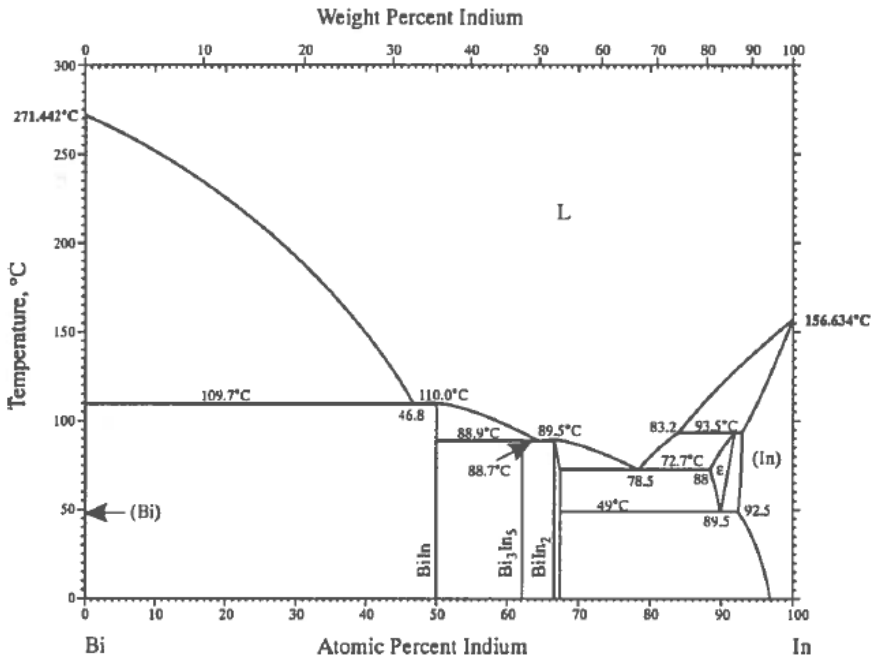

Bi-In

Bi-In

Phase	Composition, at.% In	Pearson symbol	Space group	Struktur-bericht designation	Prototype
(Bi)	0	*hR*2	$R\bar{3}m$	*A*7	αAs
BiIn	50	*tP*4	*P*4/*nmm*	*B*10	PbO
Bi_3In_5	62.5	*tI*32	*I*4/*mcm*	$D8_f$	Cr_5B_3
$BiIn_2$	66.8 to 67.7	*hP*6	$P6_3/mmc$	$B8_2$	Ni_2In
ε	88 to 92	*tI*2	...	...	...
(In)	92.5 to 100	*tI*2	*I*4/*mmm*	*A*6	In

H. Okamoto, *Phase Diagrams of Indium Alloys and Their Engineering Applications*, C.E.T. White and H. Okamoto, ed., ASM International, Materials Park, OH, 46-54 (1992)

6.1.34 Bi-Li

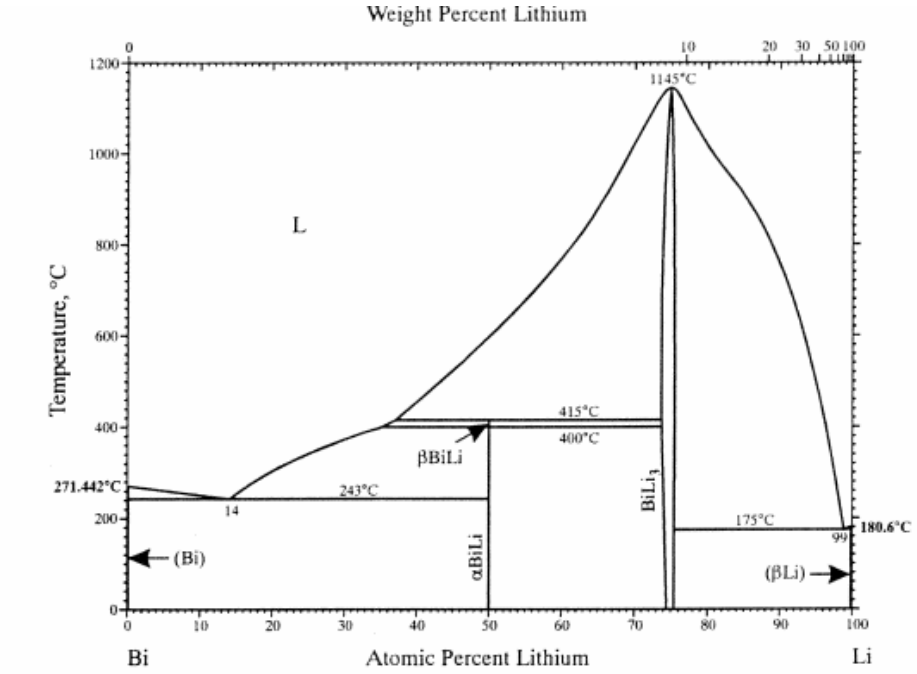

Bi-Li

Bi-Li

Phase	Composition, at.% Li	Pearson symbol	Space group	Struktur-bericht designation	Prototype
(Bi)	0	*hR*2	$R\bar{3}m$	*A*7	αAs
βBiLi	50	…	…	…	…
αBiLi	50	*tP*4	*P*4/*mmm*	$L1_0$	AuCu
$BiLi_3$	73.8 to 75.2	*cF*16	$Fm\bar{3}m$	$D0_3$	BiF_3
(βLi)	100	*cI*2	$Im\bar{3}m$	*A*2	W

J. Sangster and A.D. Pelton, *J. Phase Equilibria*, *12*(4), 447-450 (1991)

6.1.35 Bi-Na

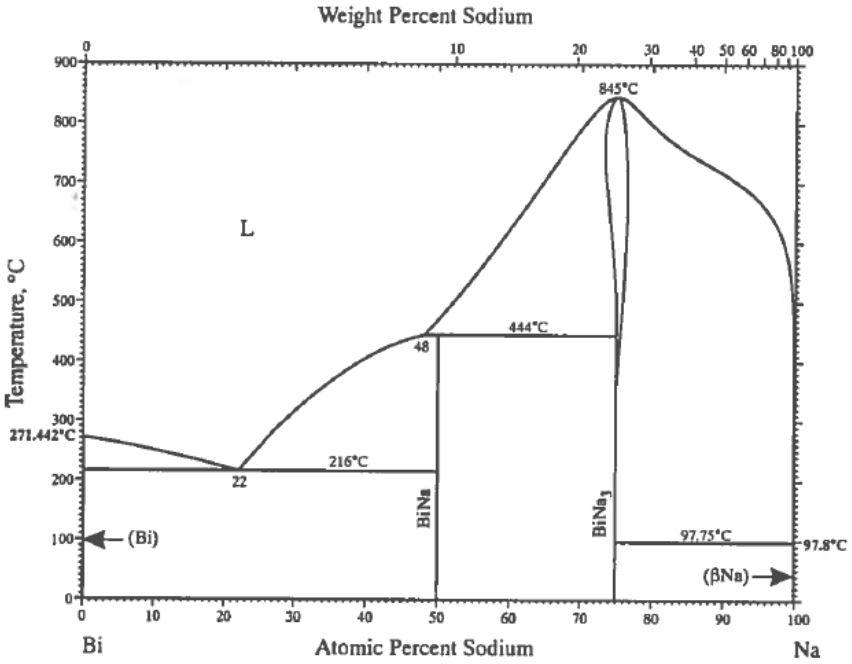

Bi-Na

Bi-Na

Phase	Composition, at.% Na	Pearson symbol	Space group	Strukturbericht designation	Prototype
(Bi)	0	*hR*2	$R\bar{3}m$	*A*7	αAs
BiNa	50	*tP*4	*P*4/*mmm*	$L1_0$	AuCu
$BiNa_3$	73.5 to 77.5	*hP*8	$P6_3/mmc$	$D0_{18}$	Na_3As
(βNa)	100	*cI*2	$Im\bar{3}m$	*A*2	W
(αNa)	100	*hP*2	$P6_3/mmc$	*A*3	Mg

J. Sangster and A.D. Pelton, *J. Phase Equilibria*, *12*(4), 451-456 (1991)

6.1.36 Bi-Pb

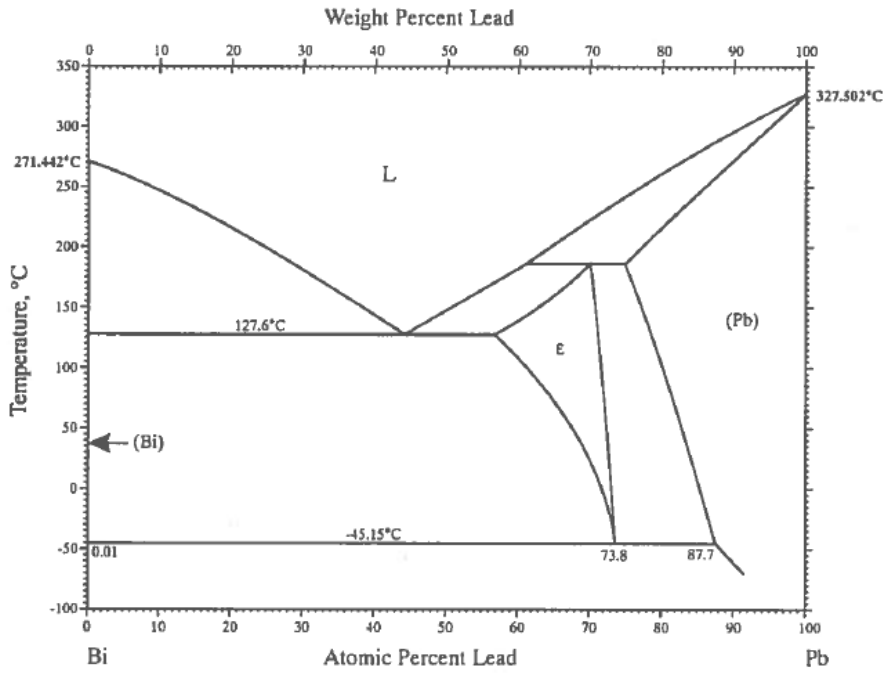

Bi-Pb

Bi-Pb

Phase	Composition, at.% Pb	Pearson symbol	Space group	Struktur-bericht designation	Prototype
(Bi)	0	*hR*2	$R\bar{3}m$	*A*7	αAs
ε	56.9 to 73.8	*hP*2	$P6_3/mmc$	*A*3	Mg
(Pb)	75 to 100	*cF*4	$Fm\bar{3}m$	*A*1	Cu

H. Okamoto, *J. Phase Equilibria*, *15*(3), 361-362 (1994)

6.1.37 Bi-Sn

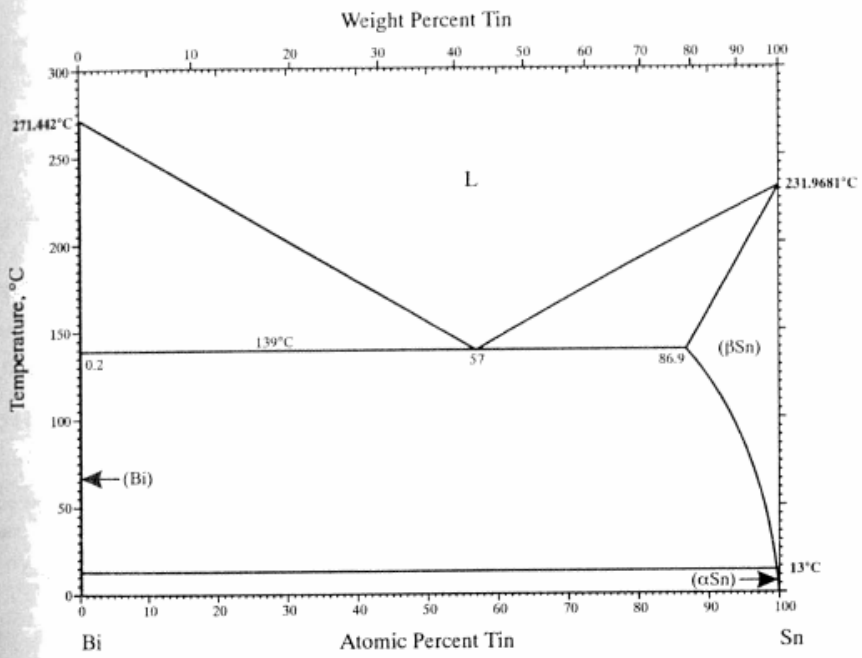

Bi-Sn

Bi-Sn

Phase	Composition, at.% Sn	Pearson symbol	Space group	Struktur-bericht designation	Prototype
(Bi)	0 to 0.2	*hR2*	$R\bar{3}m$	*A7*	αAs
(βSn)	86.9 to 100	*tI4*	$I4_1/amd$	*A5*	βSn
(αSn)	100	*cF8*	$Fd\bar{3}m$	*A4*	C (diamond)

Binary Alloy Phase Diagrams, 2nd ed., T.B. Massalski, H. Okamoto, P.R. Subramanian, and L. Kacprzak, ed., ASM International, Materials Park, OH, 794, 796 (1990)

6.1.38 Bi-Sr

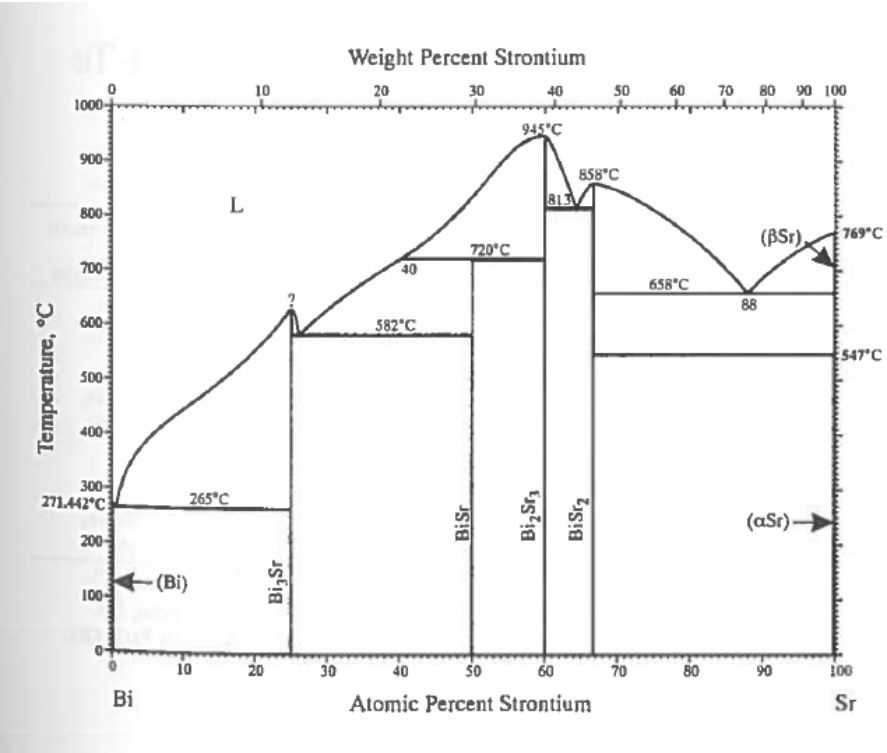

Bi-Sr

Bi-Sr

Phase	Composition, at.% Sr	Pearson symbol	Space group	Strukturbericht designation	Prototype
(Bi)	0	*hR*2	$R\bar{3}m$	*A*7	αAs
Bi_3Sr	25	*cP*4	$Pm\bar{3}m$	$L1_2$	$AuCu_3$
BiSr	50	…	…	…	…
Bi_2Sr_3	60	…	…	…	…
$BiSr_2$	66.7	*tI*12	*I*4/*mmm*	…	La_2Sb
(βSr)	100	*cI*2	$Im\bar{3}m$	*A*2	W
(αSr)	100	*cF*4	$Fm\bar{3}m$	*A*2	Cu

Binary Alloy Phase Diagrams, *2nd ed.*, T.B. Massalski, H. Okamoto, P.R. Subramanian, and L. Kacprzak, ed., ASM International, Materials Park, OH, 794, 797 (1990)

6.1.39 Bi-Ti

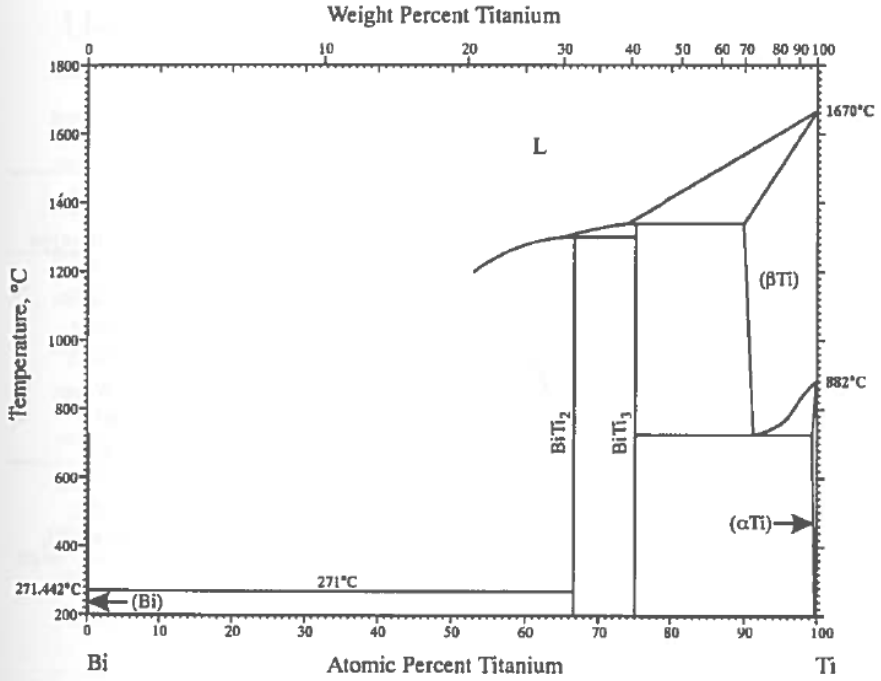

Bi-Ti

Bi-Ti

Phase	Composition, at.% Ti	Pearson symbol	Space group	Strukturbericht designation	Prototype
(Bi)	0	*hR*2	$R\bar{3}m$	*A*7	αAs
$BiTi_2$	66.7	*tP*12	$P4_2/mmc$	…	…
$BiTi_3$	75	*t***	…	…	…
(βTi)	90 to 100	*cI*2	$Im\bar{3}m$	*A*2	W
(αTi)	99 to 100	*hP*2	$P6_3/mmc$	*A*3	Mg

J.L. Murray, *Bull. Alloy Phase Diagrams*, 5(6), 610-613 (1994)

6.1.40 Bi-Zn

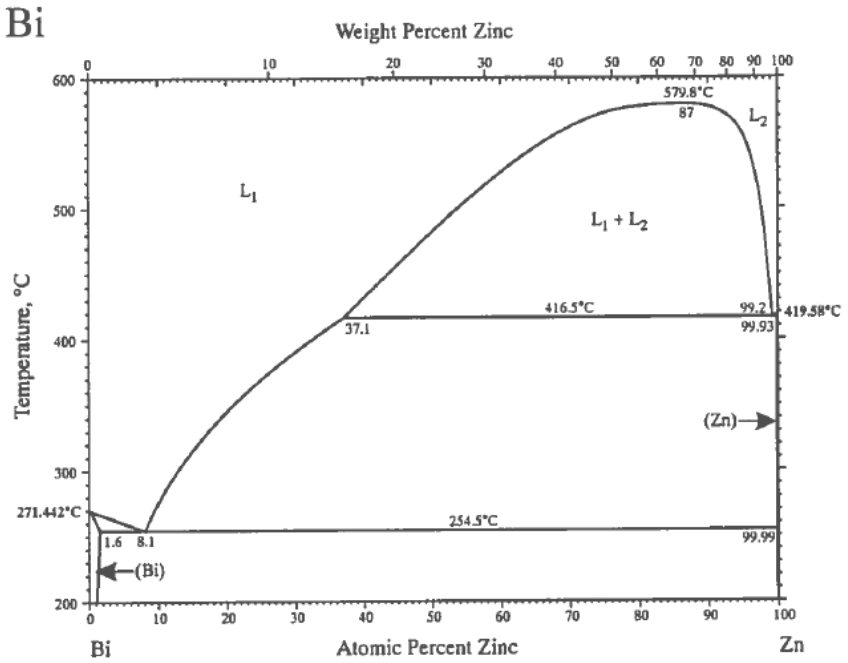

Bi-Zn

Phase	Composition, at.% Zn	Pearson symbol	Space group	Struktur-bericht designation	Prototype
(Bi)	0 to 1.6	*hR*2	$R\bar{3}m$	*A*7	αAs
(Zn)	99.93 to 100	*hP*2	$P6_3/mmc$	*A*3	Mg

D.V. Malakhov, *Calphad*, *24*(1), 1-14 (2000)

6.1.41 Cd-Li

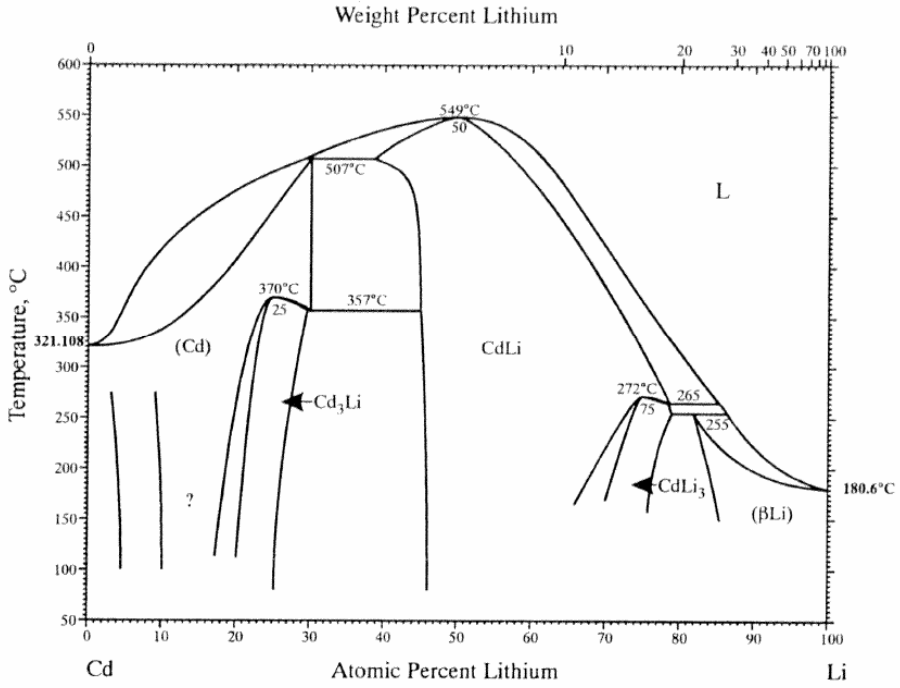

Cd-Li

Cd-Li

Phase	Composition, at.% Li	Pearson symbol	Space group	Struktur-bericht designation	Prototype
(Cd)	0 to 30	*hP*2	$P6_3/mmc$	*A*3	Mg
Cd_3Li	20 to 29	*hP*2	$P6_3/mmc$	*A*3	Mg
CdLi	38 to 78	*cF*16	$Fd\bar{3}m$	*B*32	NaTl
$CdLi_3$	65 to 78	*cF*4	$Fm\bar{3}m$	*A*1	Cu
(βLi)	82 to 100	*cI*2	$Im\bar{3}m$	*A*2	W

A.D. Pelton, *Bull. Alloy Phase Diagrams*, *9*(1), 36-41 (1988)

6.1.42 Cd-Sn

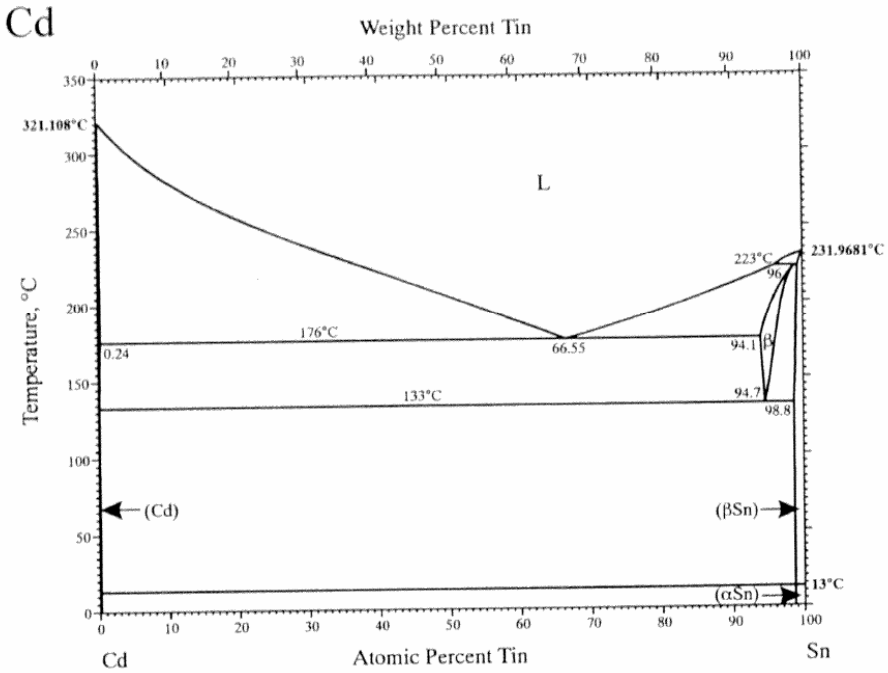

Cd-Sn

Phase	Composition, at.% Sn	Pearson symbol	Space group	Strukturbericht designation	Prototype
(Cd)	0 to 0.24	*hP*2	$P6_3/mmc$	*A*3	Mg
β	94.1 to 99	*hP*2	$P6_3/mmc$	*A*3	Mg
(βSn)	98.8 to 100	*tI*4	$I4_1/amd$	*A*5	βSn
(αSn)	? to 100	*cF*8	$Fd\bar{3}m$	*A*4	C (diamond)

J. Dutkiewicz, L. Zabdyr, Z. Moser, and J. Salawa, *Bull. Alloy Phase Diagrams*, *10*(3), 223-229 (1989)

6.1.43 Cu-Ga

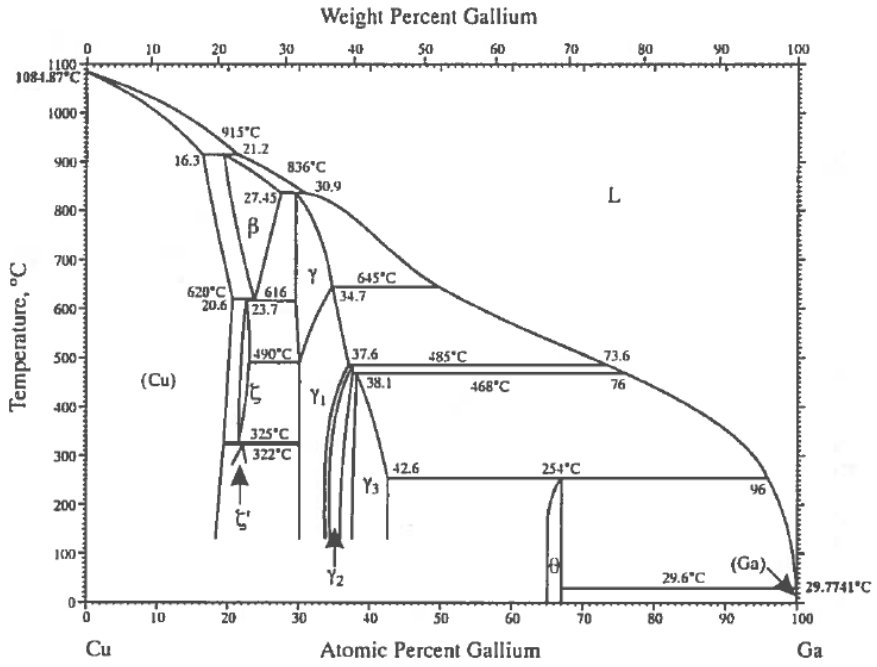

Cu-Ga

Cu-Ga

Phase	Composition, at.% Ga	Pearson symbol	Space group	Struktur-bericht designation	Prototype
(Cu)	0 to 20.6	*cF*4	$Fm\bar{3}m$	*A*1	Cu
β	19.3 to 27.45	*cI*2	$Im\bar{3}m$	*A*2	W
ζ	20.5 to 22.5	*hP*2	$P6_3/mmc$	*A*3	Mg
ζ'	21.0 to 22.4	*hP**	...	...	...
γ	29.5 to 34.7	*cP*52	$P\bar{4}3m$	$D8_3$	Al_4Cu_9
γ_1	29.8 to 37.6	*cP*52	$P\bar{4}3m$	...	...
γ_2	33.9 to 37.7	*cP**	$P\bar{4}3m$	...	...
γ_3	37.5 to 42.6	*cP**	$P\bar{4}3m$	...	...
θ	64.6 to 66.7	*tP*3	*P*4/*mmm*	...	...
(Ga)	100	*oC*8	*Cmca*	*A*11	Ga

P.R. Subramanian and D.E. Laughlin, *Phase Diagrams of Binary Copper Alloys*, P.R. Subramanian, D.J. Chakrabarti, and D.E. Laughlin, ed., ASM International, OH, 174-184 (1994)

6.1.44 Cu-Hg

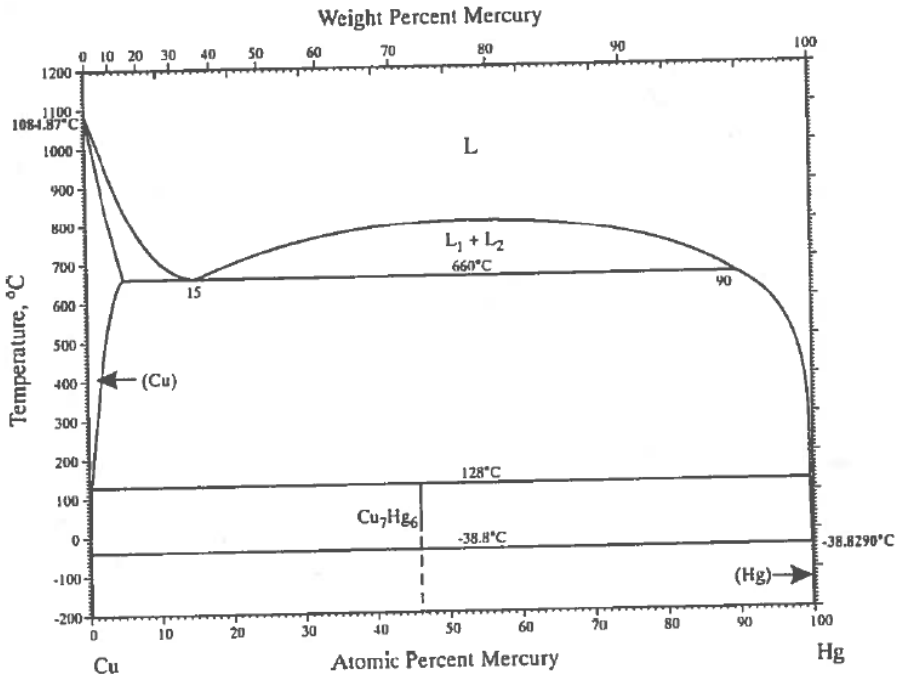

Cu-Hg

Cu-Hg

Phase	Composition, at.% Hg	Pearson symbol	Space group	Struktur-bericht designation	Prototype
(Cu)	0 to 5	*cF4*	$Fm\bar{3}m$	*A1*	Cu
Cu_7Hg_6	46	*hR52*	$R\bar{3}m$	...	...
(Hg)	100	*hR1*	$R\bar{3}m$	*A10*	αHg

D.J. Chakrabarti and D.E. Laughlin, *Bull. Alloy Phase Diagrams*, 6(6), 522-527 (1985)

6.1.45 Cu-In

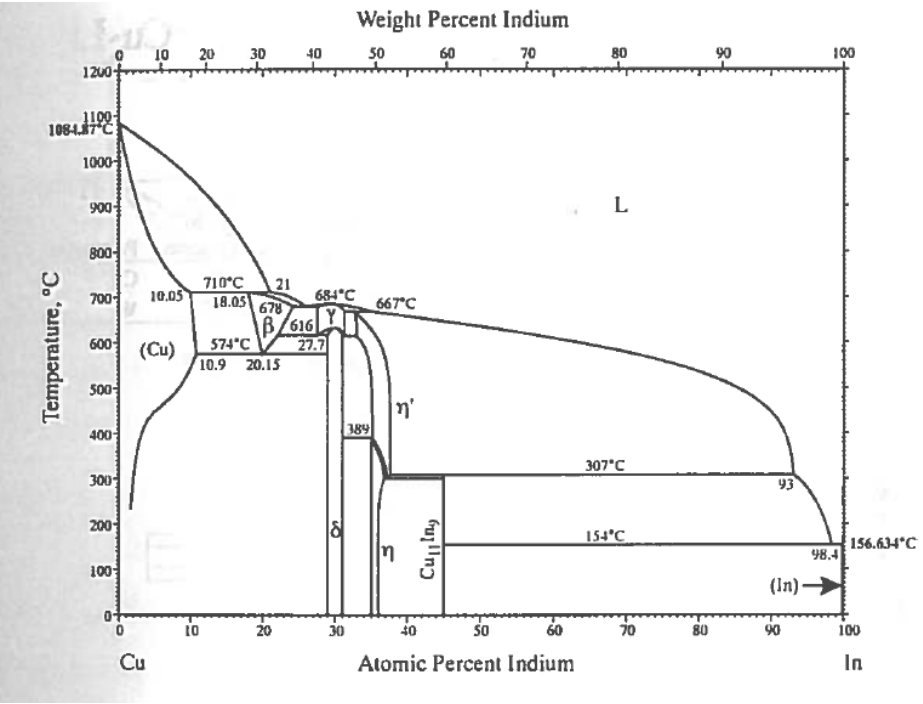

Cu-In

Cu-In

Phase	Composition, at.% In	Pearson symbol	Space group	Struktur-bericht designation	Prototype
(Cu)	0 to 10.9	*cF4*	$Fm\bar{3}m$	*A1*	Cu
β	18.05 to 24.5	*cI2*	$Im\bar{3}m$	*A2*	W
γ	27.7 to 31.3	*cP52*	$P\bar{4}3m$	...	$InMn_3$
δ	29.05 to 30.6	*aP40*	$P\bar{1}$	...	...
η'	32.8 to 37.8	*hP4*	$P6_3/mmc$	$B8_1$	NiAs
		hP6	$P6_3/mmc$	$B8_2$	Ni_2In
η	35 to 37	*o***	...	...	...
$Cu_{11}In_9$	45	*mC20*	*C2/m*	...	...
(In)	100	*tI2*	*I4/mmm*	*A6*	In

H. Okamoto, *J. Phase Equilibria*, *15*(2), 226-227 (1994)

6.1.46 Cu-Li

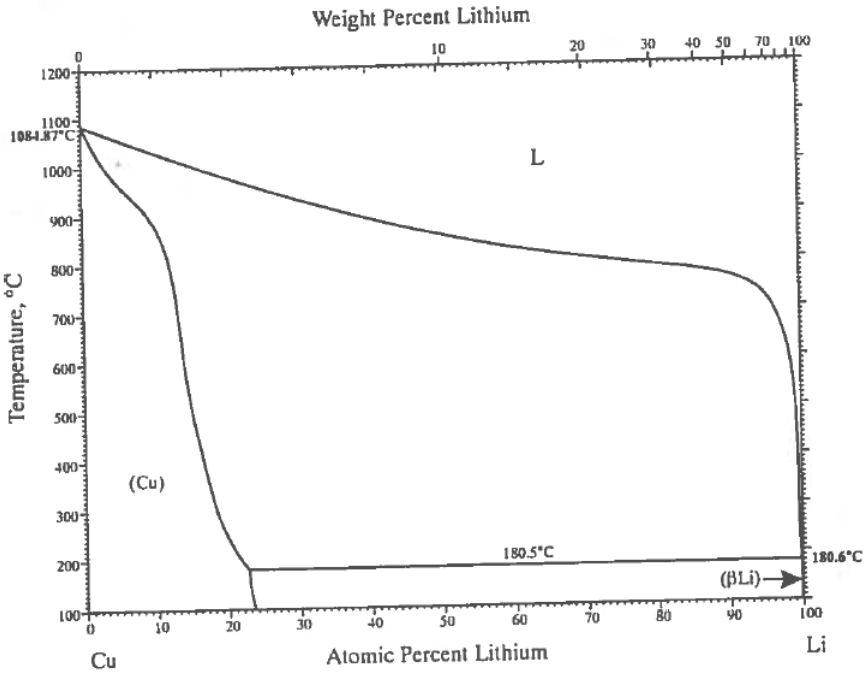

Cu-Li

Cu-Li

Phase	Composition, at.% Li	Pearson symbol	Space group	Struktur-bericht designation	Prototype
(Cu)	0 to 23.5	*cF4*	$Fm\bar{3}m$	*A1*	Cu
(βLi)	100	*cI2*	$Im\bar{3}m$	*A2*	W

A.D. Pelton, *Bull. Alloy Phase Diagrams*, 7(2), 142-144 (1986)

6.1.47 Cu-Na

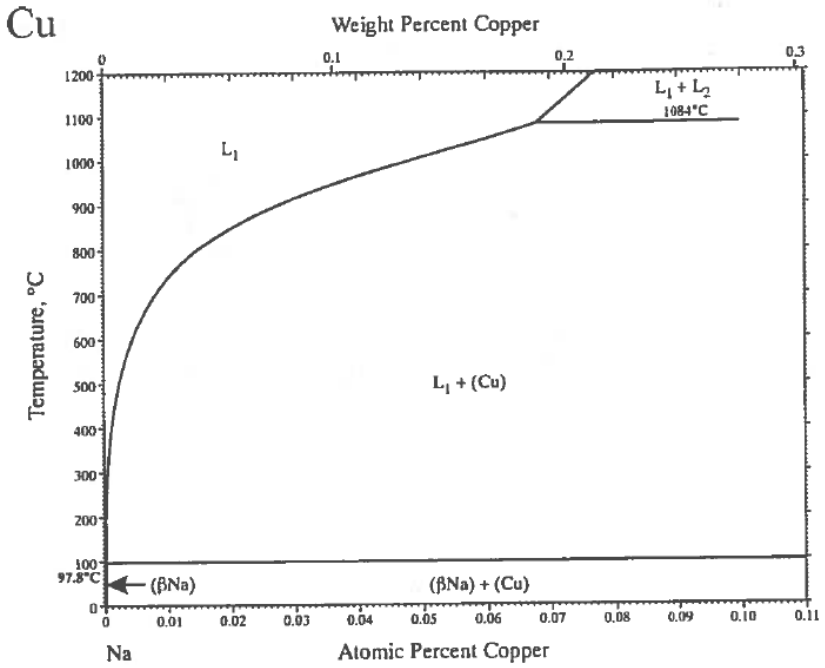

Cu-Na

Na-Cu

Phase	Composition, at.% Cu	Pearson symbol	Space group	Struktur-bericht designation	Prototype
(βNa)	0	*cI*2	$Im\bar{3}m$	*A*2	W
(Cu)	100	*cF*4	$Fm\bar{3}m$	*A*1	Cu

A.D. Pelton, *Bull. Alloy Phase Diagrams*, 7(1), 25-27 (1986)

6.1.48 Cu-Pb

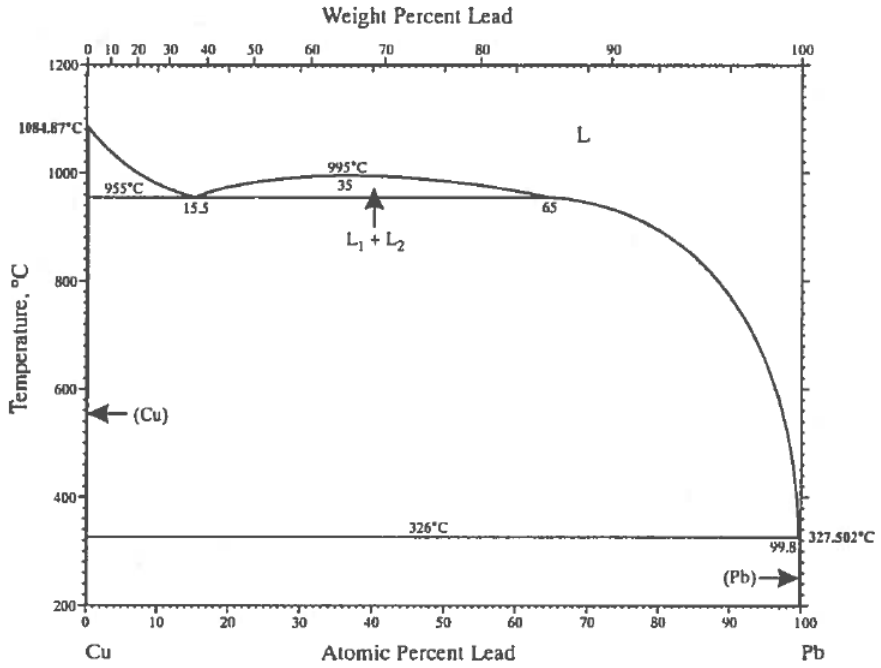

Cu-Pb

Cu-Pb

Phase	Composition, at.% Pb	Pearson symbol	Space group	Struktur-bericht designation	Prototype
(Cu)	0	*cF*4	$Fm\bar{3}m$	*A*1	Cu
(Pb)	100	*cF*4	$Fm\bar{3}m$	*A*1	Cu

D.J. Chakrabarti and D.E. Laughlin, *Bull. Alloy Phase Diagrams*, *5*(5), 503-510 (1984)

See also
H. Okamoto, *J. Phase Equilibria*, *14*(5), 649-650 (1993)

6.1.49 Cu-Sn

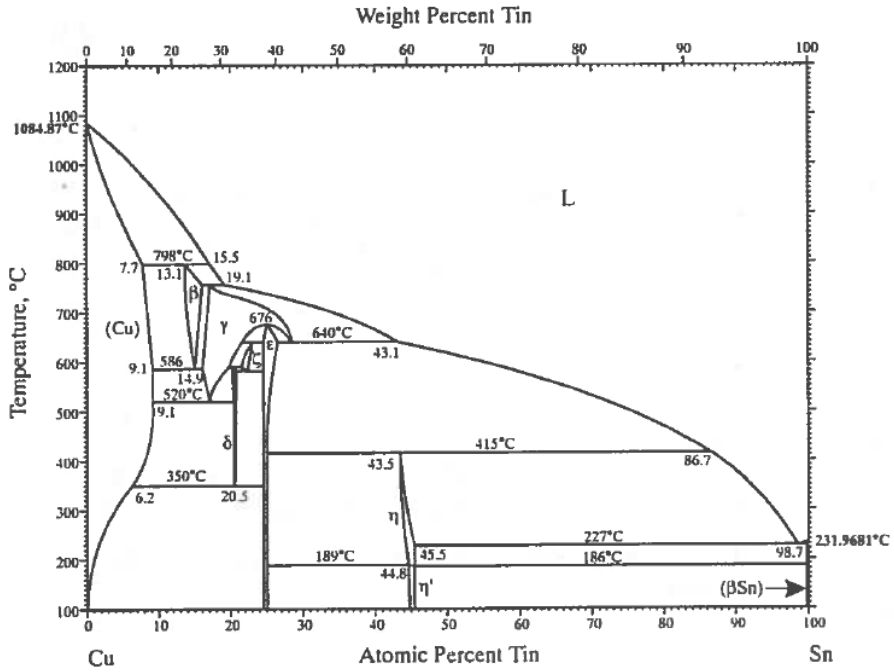

Cu-Sn

Cu-Sn

Phase	Composition, at.% Sn	Pearson symbol	Space group	Struktur-bericht designation	Prototype
(Cu)	0 to 9.1	*cF*4	$Fm\bar{3}m$	*A*1	Cu
β	13.1 to 15.7	*cI*2	$Im\bar{3}m$	*A*2	W
γ	15.4 to 27.9	*cF*16	$Fm\bar{3}m$	$D0_3$	BiF_3
δ	20.3 to 20.8	*cF*416	$F\bar{4}3m$	…	…
ζ	20.9 to 22.5	*hP*26	$P6_3$	…	…
ε	24.5 to 25.9	*oC*80	*Cmcm*	…	…
η	43.5 to 45.5	*hP*4	$P6_3/mmc$	$B8_1$	NiAs
η'	44.8 to 45.5	*hP**	…	…	…
(βSn)	100	*tI*4	$I4_1/amd$	*A*5	βSn
(αSn)	100	*cF*8	$Fd\bar{3}m$	*A*4	C (diamond)

N. Saunders and A.P. Miodownik, *Bull. Alloy Phase Diagrams*, *11*(3), 278-287 (1990)

6.1.50 Cu-Sr

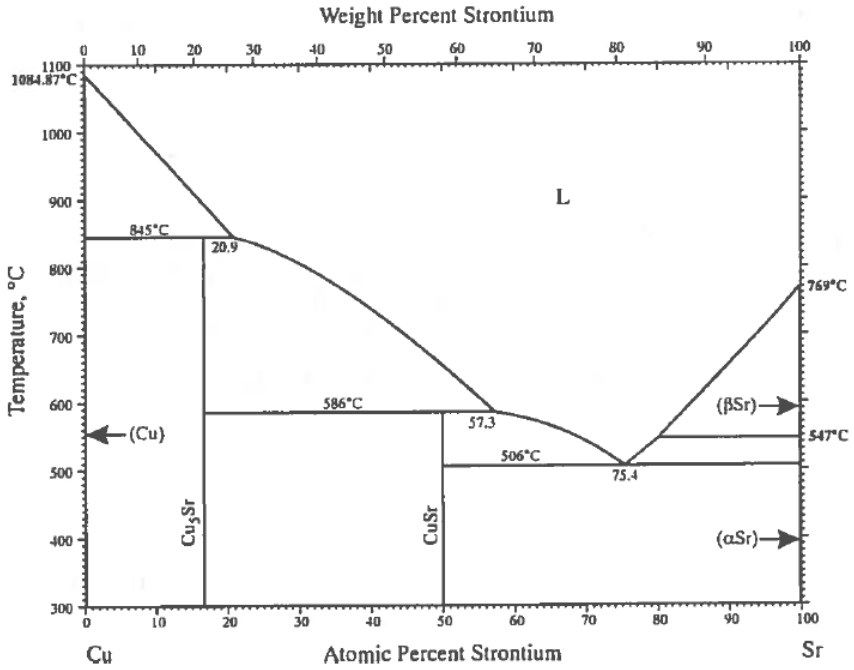

Cu-Sr

Cu-Sr

Phase	Composition, at.% Sr	Pearson symbol	Space group	Struktur-bericht designation	Prototype
(Cu)	0	*cF4*	$Fm\bar{3}m$	*A1*	Cu
Cu_5Sr	16.7	*hP6*	*P6/mmm*	$D2_d$	$CaCu_5$
CuSr	50	*hP8*	$P6_3/mmm$	…	…
(βSr)	100	*cI2*	$Im\bar{3}m$	*A2*	W
(αSr)	100	*cF4*	$Fm\bar{3}m$	*A1*	Cu

D. Risold, B. Hallstedt, L.J. Gauckler, H.L. Lukas, and S. Fries, *Calphad*, *20*(2), 151-160 (1996)

6.1.51 Cu-Ti

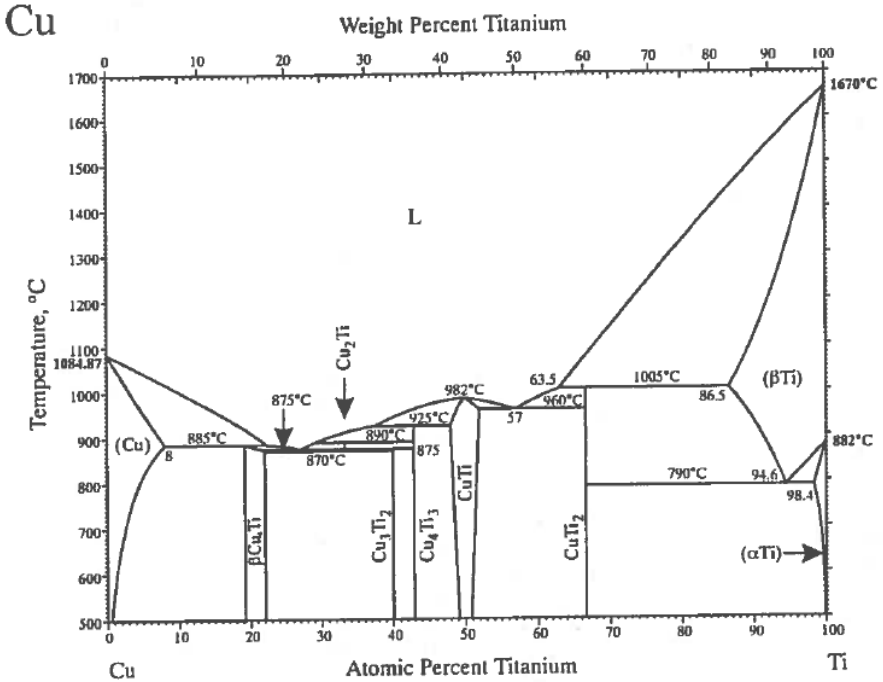

Cu-Ti

Cu-Ti

Phase	Composition, at.% Ti	Pearson symbol	Space group	Struktur-bericht designation	Prototype
(Cu)	0 to 8	*cF*4	$Fm\bar{3}m$	*A*1	Cu
βCu_4Ti	19.1 to 22	*oP*20	*Pnma*	...	Au_4Zr
αCu_4Ti*	19.1 to 22	*tI*10	*I*4/*m*	$D1_a$	$MoNi_4$
Cu_2Ti	33.3	*oC*12	*Amm*2	...	Au_2V
Cu_3Ti_2	40	*tP*10	*P*4/*nmm*	...	...
Cu_4Ti_3	42.9	*tI*14	*I*4/*mmm*	...	...
CuTi	48 to 52	*tP*4	*P*4/*nmm*	*B*11	γCuTi
$CuTi_2$	66.7	*tI*6	*I*4/*mmm*	$C11_b$	$MoSi_2$
(βTi)	86.5 to 100	*cI*2	$Im\bar{3}m$	*A*2	W
(αTi)	98.4 to 100	*hP*2	$P6_3/mmc$	*A*3	Mg

* Not shown.

J.L. Murray, *Phase Diagrams of Binary Titanium Alloys*, J.L. Murray, ed., ASM International, Metals Park, OH, 80-95 (1987)

See also

H. Okamoto, *J. Phase Equilibria*, *15*(5), 566-567 (1994)

6.1.52 Cu-Zn

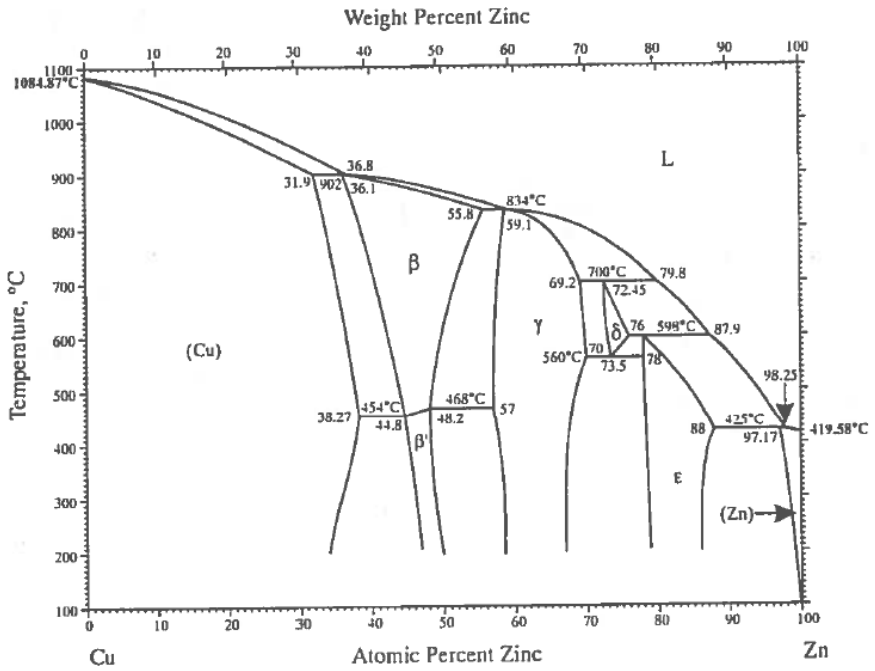

Cu-Zn

Cu-Zn

Phase	Composition, at.% Zn	Pearson symbol	Space group	Struktur-bericht designation	Prototype
(Cu)	0 to 38.27	*cF*4	$Fm\bar{3}m$	*A*1	Cu
β	36.1 to 55.8	*cI*2	$Im\bar{3}m$	*A*2	W
β'	44.8 to 50	*cP*2	$Pm\bar{3}m$	*B*2	CsCl
γ	57.0 to 70.0	*cI*52	$I\bar{4}3m$	$D8_2$	Cu_5Zn_8
δ	72.45 to 76.0	*hP*3	$P\bar{6}$	...	...
ε	78.0 to 88.0	*hP*2	$P6_3/mmc$	*A*3	Mg
(Zn)	97.17 to 100	*hP*2	$P6_3/mmc$	*A*3	Mg

A.P. Miodownik, *Phase Diagrams of Binary Copper Alloys*, P.R. Subramanian and D.E. Laughlin, ed., ASM International, Materials Park, OH, 487-496 (1994)

6.1.53 Ga-Hg

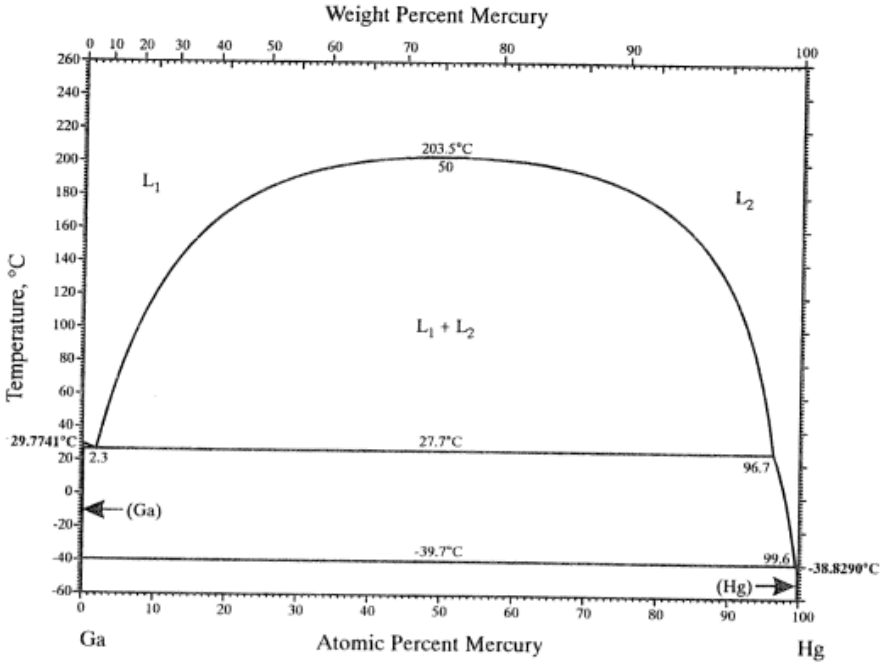

Ga-Hg

Ga-Hg

Phase	Composition, at.% Hg	Pearson symbol	Space group	Struktur-bericht designation	Prototype
(Ga)	0	*oC*8	*Cmca*	*A*11	Ga
(Hg)	100	*hR*1	$R\bar{3}m$	*A*10	αHg

C. Guminski and L. Zabdyr, *J. Phase Equilibria*, *14*(6), 719-725 (1993)

6.1.54 Ga-In

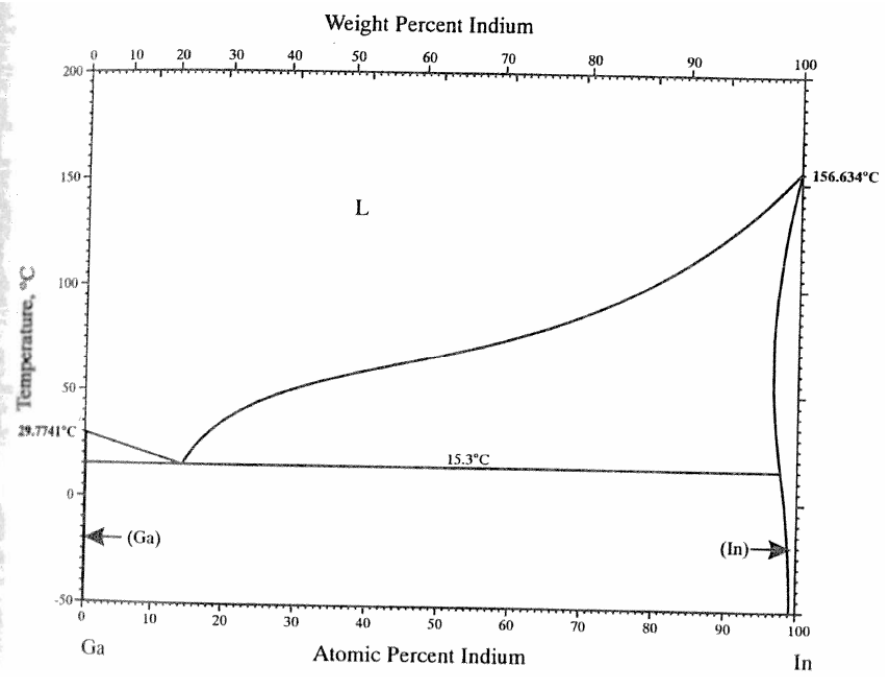

Ga-In

Ga-In

Phase	Composition, at.% In	Pearson symbol	Space group	Struktur-bericht designation	Prototype
(Ga)	0	*oC*8	*Cmca*	*A*11	Ga
(In)	96.9 to 100	*tI*2	*I*4/*mmm*	*A*6	In

T.J. Anderson and I. Ansara, *J. Phase Equilibria*, *12*(1), 64-72 (1991)

6.1.55 Ga-Li

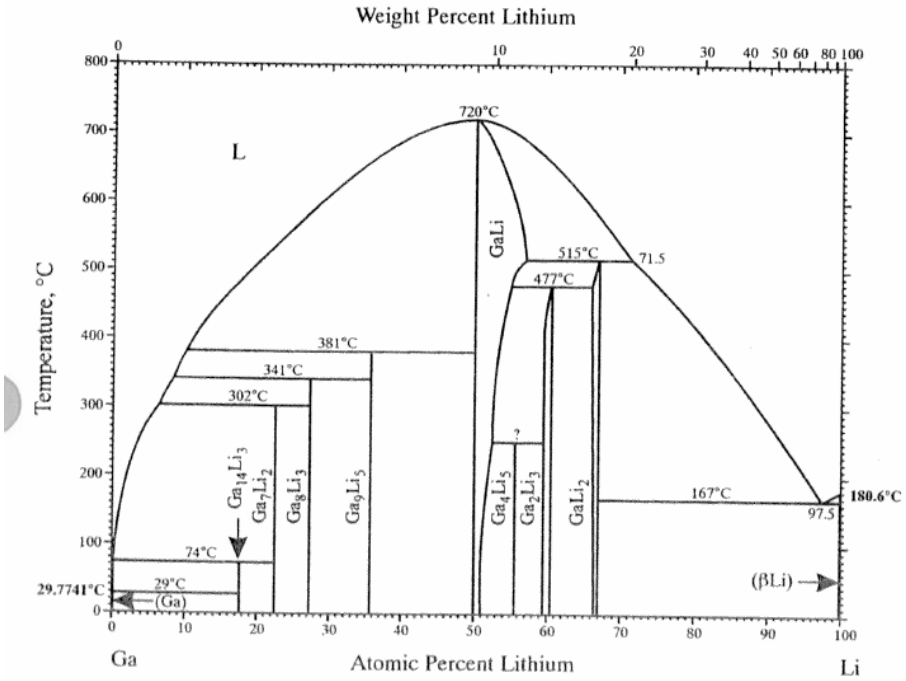

Ga-Li

Ga-Li

Phase	Composition, at.% Li	Pearson symbol	Space group	Struktur-bericht designation	Prototype
(Ga)	0	*oC*8	*Cmca*	*A*11	Ga
$Ga_{14}Li_3$	17.6	*hR*20	$R\bar{3}m$	...	...
Ga_7Li_2	22.2	*oC*304	*Cmcm*	...	...
Ga_8Li_3	27.3	...	...	...	...
Ga_9Li_5	35.7	...	...	...	...
GaLi	50 to 57	*cF*16	$Fd\bar{3}m$	*B*32	NaTl
Ga_4Li_5	55.6	*hP*9	$P\bar{3}m1$	...	...
Ga_2Li_3	59.5 to 60.5	*hR*5	$R\bar{3}m$	...	...
$GaLi_2$	66 to 67	*oC*12	*Cmcm*	*C*49	$ZrSi_2$
(βLi)	100	*cI*2	$Im\bar{3}m$	*A*2	W

H. Okamoto, *J. Phase Equilibria*, *20*(1), 92 (1999)

6.1.56 Ga-Na

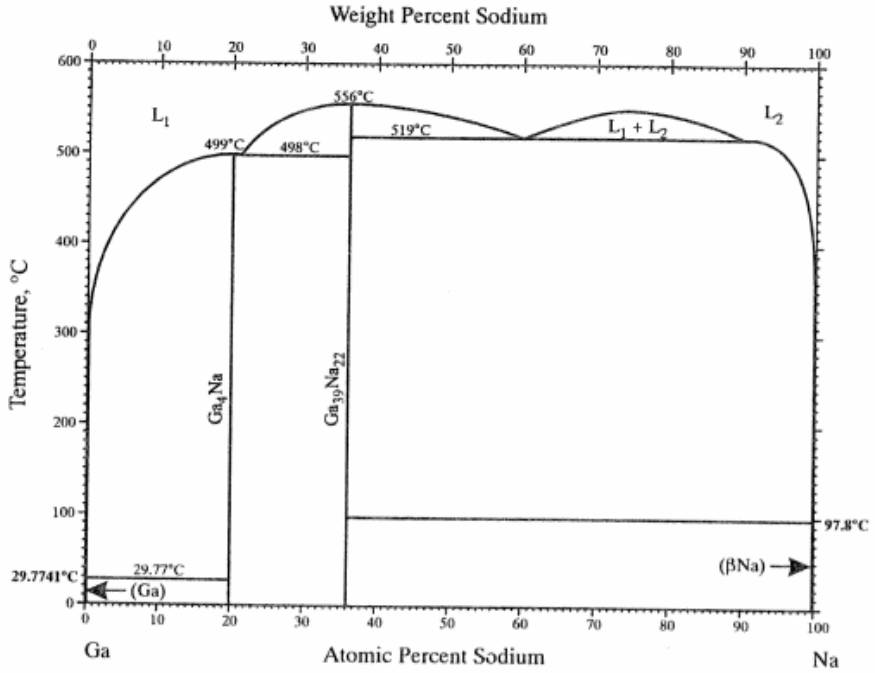

Ga-Na

Ga-Na

Phase	Composition, at.% Na	Pearson symbol	Space group	Strukturbericht designation	Prototype
(Ga)	0	*oC*8	*Cmca*	*A*11	Ga
Ga_4Na	20	*tI*10	*I*4/*mmm*	$D1_3$	Al_4Ba
$Ga_{39}Na_{22}$	36.1	*oP*244	*Pnma*	...	...
(βNa)	100	*cI*2	*Im* $\bar{3}$*m*	*A*2	W

A.D. Pelton and S. Larose, *Bull. Alloy Phase Diagrams*, *11*(4), 347-353 (1990)

6.1.57 Ga-Pb

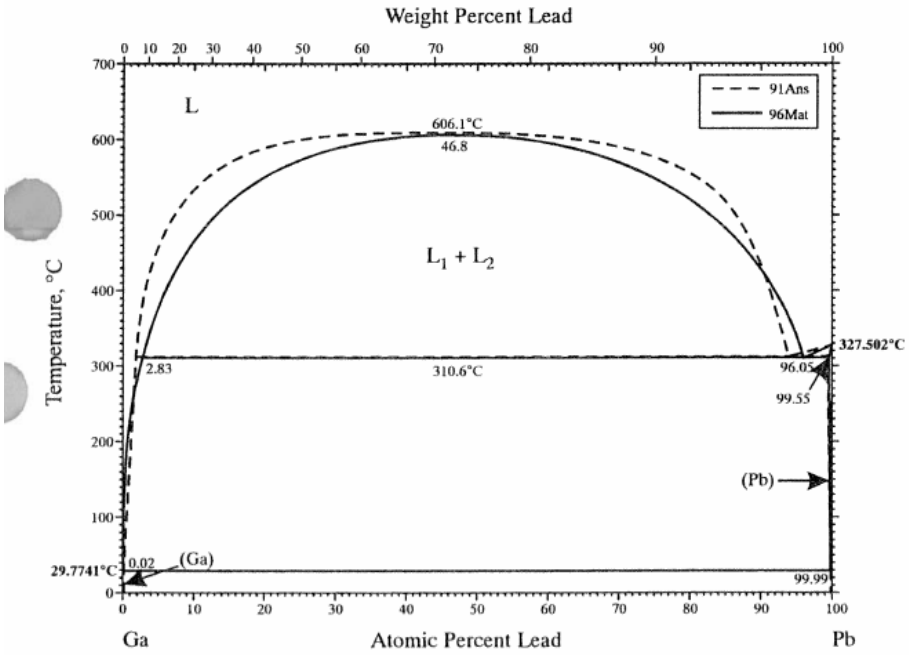

Ga-Pb

Ga-Pb

Phase	Composition, at.% Pb	Pearson symbol	Space group	Struktur-bericht designation	Prototype
(Ga)	0	*oC*8	*Cmca*	*A*11	Ga
(Pb)	? to 100	*cF*4	$Fm\bar{3}m$	*A*1	Cu

H. Okamoto, *J. Phase Equilibria*, *19*(2), 184 (1998)

6.1.58 Ga-Sn

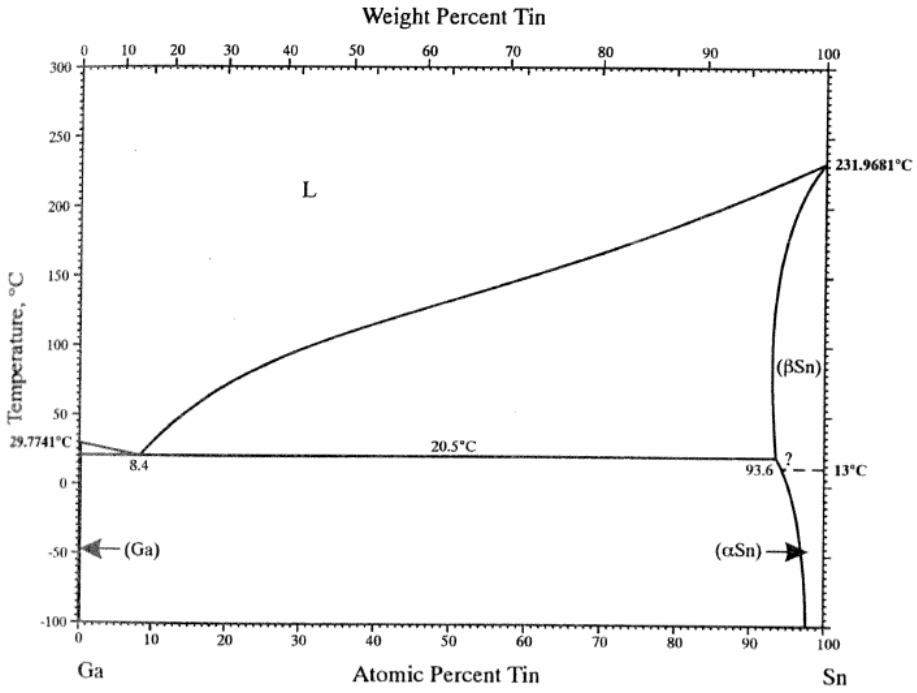

Ga-Sn

Ga-Sn

Phase	Composition, at.% Sn	Pearson symbol	Space group	Struktur-bericht designation	Prototype
(Ga)	0	*oC*8	*Cmca*	*A*11	Ga
(βSn)	93.6 to 100	*tI*4	$I4_1/amd$	*A*5	βSn
(αSn)	? to 100	*cF*8	$Fd\bar{3}m$	*A*4	C (diamond)

T.J. Anderson and I. Ansara, *J. Phase Equilibria*, *13*(2), 181-189 (1992)

6.1.59 Ga-Sr

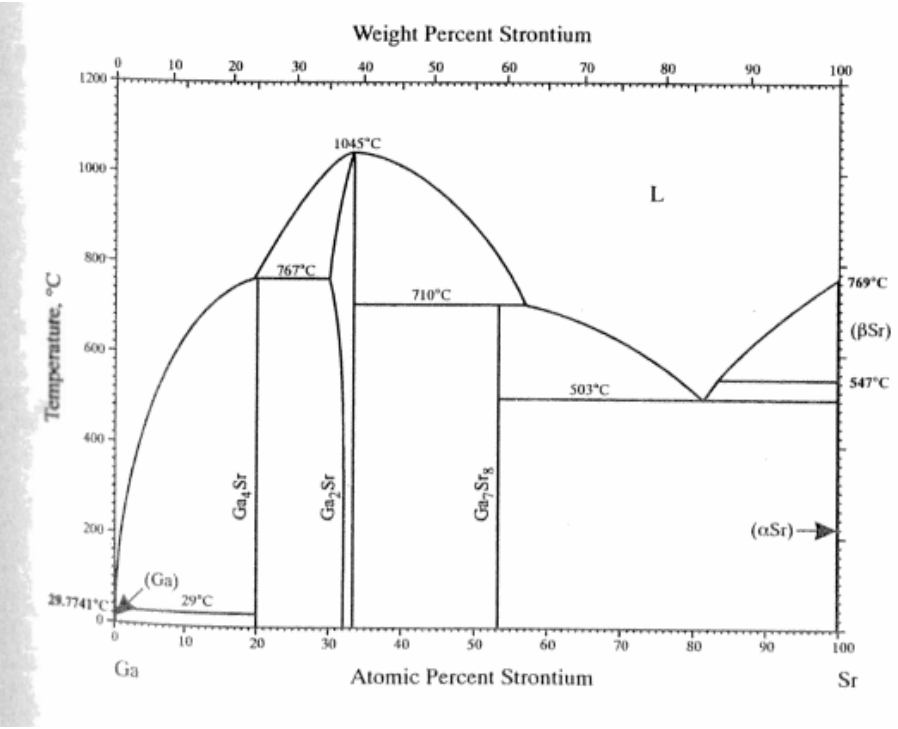

Ga-Sr

Ga-Sr

Phase	Composition, at.% Sr	Pearson symbol	Space group	Struktur-bericht designation	Prototype
(Ga)	0	*oC*8	*Cmca*	*A*11	Ga
Ga_4Sr	20	*tI*10	*I*4/*mmm*	$D1_3$	Al_4Ba
Ga_2Sr	30 to 33.3	*hP*3	*P*6/*mmm*	*C*32	AlB_2
Ga_7Sr_8	53.3	*cP*60	$P2_13$	…	Al_7Sr_8
(βSr)	100	*cI*2	$Im\bar{3}m$	*A*2	W
(αSr)	100	*cF*4	$Fm\bar{3}m$	*A*1	Cu

V.P. Itkin and C.B. Alcock, *J. Phase Equilibria*, *13*(2), 190-192 (1992)

6.1.60 Ga-Ti

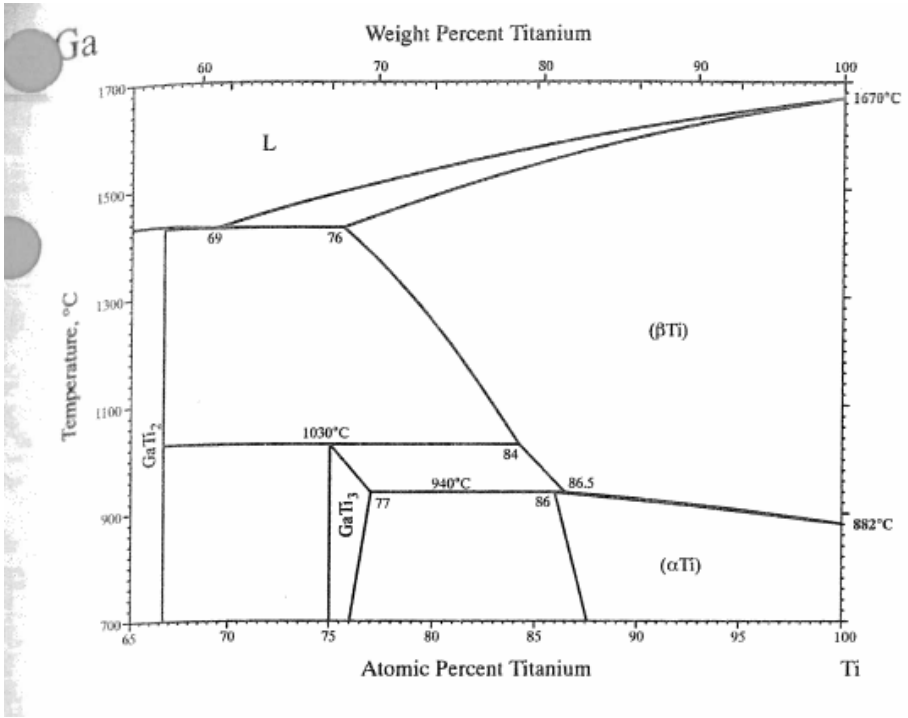

Ga-Ti

Ga-Ti

Phase	Composition, at.% Ti	Pearson symbol	Space group	Strukturbericht designation	Prototype
(Ga)	0	*oC*8	*Cmca*	*A*11	Ga
Ga_3Ti	25	*tI*8	*I*4/*mmm*	$D0_{22}$	Al_3Ti
Ga_2Ti	33.3	*tI*24	$I4_1/amd$	…	Ga_2Hf
Ga_5Ti_3	37.5	*tP*32	*P*4/*mbm*	…	Al_5Ti_3
Ga_3Ti_2	40	*tP*10	*P*4/*m*	…	…
GaTi	50	*tP*4	*P*4/*mmm*	$L1_0$	AuCu
Ga_4Ti_5	55.6	*hP*18	$P6_3/mcm$	…	…
Ga_5Ti_3	62.5	*tI*32	*I*4/*mcm*	$D8_m$	W_5Si_3
$GaTi_2$	66.7	*hP*6	$P6_3/mmc$	$B8_2$	Ni_2In
$GaTi_3$	75 to 77	*hP*8	$P6_3/mmc$	$D0_{19}$	Ni_3Sn
(βTi)	76 to 100	*cI*2	$Im\bar{3}m$	*A*2	W
(αTi)	86 to 100	*hP*2	$P6_3/mmc$	*A*3	Mg

J.L. Murray, *Bull. Alloy Phase Diagrams*, *6*(4), 327-330 (1985)

6.1.61 Ga-Zn

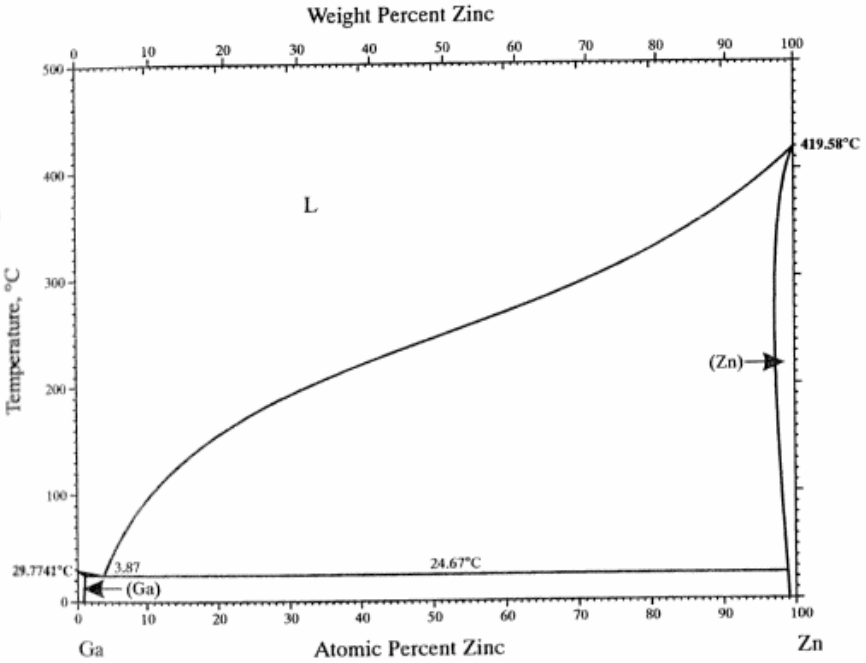

Ga-Zn

Ga-Zn

Phase	Composition, at.% Zn	Pearson symbol	Space group	Struktur-bericht designation	Prototype
(Ga)	0 to 0.8	*oC*8	*Cmca*	*A*11	Ga
(Zn)	97.64 to 100	*hP*2	$P6_3/mmc$	*A*3	Mg

J. Dutkiewicz, Z. Moser, L. Zabdyr, D.D. Gohil, T.G. Chart, I. Ansara, and C. Girard, *Bull. Alloy Phase Diagrams*, *11*(1), 77-82 (1990)

6.1.62 Hg-Li

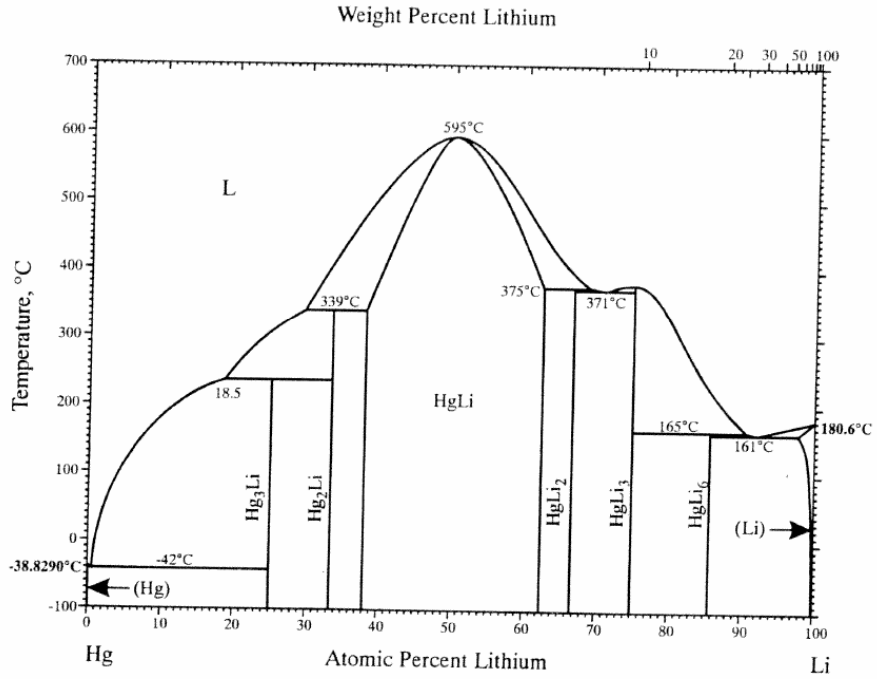

Hg-Li

Hg-Li

Phase	Composition, at.% Li	Pearson symbol	Space group	Struktur-bericht designation	Prototype
(Hg)	0	*hR*1	$R\bar{3}m$	*A*10	αHg
Hg_3Li	25	*hP*8	$P6_3/mmc$	$D0_{19}$	Ni_3Sn
Hg_2Li	33.3	…	…	…	…
HgLi	38 to 63	*cP*2	$Pm\bar{3}m$	*B*2	CsCl
$HgLi_2$	66.7	…	…	…	…
$HgLi_3$	75	*cF*16	$Fm\bar{3}m$	$D0_3$	BiF_3
$HgLi_6$	85.7	…	…	…	…
(Li)	? to 100	*cI*2	$Im\bar{3}m$	*A*2	W

Binary Alloy Phase Diagrams, *2nd ed.*, T.B. Massalski, H. Okamoto, P.R. Subramanian, and L. Kacprzak, ed., ASM International, Materials Park, OH, 2138-2139 (1990)

6.1.63 Hg-Sn

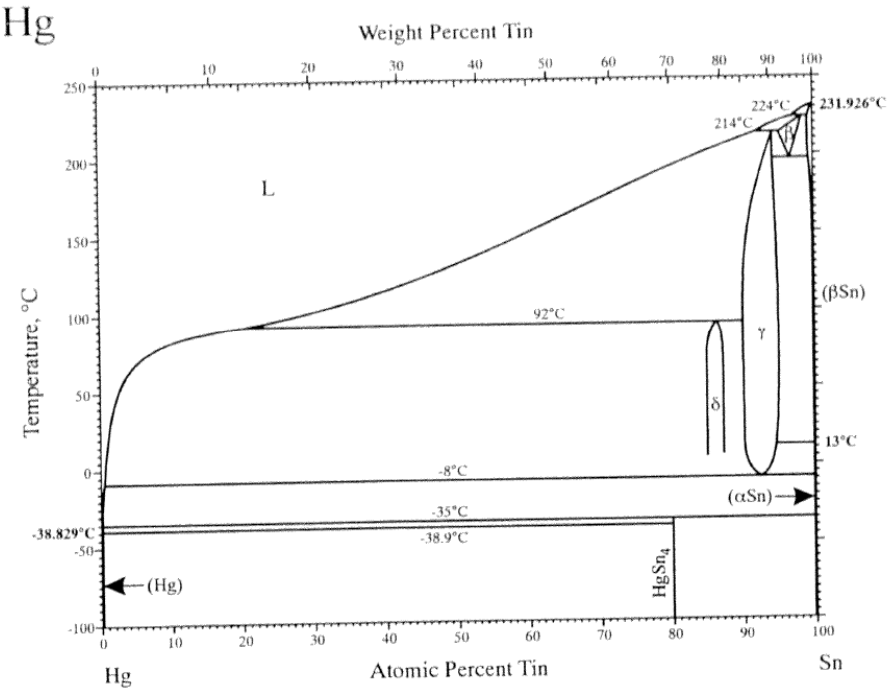

Hg-Sn

Phase	Composition, at.% Sn	Pearson symbol	Space group	Struktur-bericht designation	Prototype
(Hg)	0	*hR*1	$R\bar{3}m$	*A*10	αHg
$HgSn_4$	80	…	…	…	…
δ	85 to 87.5	*o***	…	…	…
γ	89 to 94	*hP*1	*P*6/*mmm*	…	…
β	95.5 to 98.5	…	…	…	…
(βSn)	100	*tI*4	$I4_1/amd$	*A*5	βSn
(αSn)	100	*cF*8	$Fd\bar{3}m$	*A*4	C (diamond)

L.A. Zabdyr and C. Guminski, *J. Phase Equilibria*, *14*(6), 743-752 (1993)

6.1.64 In-Li

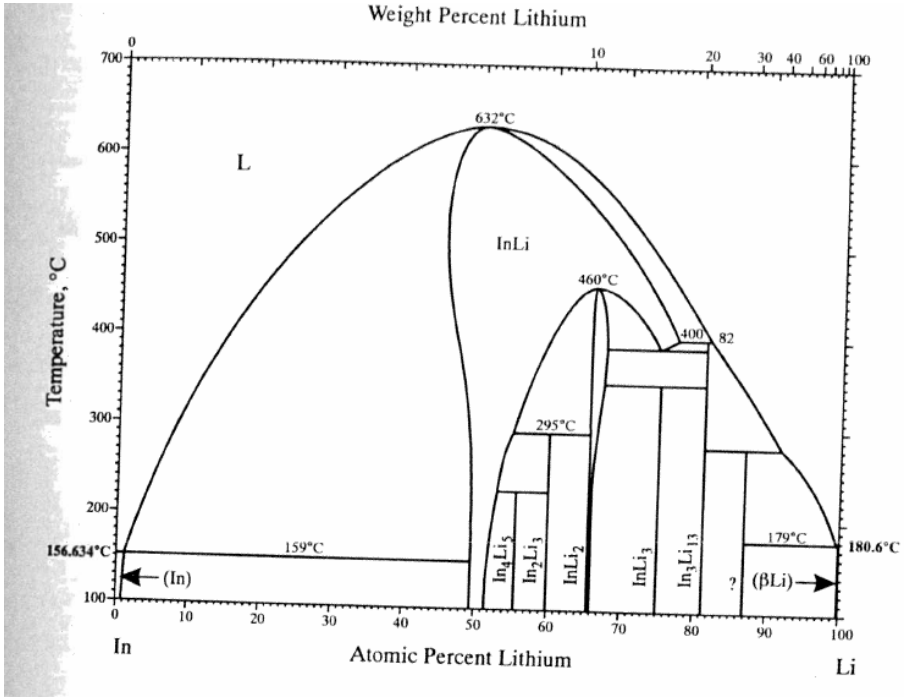

In-Li

In-Li

Phase	Composition, at.% Li	Pearson symbol	Space group	Struktur-bericht designation	Prototype
(In)	0 to 1	*tI*2	*I*4/*mmm*	*A*6	In
InLi	45 to 77	*cF*16	*Fd*$\bar{3}$*m*	*B*32	NaTl
In_4Li_5	55.6	*hP*9	*P*$\bar{3}$*m*1	…	Ga_4Li_5
In_2Li_3	60	*hR*5	*R*$\bar{3}$*m*	*C*33	Bi_2Te_3
$InLi_2$	65.6 to 67.5	*oC*12	*Cmcm*	…	$GaLi_2$
$InLi_3$	75	…	…	…	…
In_3Li_{13}	81.3	*cF*128	*Fd*$\bar{3}$*m*	…	…
?	87	…	…	…	…
(βLi)	100	*cI*2	*Im*$\bar{3}$*m*	*A*2	W
(αLi)	100	*hP*2	$P6_3/mmc$	*A*3	Mg

J. Sangster and A.D. Pelton, *J. Phase Equilibria*, *12*(1), 37-41 (1991)

6.1.65 In-Sn

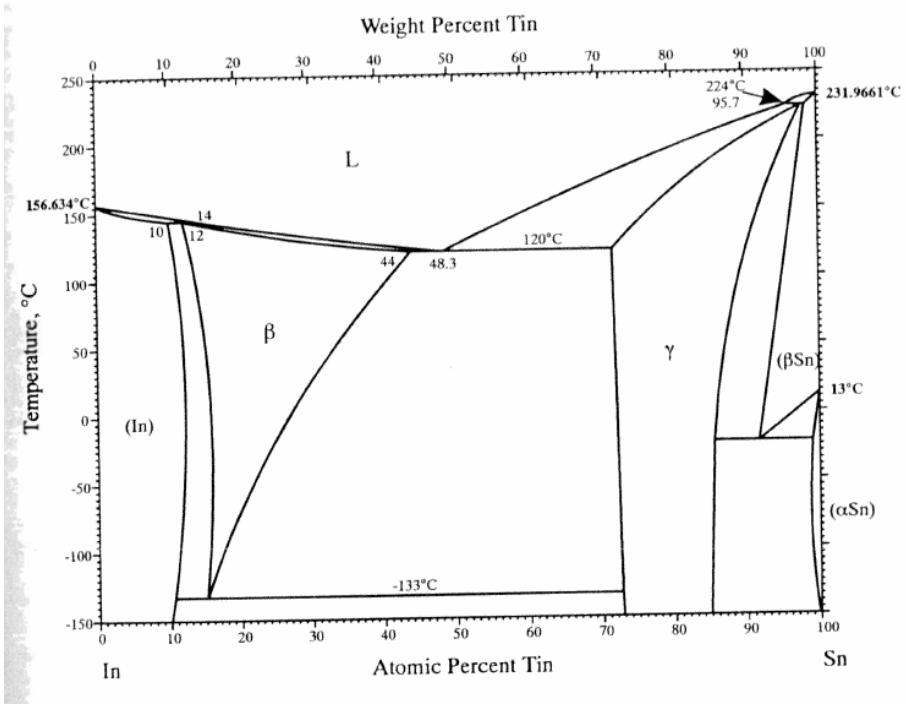

In-Sn

In-Sn

Phase	Composition, at.% Sn	Pearson symbol	Space group	Struktur-bericht designation	Prototype
(In)	0 to 12	*tI*2	*I*4/*mmm*	*A*6	In
β	12 to 44	*tI*2	*I*4/*mmm*	*A*6	In
γ	71 to 97	*hP*5	*P*6/*mmm*	…	…
(βSn)	? to 100	*tI*4	$I4_1/amd$	*A*5	βSn
(αSn)	? to 100	*cF*8	$Fd\bar{3}m$	*A*4	C (diamond)

H. Okamoto, *Phase Diagrams of Indium Alloys and Their Engineering Applications*, C.E.T. White and H. Okamoto, ed., ASM International, Materials Park, OH, 255-257 (1992)

6.1.66 Li-Na

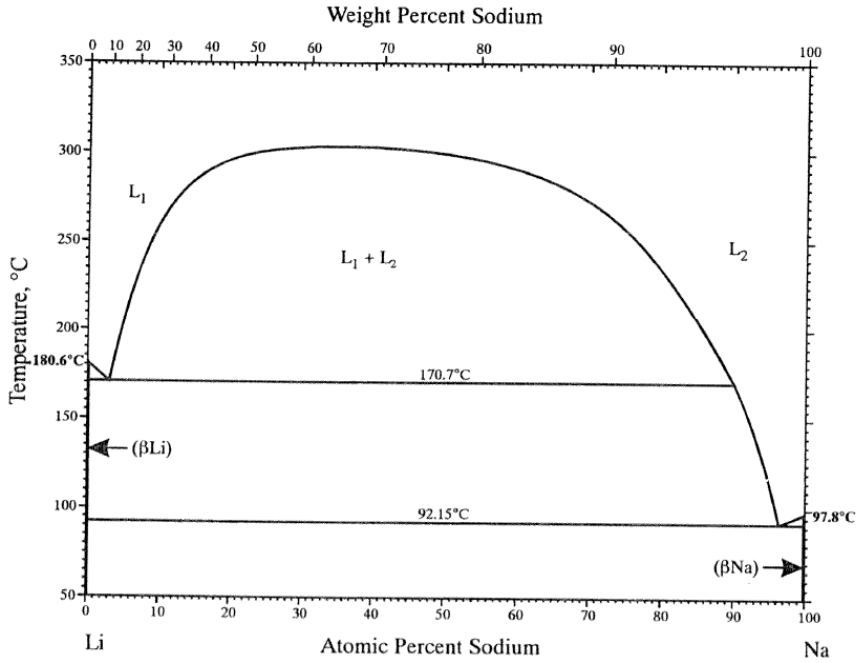

Li-Na

Li-Na

Phase	Composition, at.% Na	Pearson symbol	Space group	Struktur-bericht designation	Prototype
(βLi)	0	*cI*2	$Im\bar{3}m$	*A*2	W
(βNa)	100	*cI*2	$Im\bar{3}m$	*A*2	W

C.W. Bale, *Bull. Alloy Phase Diagrams*, *10*(3), 265-268 (1989)

6.1.67 Li-Pb

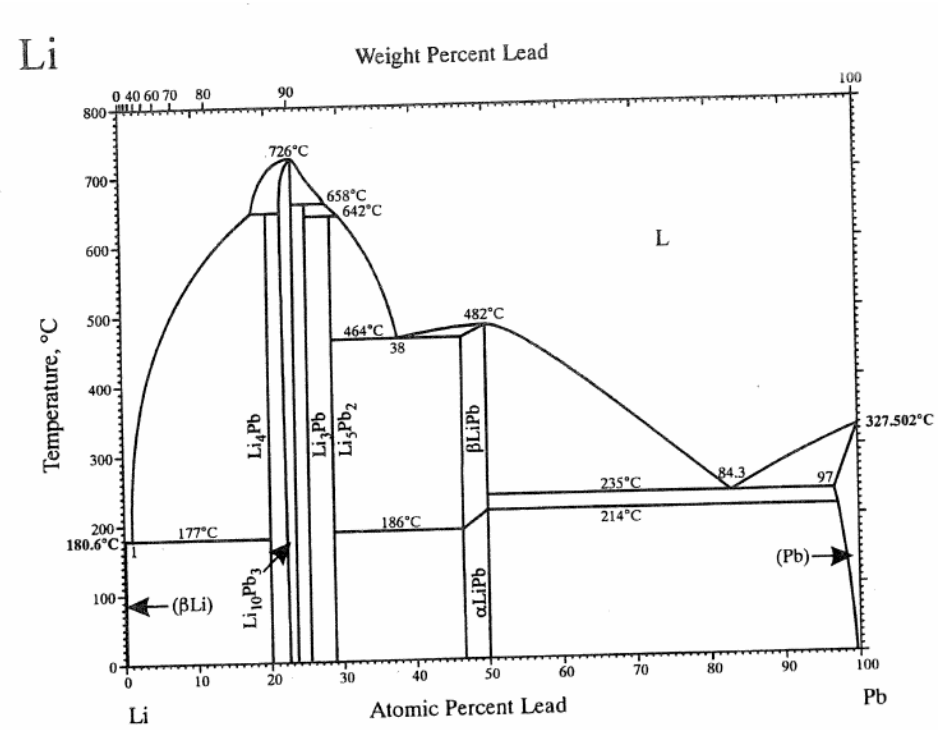

Li-Pb

Phase	Composition, at.% Pb	Pearson symbol	Space group	Struktur-bericht designation	Prototype
(βLi)	0	*cI*2	$Im\bar{3}m$	*A*2	W
Li_4Pb	20	…	…	…	…
$Li_{10}Pb_3$	22.5 to 23.5	*cP*52	$P\bar{4}3m$	$D8_3$	Al_4Cu_9
Li_3Pb	25	*cF*16	$Fm\bar{3}m$	$D0_3$	BiF_3
Li_5Pb_2	28.6	…	…	…	…
βLiPb	47 to 50	*cP*2	$Pm\bar{3}m$	*B*2	CsCl
αLiPb	47 to 50	*hR*2	$R\bar{3}m$	…	…
(Pb)	97 to 100	*cF*4	$Fm\bar{3}m$	*A*1	Cu

H. Okamoto, *J. Phase Equilibria*, *14*(6), 770 (1993)

6.1.68 Li-Sb

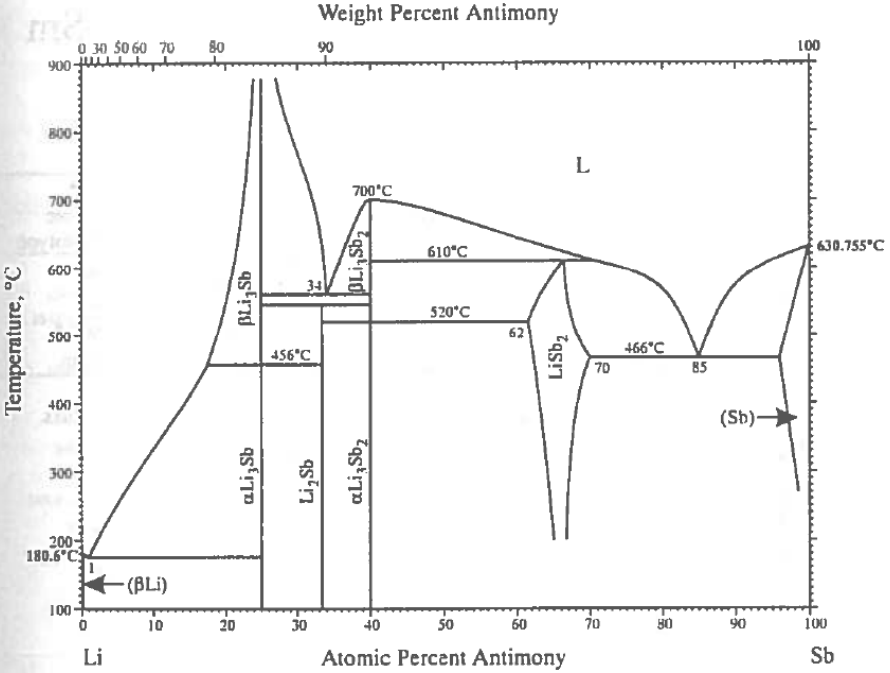

Li-Sb

Phase	Composition, at.% Sb	Pearson symbol	Space group	Strukturbericht designation	Prototype
(βLi)	0	*cI*2	$Im\bar{3}m$	*A*2	W
βLi_3Sb	25	*hP*8	$P6_3/mmc$	$D0_{18}$	Na_3As
αLi_3Sb	25	*cF*16	$Fm\bar{3}m$	$D0_3$	BiF_3
Li_2Sb	33.3	*hP*16	$P\bar{6}2c$	…	…
βLi_3Sb_2	40	…	…	…	…
αLi_3Sb_2	40	…	…	…	…
$LiSb_2$	62 to 70	…	…	…	…
(Sb)	96 to 100	*hR*2	$R\bar{3}m$	*A*7	αAs

H. Okamoto, *J. Phase Equilibria*, *17*(3), 271 (1996)

6.1.69 Li-Sn

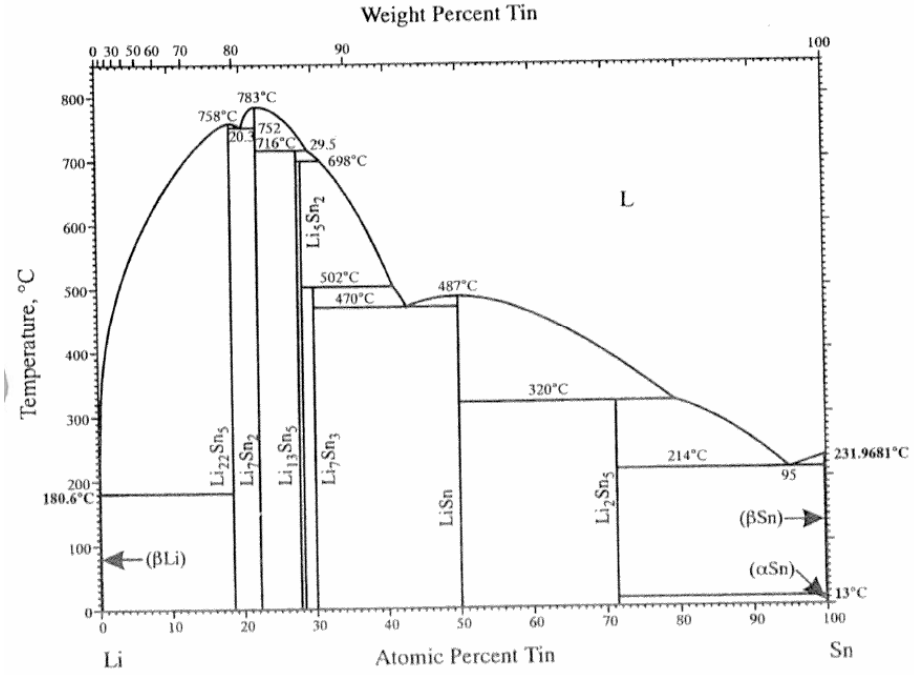

Li-Sn

Li-Sn

Phase	Composition, at.% Sn	Pearson symbol	Space group	Struktur-bericht designation	Prototype
(βLi)	0	*cI*2	$Im\bar{3}m$	*A*2	W
$Li_{22}Sn_5$	18.5	*cF*432	*F*23	…	$Li_{22}Pb_5$
Li_7Sn_2	22.2	*oC*36	*Cmmm*	…	…
$Li_{13}Sn_5$	27.8	*hP*18	$P\bar{3}m1$	…	…
Li_5Sn_2	28.6	*hR*7	$R\bar{3}m$	$D8_i$	Mo_2B_5
Li_7Sn_3	30	*mP*20	$P2_1/m$	…	…
LiSn	50	*mP*6	*P*2/*m*	…	…
Li_2Sn_5	71.4	*tP*14	*P*4/*mbm*	…	…
(βSn)	100	*tI*4	$I4_1/amd$	*A*5	βSn
(αSn)	100	*cF*8	$Fd\bar{3}m$	*A*4	C (diamond)

J. Sangster and C.W. Bale, *J. Phase Equilibria*, *19*(1), 70-75 (1998)

6.1.70 Li-Sr

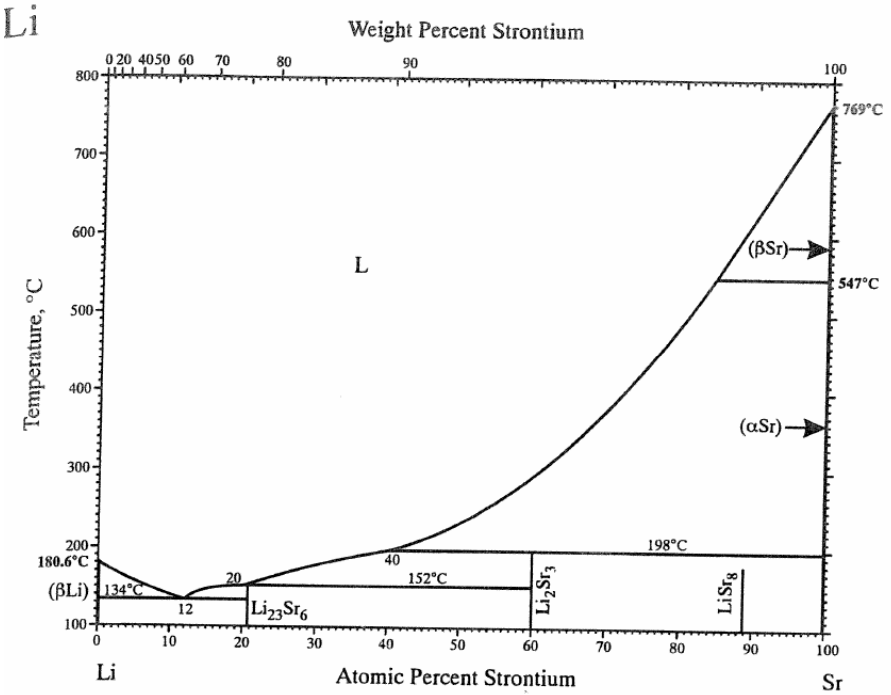

Li-Sr

Li-Sr

Phase	Composition, at.% Sr	Pearson symbol	Space group	Struktur-bericht designation	Prototype
(βLi)	0	*cI*2	*Im* $\bar{3}$*m*	*A*2	W
$Li_{23}Sr_6$	20.7	*cF*116	*Fm* $\bar{3}$*m*	$D8_a$	$Mn_{23}Th_6$
Li_2Sr_3	60	*tP*20	$P4_2/mnm$	…	Al_2Zr_3
$LiSr_8$	88.9	*t***	…	…	…
		*hP**	…	…	…
(βSr)	100	*cI*2	*Im* $\bar{3}$*m*	*A*2	W
(αSr)	100	*cF*4	*Fm* $\bar{3}$*m*	*A*1	Cu

C.W. Bale and A.D. Pelton, *Bull. Alloy Phase Diagrams*, *10*(3), 278-280 (1989)

6.1.71 Li-Ti

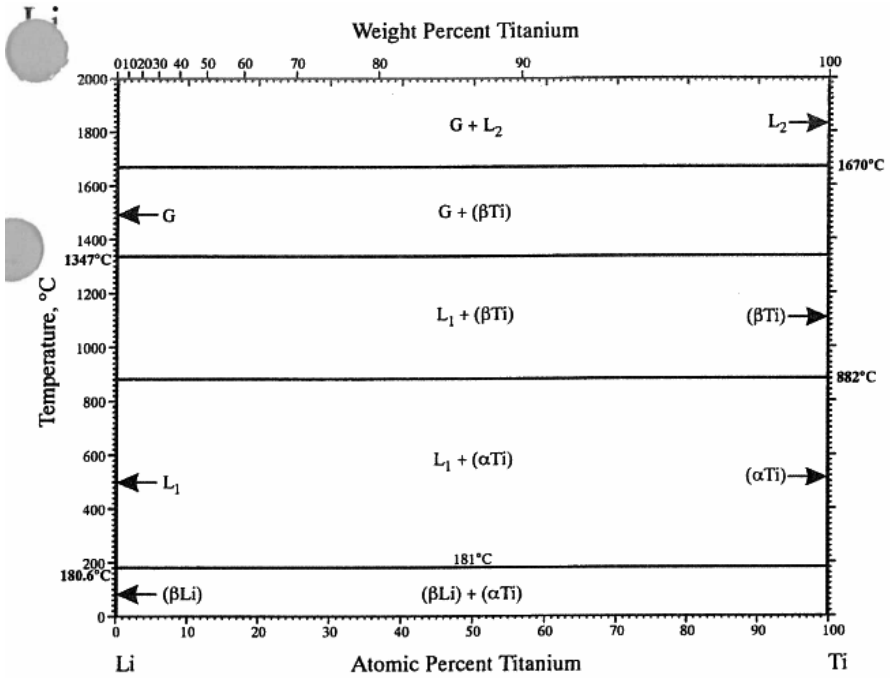

Li-Ti

Li-Ti

Phase	Composition, at.% Ti	Pearson symbol	Space group	Struktur-bericht designation	Prototype
(βLi)	0	*cI*2	$Im\bar{3}m$	*A*2	W
(βTi)	100	*cI*2	$Im\bar{3}m$	*A*2	W
(αTi)	100	*hP*2	$P6_3/mmc$	*A*3	Mg

C.W. Bale, *Bull. Alloy Phase Diagrams*, *10*(2), 135-138 (1989)

6.1.72 Li-Zn

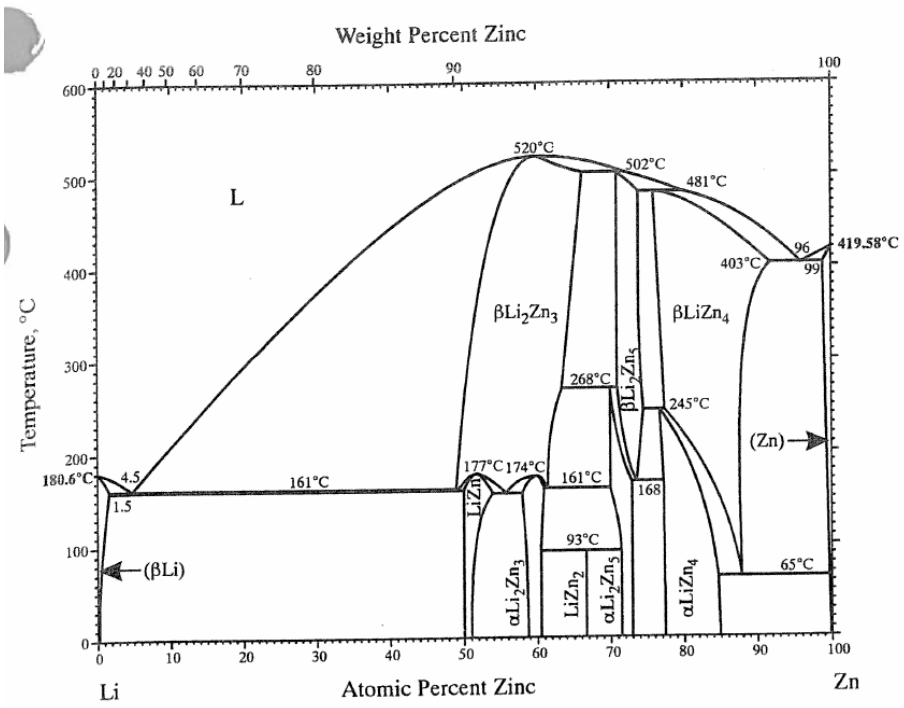

Li-Zn

Li-Zn

Phase	Composition, at.% Zn	Pearson symbol	Space group	Struktur-bericht designation	Prototype
(βLi)	0 to 1.5	*cI*2	$Im\bar{3}m$	*A*2	W
LiZn	50 to 54	*cF*16	$Fd\bar{3}m$	*B*32	NaTl
βLi_2Zn_3	50 to 67	…	…	…	…
αLi_2Zn_3	58 to 61	*c***	…	…	…
$LiZn_2$	66.7	…	…	…	…
βLi_2Zn_5	71 to 74.5	…	…	…	…
αLi_2Zn_5	70 to 73	*h***	…	…	…
$\beta LiZn_4$	75 to 90	*hP*2	$P6_3/mmc$	…	…
$\alpha LiZn_4$	77 to 85	*h***	…	…	…
(Zn)	99 to 100	*hP*2	$P6_3/mmc$	*A*3	Mg

A.D. Pelton, *J. Phase Equilibria*, *12*(1), 42-45 (1991)

6.1.73 Na-Pb

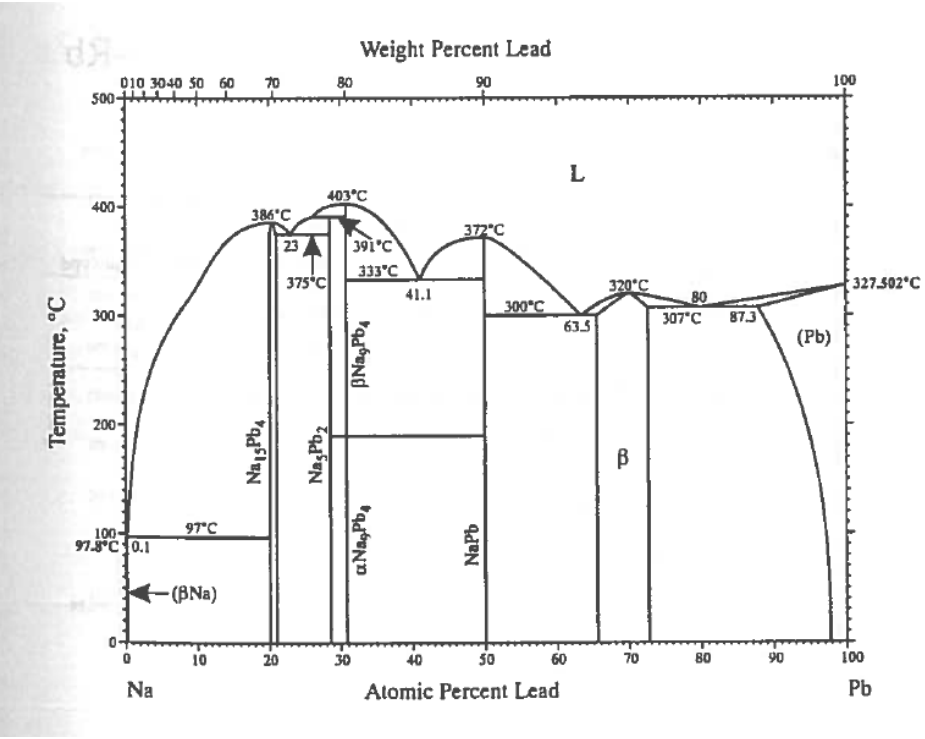

Na-Pb

Phase	Composition, at.% Pb	Pearson symbol	Space group	Strukturbericht designation	Prototype
(βNa)	0	*cI*2	$Im\bar{3}m$	*A*2	W
(αNa)	0	*hP*2	$P6_3/mmc$	*A*3	Mg
$Na_{15}Pb_4$	20 to 21	*cI*76	$I\bar{4}3d$	$D8_6$	$Cu_{15}Si_4$
Na_5Pb_2	28.6	*hR*7	$R\bar{3}m$	…	…
βNa_9Pb_4	30.8	…	…	…	…
αNa_9Pb_4	30.8	*hP*26	$P6_3/mmc$	…	…
NaPb	50	*tI*64	$I4_1/acd$	…	…
β	65.5 to 72.5	*cP*4	$Pm\bar{3}m$	$L1_2$	$AuCu_3$
(Pb)	87.3 to 100	*cF*4	$Fm\bar{3}m$	*A*1	Cu

Binary Alloy Phase Diagrams, 2nd ed., T.B. Massalski, H. Okamoto, P.R. Subramanian, and L. Kacprzak, ed., ASM International, Materials Park, OH, 2722-2723 (1990)

6.1.74 Na-Sb

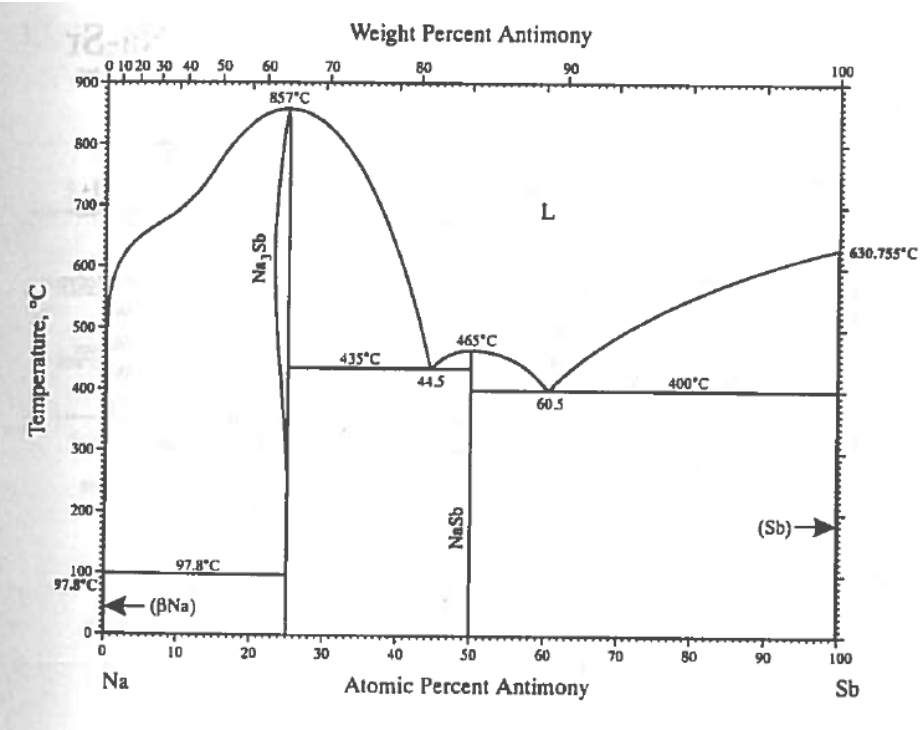

Na-Sb

Na-Sb

Phase	Composition, at.% Sb	Pearson symbol	Space group	Struktur-bericht designation	Prototype
(βNa)	0	*cI*2	$Im\bar{3}m$	*A*2	W
(αNa)	0	*hP*2	$P6_3/mmc$	*A*3	Mg
Na_3Sb	23 to 25.2	*hP*8	$P6_3/mmc$	$D0_{18}$	Na_3As
		*hP*24	$P6_3cm$	$D0_{21}$	Cu_3P
NaSb	50	*mP*16	$P2_1c$	...	LiAs
(Sb)	100	*hR*2	$R\bar{3}m$	*A*7	αAs

J. Sangster and A.D. Pelton, *J. Phase Equilibria*, *14*(2), 250-255 (1993)

6.1.75 Na-Sn

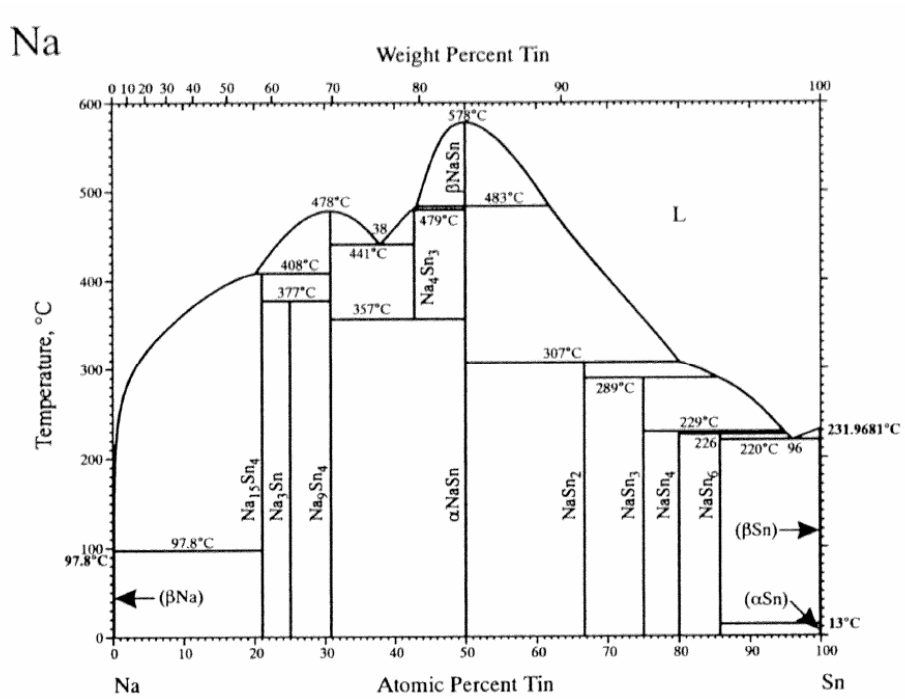

Na-Sn

Phase	Composition, at.% Sn	Pearson symbol	Space group	Strukturbericht designation	Prototype
(βNa)	0	*cI*2	$Im\bar{3}m$	*A*2	W
(αNa)	0	*hP*2	$P6_3/mmc$	*A*3	Mg
$Na_{15}Sn_4$	21.1	*oP*40	*Pnma*	…	…
		*cI*76	$I\bar{4}3d$	$D8_6$	$Cu_{15}Si_4$
Na_3Sn	25	…	…	…	…
Na_9Sn_4	30.8	*oC*52	*Cmcm*	…	…
Na_4Sn_3	42.9	…	…	…	…
βNaSn	50	…	…	…	…
αNaSn	50	*tI*64	$I4_1/acd$	…	…
$NaSn_2$	66.7	…	…	…	…
$NaSn_3$	75	…	…	…	…
$NaSn_4$	80	…	…	…	…
$NaSn_6$	85.7	…	…	…	…
(βSn)	100	*tI*4	$I4_1/amd$	*A*5	βSn
(αSn)	100	*cF*8	$Fd\bar{3}m$	*A*4	C (diamond)

J. Sangster and A.D. Pelton, *J. Phase Equilibria*, *19*(1), 76-81 (1998)

6.1.76 Na-Sr

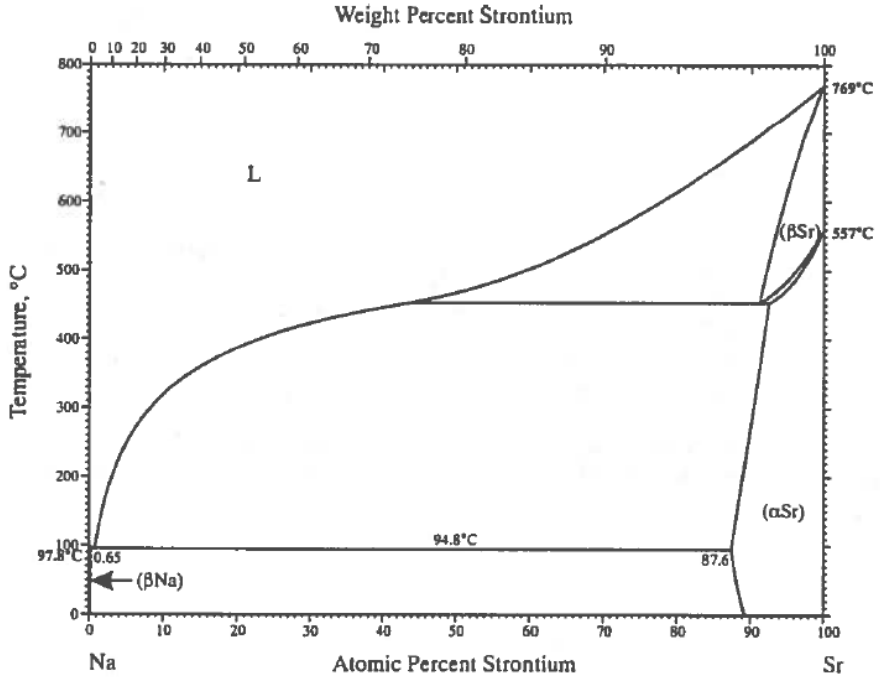

Na-Sr

Na-Sr

Phase	Composition, at.% Sr	Pearson symbol	Space group	Strukturbericht designation	Prototype
(βNa)	0	*cI*2	$Im\bar{3}m$	*A*2	W
(αNa)	0	*hP*2	$P6_3/mmc$	*A*3	Mg
(βSr)	90 to 100	*cI*2	$Im\bar{3}m$	*A*2	W
(αSr)	87.6 to 100	*cF*4	$Fm\bar{3}m$	*A*1	Cu

A.D. Pelton, *Bull. Alloy Phase Diagrams*, 6(1), 43-45 (1985)

6.1.77 Na-Ti

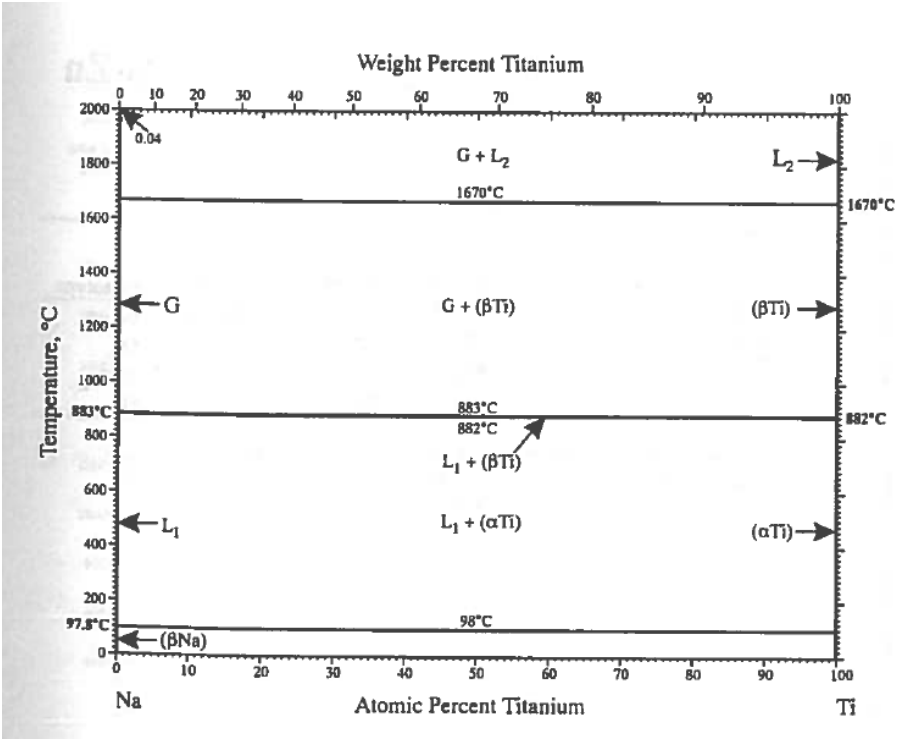

Na-Ti

Na-Ti

Phase	Composition, at.% Ti	Pearson symbol	Space group	Struktur-bericht designation	Prototype
(βNa)	0	*cI*2	$Im\bar{3}m$	*A*2	W
(αNa)	0	*hP*2	$P6_3/mmc$	*A*3	Mg
(βTi)	100	*cI*2	$Im\bar{3}m$	*A*2	W
(αTi)	100	*hP*2	$P6_3/mmc$	*A*3	Mg

C.W. Bale, *Phase Diagrams of Binary Titanium Alloys*, J.L. Murray, ed., ASM International, Metals Park, OH, 187 (1987)

6.1.78 Na-Zn

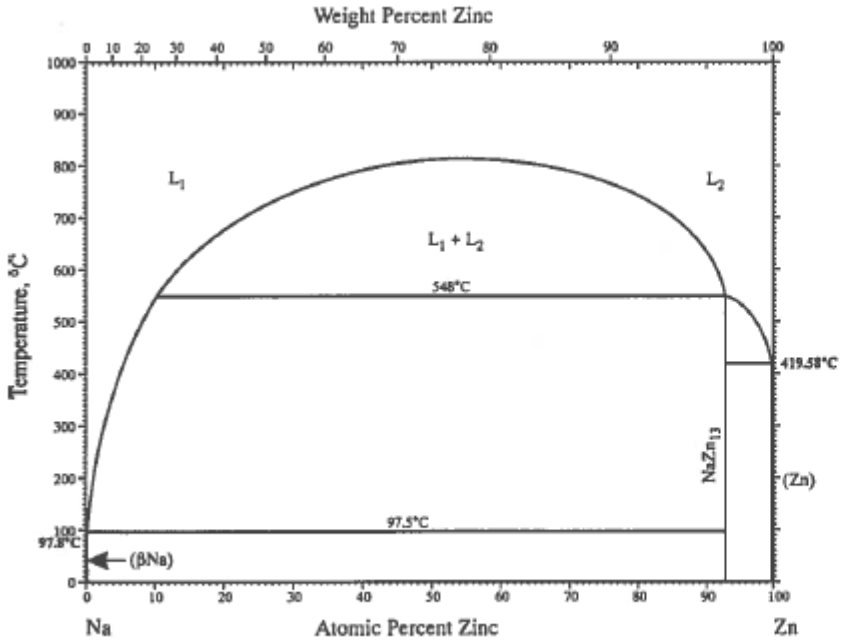

Na-Zn

Phase	Composition, at.% Zn	Pearson symbol	Space group	Struktur-bericht designation	Prototype
(βNa)	0	*cI*2	$Im\bar{3}m$	*A*2	W
(αNa)	0	*hP*2	$P6_3/mmc$	*A*3	Mg
$NaZn_{13}$	92.9	*cF*112	$Fm\bar{3}c$	$D2_3$	$NaZn_{13}$
(Zn)	100	*hP*2	$P6_3/mmc$	*A*3	Mg

H. Cetin and R.G. Ross, *J. Phase Equilibria*, *12*(1), 6-9 (1991)

6.1.79 Pb-Sn

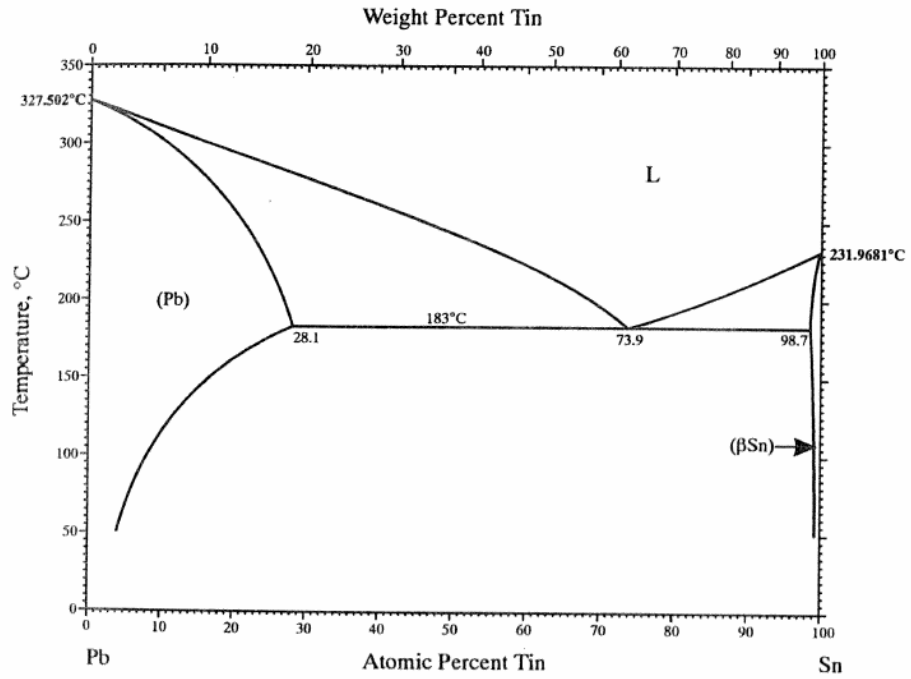

Pb-Sn

Pb-Sn

Phase	Composition, at.% Sn	Pearson symbol	Space group	Struktur-bericht designation	Prototype
(Pb)	0 to 28.1	*cF*4	$Fm\bar{3}m$	*A*1	Cu
(βSn)	98.7 to 100	*tI*4	$I4_1/amd$	*A*5	βSn
(αSn)	100	*cF*8	$Fd\bar{3}m$	*A*4	C (diamond)

I. Karakaya and W.T. Thompson, *Bull. Alloy Phase Diagrams*, *9*(2), 144-152 (1988)

6.1.80 Pb-Sr

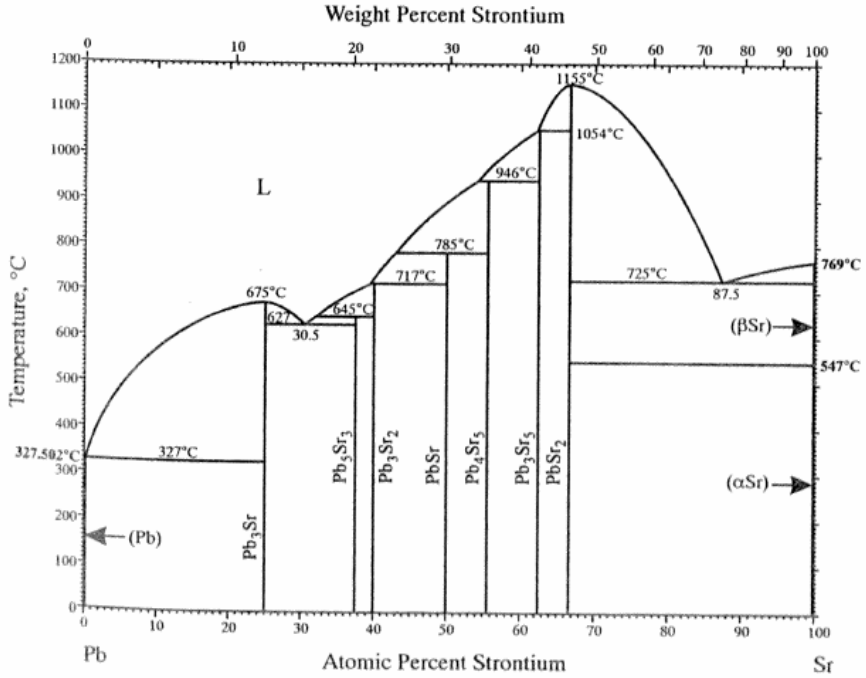

Pb-Sr

Pb-Sr

Phase	Composition, at.% Sr	Pearson symbol	Space group	Struktur-bericht designation	Prototype
(Pb)	0	*cF*4	$Fm\bar{3}m$	*A*1	Cu
Pb_3Sr	25	*tP*4	*P*4/*mmm*	$L6_0$	Pb_3Sr
Pb_5Sr_3	37.5	*t***	…	…	…
Pb_3Sr_2	40	*t***	…	…	…
PbSr	50	*oC*8	*Cmcm*	B_f	CrB
Pb_4Sr_5	55.6	*oP*36	*Pnma*	…	…
Pb_3Sr_5	62.5	*tI*32	*I*4/*mcm*	$D8_l$	Cr_5B_3
$PbSr_2$	66.7	*oP*12	*Pnma*	*C*23	Co_2Si
(βSr)	100	*cI*2	$Im\bar{3}m$	*A*2	W
(αSr)	100	*cF*4	$Fm\bar{3}m$	*A*1	Cu

Binary Alloy Phase Diagrams, 2nd ed., T.B. Massalski, H. Okamoto, P.R. Subramanian, and L. Kacprzak, ed., ASM International, Materials Park, OH, 3017-3018 (1990)

6.1.81 Pb-Ti

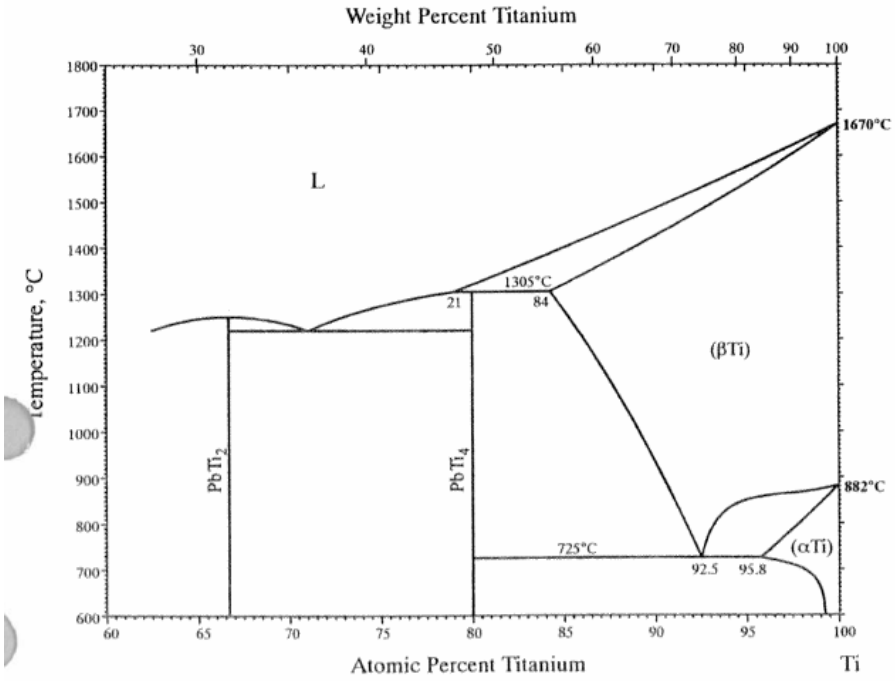

Pb-Ti

Pb-Ti

Phase	Composition, at.% Ti	Pearson symbol	Space group	Struktur-bericht designation	Prototype
(Pb)	0	*cF*4	$Fm\bar{3}m$	*A*1	Cu
$PbTi_2$	66.7	…	…	…	…
$PbTi_4$	80	*hP*8	$P6_3/mmc$	$D0_{19}$	Ni_3Sn
(βTi)	84 to 100	*cI*2	$Im\bar{3}m$	*A*2	W
(αTi)	95.8 to 100	*hP*2	$P6_3/mmc$	*A*3	Mg

J.L.Murray, *Bull. Alloy Phase Diagrams*, *5*(6), 613-615 (1984)

6.1.82 Pb-Zn

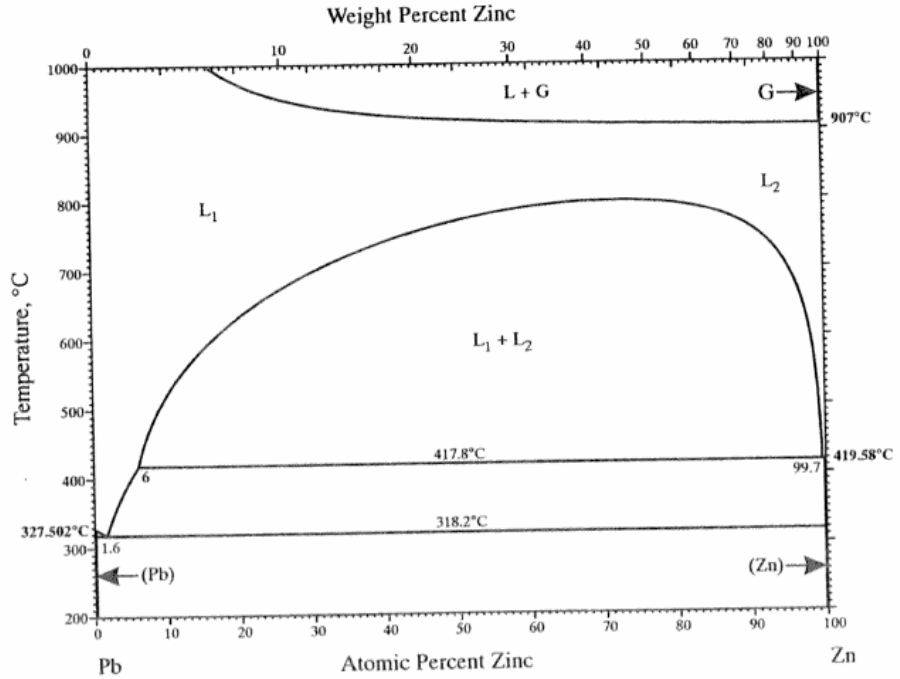

Pb-Zn

Pb-Zn

Phase	Composition, at.% Zn	Pearson symbol	Space group	Struktur-bericht designation	Prototype
(Pb)	0	*cF*4	$Fm\bar{3}m$	*A*1	Cu
(Zn)	100	*hP*2	$P6_3/mmc$	*A*3	Mg

Binary Alloy Phase Diagrams, *2nd ed.*, T.B. Massalski, H. Okamoto, P.R. Subramanian, and L. Kacprzak, ed., ASM International, Materials Park, OH, 3029, 3031 (1990)

6.1.83 Sn-Sr

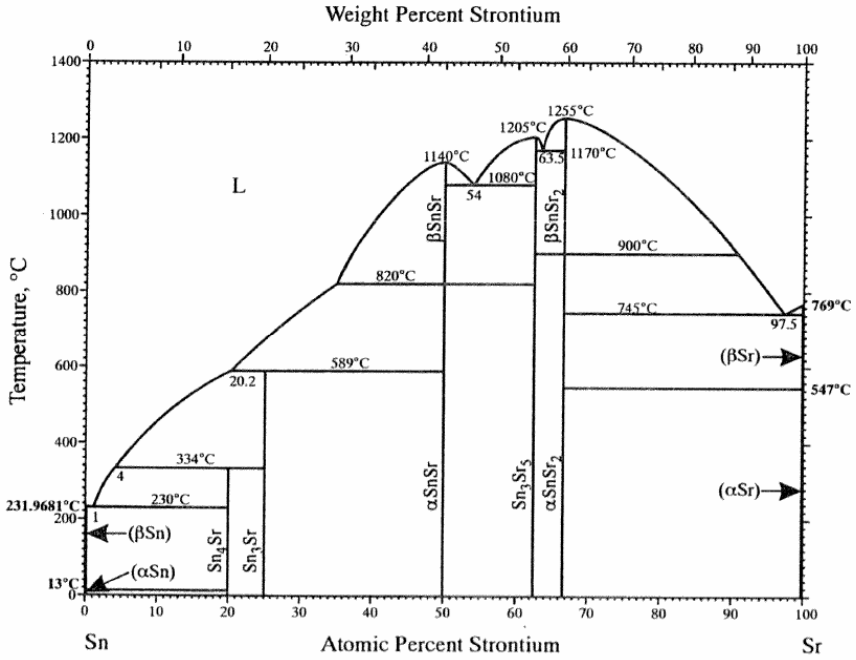

Sn-Sr

Sn-Sr

Phase	Composition, at.% Sr	Pearson symbol	Space group	Struktur-bericht designation	Prototype
(βSn)	0	*tI*4	$I4_1/amd$	*A*5	βSn
(αSn)	0	*cF*8	$Fd\bar{3}m$	*A*4	C (diamond)
Sn_4Sr	20	…	…	…	…
Sn_3Sr	25	…	…	…	…
βSnSr	50	…	…	…	…
αSnSr	50	*oC*8	*Cmcm*	B_f	CrB
Sn_3Sr_5	62.5	*tI*32	*I*4/*mcm*	$D8_l$	Cr_5B_3
$\beta SnSr_2$	66.7	…	…	…	…
$\alpha SnSr_2$	66.7	*oP*12	*Pnma*	*C*23	Co_2Si
(βSr)	100	*cI*2	$Im\bar{3}m$	*A*2	W
(αSr)	100	*cF*4	$Fm\bar{3}m$	*A*1	Cu

Binary Alloy Phase Diagrams, 2nd ed., T.B. Massalski, H. Okamoto, P.R. Subramanian, and L. Kacprzak, ed., ASM International, Materials Park, OH, 3398, 3400-3401 (1990)

6.1.84 Sn-Ti

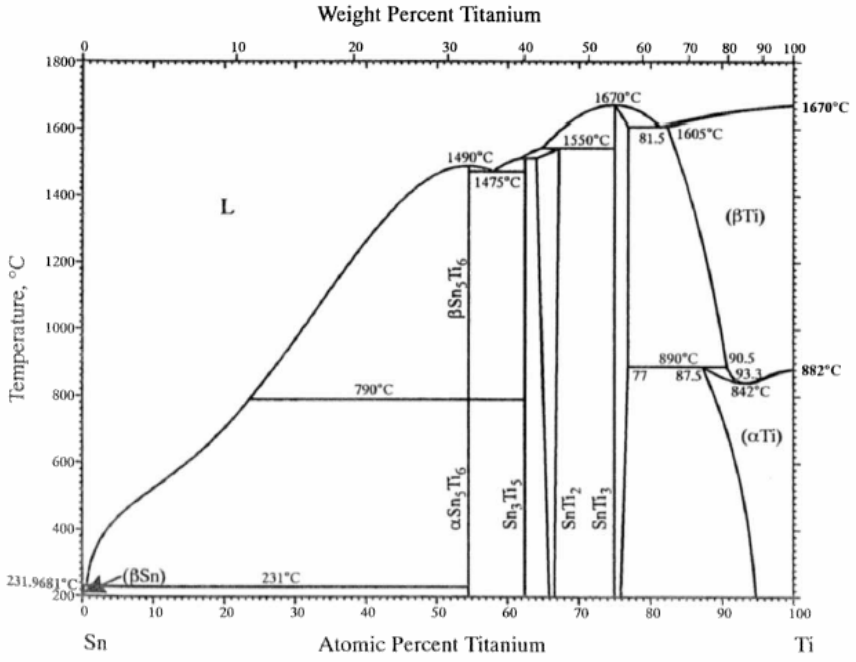

Sn-Ti

Sn-Ti

Phase	Composition, at.% Ti	Pearson symbol	Space group	Struktur-bericht designation	Prototype
(βSn)	0 to 0.02	*tI*4	$I4_1/amd$	*A*5	βSn
(αSn)	0	*cF*8	$Fd\bar{3}m$	*A*4	C (diamond)
βSn_5Ti_6	54.5	*hP*22	$P6_3/mmc$	…	…
αSn_5Ti_6	54.5	*oI*44	*Immm*	…	Nb_6Sn_5
Sn_3Ti_5	62.5	*hP*16	$P6_3/mcm$	$D8_8$	Mn_5Si_3
$SnTi_2$	64.1 to 67.3	*hP*6	$P6_3/mmc$	$B8_2$	Ni_2In
$SnTi_3$	75 to 77	*hP*8	$P6_3/mmc$	$D0_{19}$	Ni_3Sn
(βTi)	82.5 to 100	*cI*2	$Im\bar{3}m$	*A*2	W
(αTi)	87.5 to 100	*hP*2	$P6_3/mmc$	*A*3	Mg

J.L. Murray, *Phase Diagrams of Binary Titanium Alloys*, J.L. Murray, ed., ASM International, Metals Park, OH, 294-299 (1987)

6.1.85 Sn-Zn

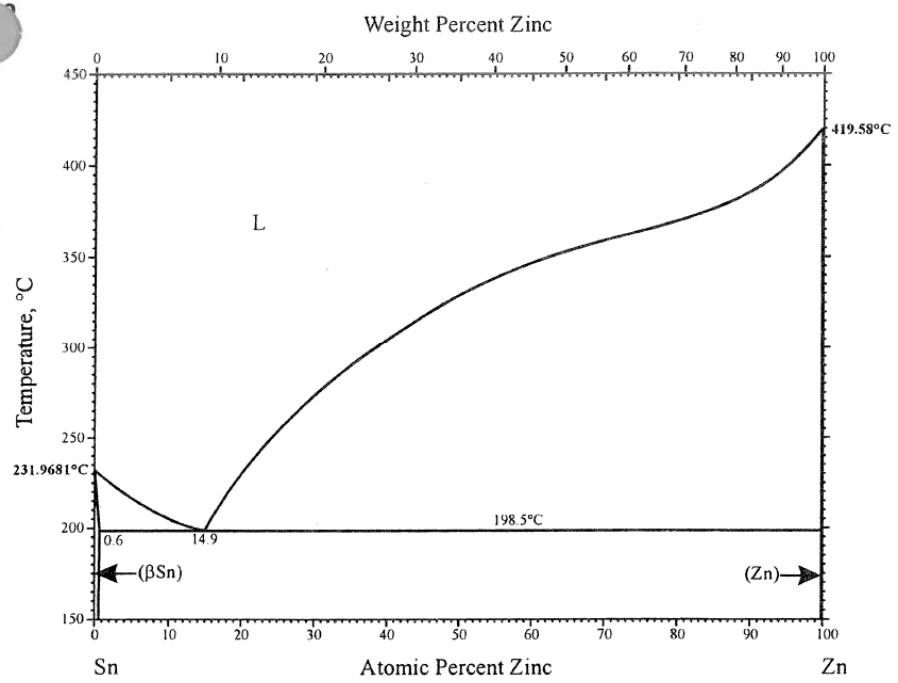

Sn-Zn

Sn-Zn

Phase	Composition, at.% Zn	Pearson symbol	Space group	Struktur-bericht designation	Prototype
(βSn)	0 to 0.6	*tI*4	$I4_1/amd$	*A*5	βSn
(αSn)	0	*cF*8	$Fd\bar{3}m$	*A*4	C (diamond)
(Zn)	100	*cI*2	$Im\bar{3}m$	*A*2	W

Z. Moser, J. Dutkiewicz, W. Gasior, and J. Salawa, *Bull. Alloy Phase Diagrams*, *6*(4), 330-334 (1985)

6.1.86 Sr-Ti

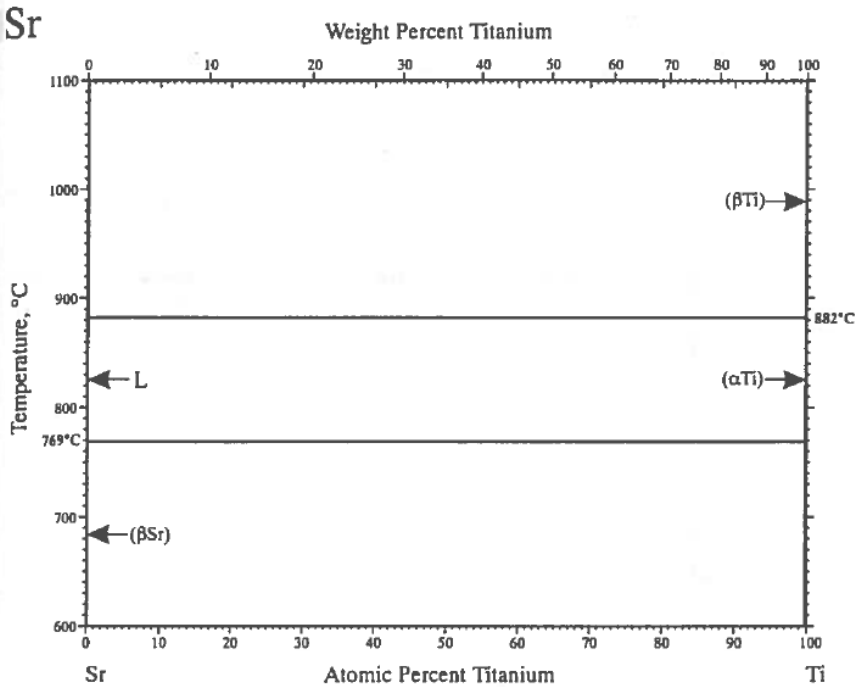

Sr-Ti

Sr-Ti

Phase	Composition, at.% Ti	Pearson symbol	Space group	Strukturbericht designation	Prototype
(βSr)	0	*cI*2	$Im\bar{3}m$	*A*2	W
(αSr)	0	*cF*4	$Fm\bar{3}m$	*A*1	Cu
(βTi)	99.9941 to 100	*cI*2	$Im\bar{3}m$	*A*2	W
(αTi)	99.981 to 100	*hP*2	$P6_3/mmc$	*A*3	Mg

J.L. Murray, *Phase Diagrams of Binary Titanium Alloys*, J.L. Murray, ed., ASM International, Metals Park, OH, 300-301 (1987)

6.1.87 Sr-Zn

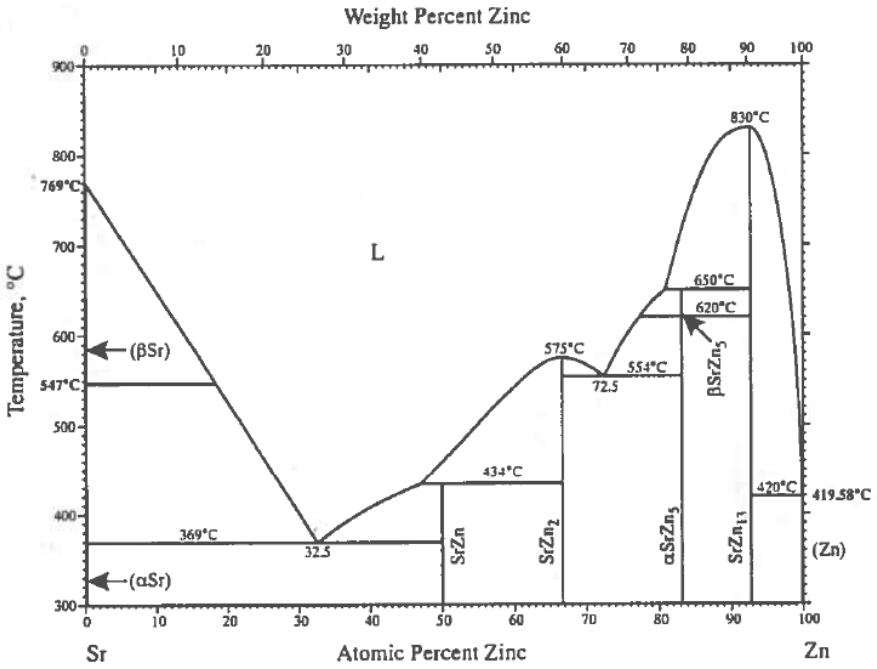

Sr-Zn

Sr-Zn

Phase	Composition, at.% Zn	Pearson symbol	Space group	Strukturbericht designation	Prototype
(βSr)	0	*cI*2	*Im* $\bar{3}$*m*	*A*2	W
(αSr)	0	*cF*4	*Fm* $\bar{3}$*m*	*A*1	Cu
SrZn	50	*oP*8	*Pnma*	*B*27	FeB
$SrZn_2$	66.7	*oI*12	*Imma*	...	$CeCu_2$
$\beta SrZn_5$	83.3	*hP*6	*P*6/*mmm*	$D2_d$	$CaCu_5$
$\alpha SrZn_5$	83.3	*oP*24	*Pnma*	...	...
$SrZn_{13}$	92.9	*cF*112	*Fm* $\bar{3}$*c*	$D2_3$	$NaZn_{13}$
(Zn)	100	*hP*2	$P6_3/mmc$	*A*3	Mg

Binary Alloy Phase Diagrams, 2nd ed., T.B. Massalski, H. Okamoto, P.R. Subramanian, and L. Kacprzak, ed., ASM International, Materials Park, OH, 3425, 3427 (1990)

6.1.88 Ti-Zn

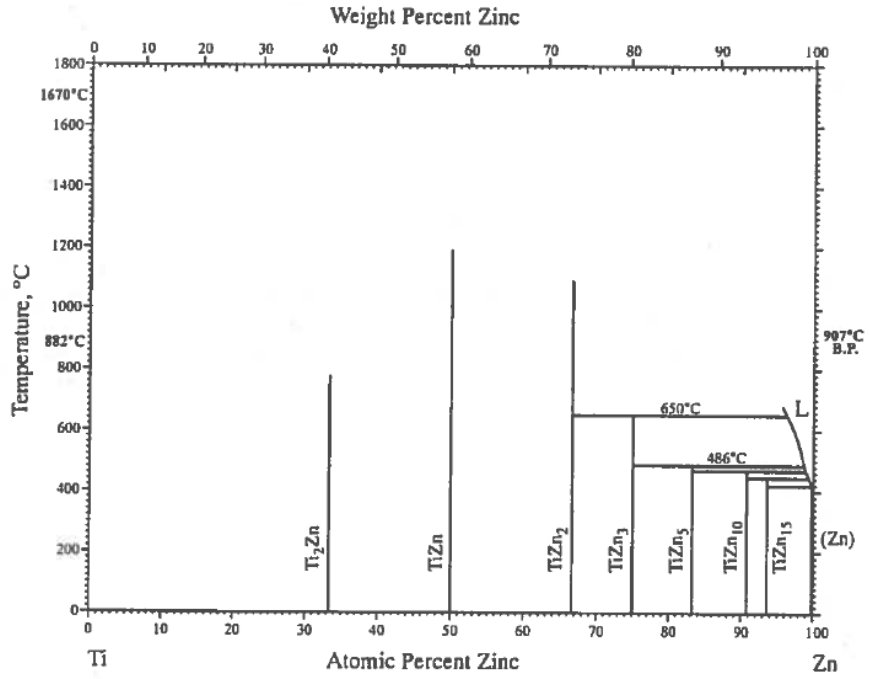

Ti-Zn

Ti-Zn

Phase	Composition, at.% Zn	Pearson symbol	Space group	Struktur-bericht designation	Prototype
(βTi)	0	*cI*2	$Im\bar{3}m$	*A*2	W
(αTi)	0	*hP*2	$P6_3/mmc$	*A*3	Mg
Ti_2Zn	33.3	*tI*6	*I*4/*mmm*	$C11_b$	$MoSi_2$
TiZn	50	*cP*2	$Pm\bar{3}m$	*B*2	CsCl
$TiZn_2$	66.7	*hP*12	$P6_3/mmc$	*C*14	$MgZn_2$
$TiZn_3$	75	*cP*4	$Pm\bar{3}m$	$L1_2$	$AuCu_3$
$TiZn_5$	83.3	…	…	…	…
$TiZn_{10}$	90.9	…	…	…	…
$TiZn_{15}$	93.7	*oC*68	*Cmcm*	…	…
(Zn)	100	*hP*2	$P6_3/mmc$	*A*3	Mg

J.L. Murray, *Phase Diagrams of Binary Titanium Alloys*, J.L. Murray, ed., ASM International, Metals Park, OH, 340-345 (1987)